SANDIA REPORT
SAND99–0752
Unlimited Release
Printed April 1999

Structural Analyses of the JPL Mars Pathfinder Impacts

Kenneth W. Gwinn

Prepared by
Sandia National Laboratories
Albuquerque, New Mexico 87185 and Livermore, California 94550

Sandia is a multiprogram laboratory operated by Sandia Corporation, a Lockheed Martin Company, for the United States Department of Energy under Contract DE-AC04-94AL85000.

Sandia National Laboratories

Issued by Sandia National Laboratories, operated for the United States Depart-ment of Energy by Sandia Corporation.

Available to DOE and DOE contractors from
Office of Scientific and Technical Information
P.O. Box 62
Oak Ridge, TN 37831

Prices available from (703) 605-6000
Web site: http://www.ntis.gov/ordering.htm

Available to the public from
National Technical Information Service
U.S. Department of Commerce
5285 Port Royal Rd
Springfield, VA 22161

NTIS price codes
Printed copy: A06
Microfiche copy: A01

SAND99-0752
Unlimited Release
Printed April 1999

Structural Analyses of the JPL Mars Pathfinder Impacts

Kenneth W. Gwinn
Engineering and Manufacturing Mechanics
Sandia National Laboratories
P.O. Box 5800
Albuquerque, NM 87185-0437

ABSTRACT

The purpose of this report is to detail the general design loadings determined from an analytical study of the Jet Propulsion Laboratory (JPL) Mars Pathfinder vehicle landing onto the Martian surface. The Pathfinder is a tetrahedral shaped structure that is protected by large airbags attached to the four faces of the lander. This lander system uses airbags to envelope the lander experiment package, protecting it with large deformation upon contact. The airbags protect the lander by deforming, thereby lengthening the impact duration in order to limit the accelerations into the Pathfinder structure. The loadings onto the Pathfinder during several impact scenarios have been predicted using explicit finite element analysis. This report details these results.

This structure exhibits extreme geometric nonlinearity during the impacts; specifically, the contact and interaction of fabric surfaces with the large deformation, which necessarily results from membrane structures, introduces great complexity to analyses. The analytical approach and the model used to predict the loading is described in detail. Results from the analysis show the stress in the fabric airbags, forces in the internal tendon support system, forces in the latches and hinges that allow the lander to deploy after impact, and deceleration of the lander components. All of these results provide the JPL engineers with design guidance for the success of this novel lander system.

This page intentionally left blank.

Acknowledgments

Tom Rivellini, JPL, allowed this analysis technique to be developed while under the time constraints of a flight program, and his initiative and patience during this process is greatly appreciated.

Kurt Metzinger, 9117, a colleague in the Materials and Solid Mechanics Department at Sandia, was invaluable in assisting with the setup of the contacts in the analysis. The author acknowledges his contribution to this program.

This page intentionally left blank.

Table of Contents

List of Figures

Introduction

The exploration of Mars includes a survey by a small instrument-laden lander, called the Mars Pathfinder, for initial definition of the Martian environment. This program, managed by the Jet Propulsion Laboratory, calls for the lander to impact on the surface using a parachute-retarding system and a bridle mounted retro-rocket system to slow down and orient the airbag protected lander. The airbags are designed to protect the vehicle by limiting not only contact with the surface but also the decelerations of the vehicle. This type of landing precludes the use of a much heavier, complicated, and expensive actively controlled rocket system normally associated with this type of landing.

The Pathfinder lander is a tetrahedron structure with three articulated 'petals,' which are used to right the structure onto its base, the fourth petal. An airbag is connected to each of the four faces of the tetrahedron at six corner locations with tethers. These tethers run across the outside of the airbags through the troughs formed by the bag intersection to a central cusp; penetrating through the central cusp, they continue inside the airbags and connect to the six lander corners by penetrating the airbags and joining with the exterior tethers.

The Pathfinder lander will deliver an instrumentation package and robotic rover to the surface of Mars. Acceptable deceleration loads and protection of these packages are the prime design parameters for JPL. The design of the airbag system is of vital importance for the success of the mission. This paper describes the structural analyses of the various parts of this system that were used in support of this design process. Explicit finite element analyses of the impact were completed for a variety of impact orientations and surface roughness. These analyses determined fabric stress in the airbags, loads in a variety of internal tethers used to maintain shape, and accelerations and loadings of various portions of the lander including the hinge and latch forces.

Details of the very complex geometry and analysis technique follow, along with the results and comparisons with scale model tests. These results are available to JPL to assist in the design of the Pathfinder components.

Analysis Methodology

The analysis of a large membrane structure impacting a surface is inherently nonlinear, especially when the structure is composed of airbags laying on top of each other. The only way to effectively model a structure of this type is with an explicitly integrated finite element code. Because of the stable shell/membrane contact experience with ABAQUS/Explicit [1], this code was used for the analysis. Because of the complex geometry of the bag design, the mesh was created using Patran [2]. These were the tools used to define the analytical model.

The design of the bags is such that there is substantial interference between the neighboring bags prior to inflation. The bags come to equilibrium by laying on top of each other during inflation. The areas of contact between the bags is a function of the bag geometry, fabric stiffness, and the pressure used to inflate the bags. Also, internal tethers are used to provide support for the lander, while providing shear reactions to the lander for an oblique impact. The initial overlapped airbag shape produces preloads in the tethers. The tether force and relative angle to the lander can only be determined with a nonlinear model of the system, in this case a finite element model.

Producing the initial inflated shape is the most challenging part of the analysis. A technique had to be devised whereby this initial geometry could be defined. The JPL design of the airbags is a combination of intersecting spheres protecting each face of the lander tetrahedron. The airbags on the adjacent faces overlap, thereby protecting the 'gaps' between the airbags. This overlap causes great difficulties in producing the finite element model of the Pathfinder system and is also of extreme importance in producing the correct preloads in the membrane of the airbags and the tethers.

The airbags had to first be physically separated to remove the interference between the bags. This is because of the contact algorithms used in finite element analysis (only small overlaps can be corrected with ABAQUS/Explicit without changing the geometry of the airbags). Once the overlap is removed, the contact identification could then be turned on locally between the airbags. At this point the airbags were reinflated using internal pressure loading.

The airbags achieve an equilibrium state after reinflation. Because the thin shell elements are now in a stable, well-formed state, global contacts between the complete airbags can now be turned on (local surface contact was used for the preliminary reinflation). The contact algorithm recognizes that a complete volume is defined for each airbag, and a robust set of contacts are now possible for the subsequent impact with even the rough, penetrating surface.

Once the 'initial' finite element model has been produced by the techniques stated above, the actual impact analysis can proceed. A body acceleration field is now used to produce the desired velocity of impact. (Generally this step occurs over 10 msec; a body or gravity loading is used to prevent stress buildup in the respective portions of the structure.) At the end of this analysis step, the body or gravity loading is reduced to simulate the gravity of Mars.

The implementation of the analysis technique is described next.

Analytical Model

The construction patterns for the lander and airbag systems were obtained from JPL. The geometry base for the airbag model in the 'as designed' state is shown in Figure 1, and the panels from which the airbags are constructed are show as outlines.

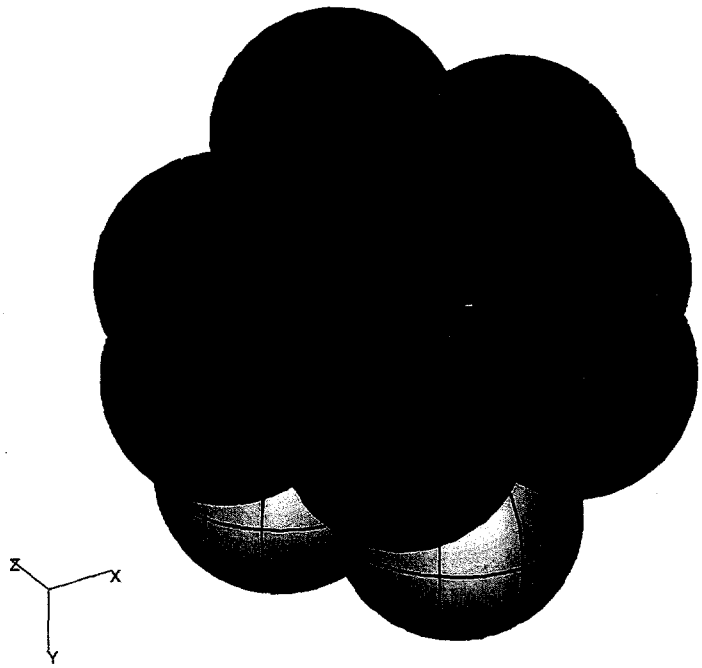

Figure 1.Geometry Pattern of the Pathfinder Airbags

The finite element model in the 'as designed' state is shown in Figure 2 (the figures shown in this section show two views of the mesh: one view with a cutting plane to show the inside details of the model and another view of the mesh exterior). The overlap in the 'as designed' model is clearly visible in the figure. Because of the complex construction of the airbags, the analytical model geometry mimicked the patterns used to piece the structure together. In this manner the initial state of stress in the airbags and internal tendons could be simulated directly (excess material or using simpler approximations to the 'as designed' geometry produces an inaccurate initial state of stress in the components). At this point a velocity boundary condition is applied to the sphere centerpoints of each airbag to uncover the airbag interference. This state is shown in Figure 3. (Because an elastic material behavior is used, this extreme deformation does not affect the final stress state in the airbags.)

At this stage in the analysis, the contact surface definition is initiated so that the local area of interference recognizes the position of its opposing surface, and a boundary condition is now imposed by the analysis code to prevent penetration. As the bags are then reinflated, they lay on top of each other in the state of equilibrium between the airbag pairs.

Only the shell elements local to the zone of interference are used for this initial contact definition. During the actual lander impact, gross bag-to-bag motion and interaction will occur, as well as bag

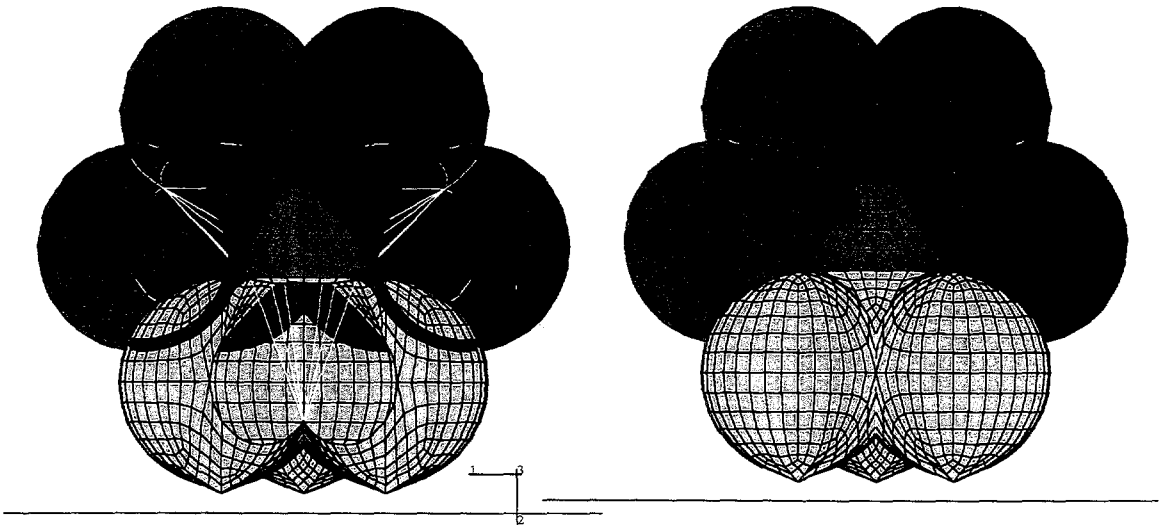

Figure 2.Initial Mesh in the 'As Designed State'

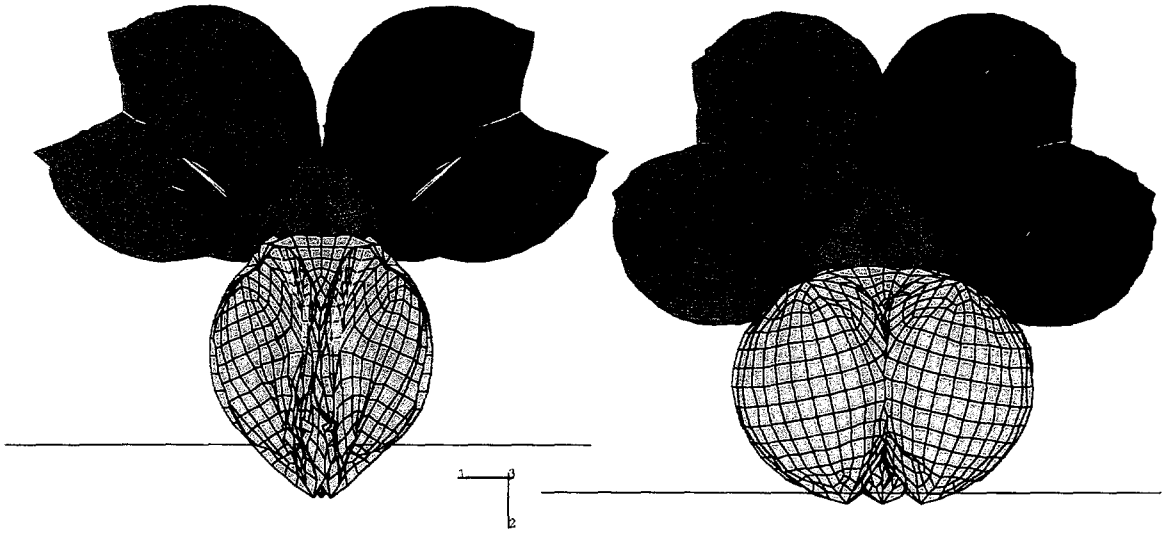

Figure 3.Mesh After Uncovering Interference Regions

penetration for the rough surface impact; therefore, a more robust contact is desired for the final analysis step. Because the elements are well shaped after reinflation, a robust contact definition is now possible. This new contact definition takes advantage of the volume treatment which ABAQUS/Explicit uses for a closed volume. (Local penetration which causes surface normal reversal does not confuse the contact set.) This robust contact will be illustrated in the results portion of this paper. Complete volume sets defined by the entire airbags are now initialized, which now makes the rotating lander/impact surface contact possible. This state where the airbags are in equilibrium is shown in Figure 4.

Several analysis steps are required to produce the actual 'initial' finite element mesh shown above because of the nature of the complex interacting geometry. The internal portions of the model visible in the cutting plane views are described below.

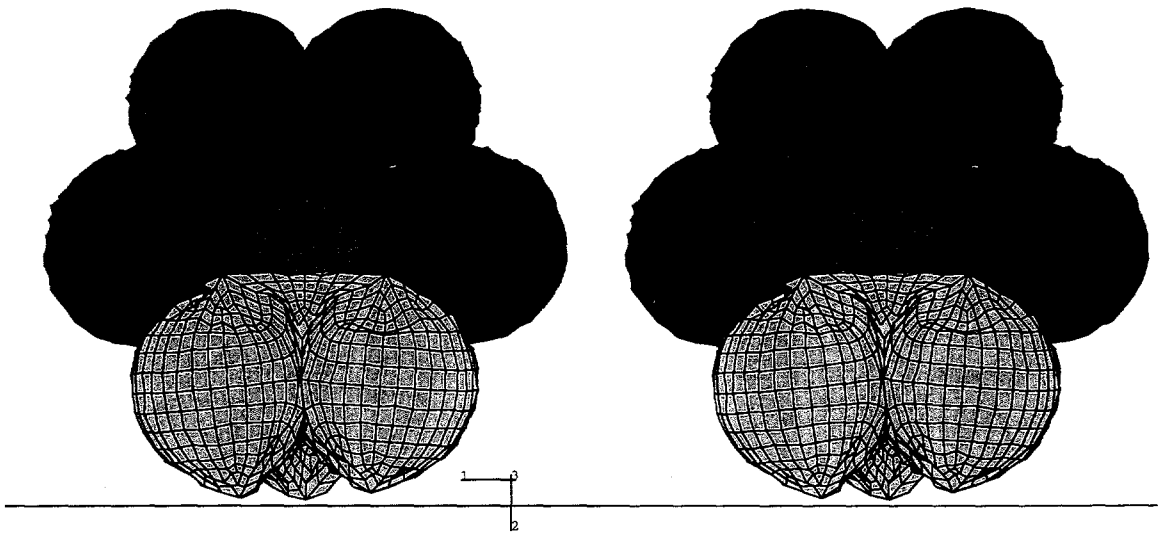

Figure 4.Equilibrium Mesh Position After Contacts Reestablished

Fabric Material Behavior

The data used to define the material behavior was determined from high strain-rate testing of parachute materials [3]. For Kevlar, the airbag and tether construction materials, the strain-rate sensitivity is not very great, so little deviation from static data occurs. Strain-to-failure of 5% was determined from these tests, also indicating little strain-rate sensitivity. Data from the same reference shows that negligible temperature effects occur in Kevlar, so the exact temperature of the deployment does not affect the material response. The reduction to the properties necessary for the analytical model produced a Young's modulus of 1.13×10^6 psi, Poisson's ratio of 0.17, and a thickness of 0.0105 in. (It should be noted that these moduli are thickness dependent to produce a resultant fabric strength that is measured in lb/in, and must always be used together.) Multiplying the resulting stress by the associated thickness used to define the Young's modulus results in the required fabric strength in lb/in, used to specify the Kevlar cloth. Results quantities for the cloth portion of the lander have been reduced to lb/in quantities in this report.

Thin shell elements were used for the model of the airbags. These were used to increase the stability of the elements during the numerous contacts. The bending stiffness terms with shell definitions which are 0.0105 in thick, are very small but not zero. It is these non-zero terms that increase the stability of the shells during contact. Fabric made of Kevlar also has some finite bending stiffness, so this approximation is felt to be appropriate.

Tendon Description

The tendons in the model were modeled as 1-dimensional extension elements. These elements carry no moment at the nodes, which models the response of the tendons very well. The tendons coexist with the shell elements in the 'troughs' of the airbags and protrude through the center of each of the airbags. Six tendons are connected to this central cusp and proceed inside the airbags to the corner locations where the lander contacts the airbags. Because 1-dimensional elements are

used to define these tendons, axial force is the only quantity carried by these tendons and is reported as a force quantity during the impacts.

Lander Description

The lander body is formed by a base plate and three 'petals,' which hinge about this plate. This was modeled using shell elements for each of the petals and the base plate. These lander elements all used the material behavior of aluminum with the required thickness (0.348 in) to bring the body of the lander to the correct assembled weight of 583 lb. This weight includes components that are mounted to the various lander plates.

As was mentioned above, the lander uses hinges for the connection of the petals to the base plate, as well as latches to maintain the top positions of the petals prior to unfolding. Clearly the load on this hardware is important to the survivability of the lander. A method to determine these loads in the rotating environment of the landing is required for the designers. This is modeled by using connections only at these discrete points of the lander body. A coordinate frame is defined at each of the connections to cause output of the results quantities in the plane of each of the petals. As is shown in the results section of this report, the forces are reported in the plane of the petal or base plate for the direction colinear with the edge and normal to this edge. These quantities were determined from the stress in the element adjacent to this hardware and using a representative area of the hardware to relate the actual force quantity reported.

Model Loading

Testing in the high altitude chamber at Sandia [4] showed that the actual pressure-time-history during the impacts did not vary greatly. The actual time of contact is ~ 40 msec, so a great amount of gas flow between the airbags is not expected. Because of this information, a pressure loading was used to load the airbags - i.e. no pressure/volume relationship is used for this model- for this structural analysis and is appropriate.

Model Validation

Testing at the Sandia Coyote Canyon Test Facility [4] of a scale model (.38 scale factor) was used to validate and calibrate the analytical model shown earlier. Primarily the maximum deceleration and pressure were used to refine the analytical model.

The test chosen for the validation is the vertical impact test case. This test had the smallest deviation from an impact normal to the surface. Peak deceleration of 20 g's (total vector sum) was measured from this test. The internal pressure during the test was 1.2 psig. Deformation of the finite element model at the peak deceleration time of 22 msec is similar to that shown for the Mars 1 analyses for normal impact. Placing this internal pressure inside the analytical model and simulating the impact velocity, a net acceleration of 22.5 g's was produced. Several parameter studies were performed on the model, and the following information was determined: 1) Moduli of the fabric (within the range of experimental error for Kevlar) did not have a great affect on the deceleration; 2) the internal pressure of the airbag system defines the deceleration of the lander system; 3) tether forces are dependent on the initial pressure, and causes an effective stiffening of the lander system - i.e. tethers raise the peak deceleration by causing greater surface area to be engaged more quickly in time.

The analytical model was found to be approximately 15% 'stiffer,' or had a slightly higher peak deceleration during the impacts. This is because of the mesh chosen for the model, and this effect is visible in the deformed mesh plot shown in Figure A7. A certain amount of 'wrinkling' occurs in the mesh at the contact line with the surface of impact. Because this mesh-dependent 'wrinkling' occurs at the maximum radius of the airbags, the surface area of contact, and thereby the deceleration, is dependent on the mesh chosen for the analysis.

It is not surprising that the results from an analysis of this type would be mesh dependent, given the direct coupling of geometry/pressure to the results (finite element results are normally stiffer than the actual response). The most important point to be learned is that the results are now verified with test data (similar results were also found for higher speed tests). Knowing that the analytical response is slightly stiffer validates the model as a design tool. These results are slightly conservative for the primary design quantity - the maximum deceleration of the Pathfinder lander.

An additional result used to validate the model was surface friction between the impact plane and the Kevlar airbags. Virtually no relative motion was observed between the impact surface and the airbags during an oblique impact test. To prevent motion in the analytical model, a coefficient of

friction of 2.0 was required. This value seems high and unrealistic but is in reality a function of the contact surface between a rigid and a very flexible surface. All the oblique analyses completed here used this coefficient of friction.

Now that the model has been validated, the analyses of the four impact cases were completed. Results for one of the analysis cases are presented below.

Analysis Results

Four analyses were chosen by JPL to envelop the range of stresses and loadings for the Pathfinder lander. These were 1) vertical impact onto a smooth surface at 20 m/sec; 2) oblique impact at 20 m/sec vertical and horizontal velocity onto a smooth surface; 3) oblique impact onto a rough surface (0.5 m tall 'rocks,' as determined from previous Mars surveys by JPL); and 4) oblique impact onto a smooth, 30° inclined surface.

For all of these analyses, the time-history results for deceleration of the lander, tether loads, hinge and latch forces are given. Also reported are the lander displacements, velocities, rotation, and rotational velocities. These are intended to quantify and envelope the motion experienced by the lander during each event. The final output quantity reported for each analysis is the stress in the airbag fabric. A global view of the state of stress is shown in the airbags at the point of maximum stress. This fabric stress is reported as maximum principal stress so that the absolute maximum will be quantified. A time-history of an element in this maximum area is also shown to understand how this stress develops in time.

As is illustrated in the acceleration and displacement time-histories for the first analysis, the contact and speed-up phase of the analysis described earlier is apparent in the results. This part of the analysis is shown for illustrative purposes only, and individual results from these periods of the analysis should not be interpreted as representative of the impact portion of the analysis. Approximately 43 msec are required to complete these phases of the analysis, so results after this time should be interpreted as the 'real' portion of the analysis. As an example, the velocity time-histories shown indicate a zero initial value until the speedup to the appropriate impact velocity is achieved. This impact velocity shows as a high positive value. At this point the impact occurs, and a slowdown to zero and the subsequent rebound is found. This portion of the velocity is the portion of interest to the designers and is the only portion that should be used for understanding the impact scenarios.

Latch forces are shown for the petal identifiers 2 to 4 (1 is the base plate). Each analysis shows the forces for the latch which joins petals 2 to 4 (for both in-line with the edge and normal to the edge of each petal) and similarly for petal latches between petals 2 to 3 and 3 to 4. The hinges, of which there are two on each side, are similarly presented as force between the base plate and petals 2 to 4 for both in-line and normal forces. As mentioned previously, these results for the latches and hinges are all presented as force quantities.

All values shown are presented in English units of lb/inch/seconds. This is because of the model construction which used English units. Two significant digits of accuracy are felt to be adequate for a design study analysis of this type. All of these results are all detailed in the next four sections for the respective impact conditions.

Mars 1 - Vertical Impact

The plots of the deformed mesh (which presents both an outside view and an inside view of the lander system using a clipping plane) during the normal impact onto a smooth plane are shown in Figures A1 - A8. These figures are snapshots of the mesh at 37.5 msec increments from 0 to 262.5 msec. Internal views are shown adjacent to the outside view to demonstrate the tendon response before, during, and after the impact. Prior to impact the tendons are preloaded or tight. During the impact, the tendons go slack and are then reloaded after the lander rebounds and allows the bottom airbag to fully resize. The acceleration time-history is shown in Figure A9, and a 48 g maximum acceleration was found from the analysis in the normal direction, Y. The velocity time history for this event is shown in Figure A10, where a rebound velocity of 320 in/sec was determined from the analysis. Rotational results quantities are shown in Figures A11 and A12, where the maximum rotation of 0.02 radians and a maximum rotational velocity of 4 rad/sec were found respectively. Displacement of the lander center-of-gravity (c.g.) during the impact is shown in Figure A13, and a maximum penetration of 40 in was determined.

Tendon forces found for the four airbags were 1000 lb for the bottom or impacting airbag; 2200 lb, 1700 lb, and 2400 lb were determined for bags 2 to 4, respectively, and the time-histories of these tendon forces are shown in Figures A14 to A17. Latch forces during the event are shown in Figure A18, and a maximum of 5300 lb was determined. For the hinges on the baseplate, a maximum force of 2300 lb was found. This time-history is shown in Figure A19.

The maximum normalized fabric force found for this event was 210 lb/in (fabric force is the stress multiplied by the thickness, 0.0105 in). The stress distribution corresponding to this condition is shown in Figure A20, where the bottom airbag alone is shown. A portion of the airbag where the lander is protruding is visible and is responsible for the higher stress region.

Mars 2 - Oblique Impact

The plots of the deformed mesh (outside view and an inside view of the system using a clipping plane) during the normal impact onto a smooth plane are shown in Figures B1 - B7. These figures, which show the external and internal views of the Pathfinder, are snapshots of the mesh at 37.5 msec increments from 0 to 225 msec. As the lander impacts the surface, the bottom airbag is prevented from sliding using friction. This causes the upper portion of the lander to roll over, whereby the tendons are being stretched in the forward bag. The acceleration time-history is shown in Figure B8, and a 39 g maximum normal acceleration and a 20 g tangential acceleration were found from the analysis, giving a total of 44 g. The velocity time-history for this event is shown in Figure B9, where a rebound velocity of 330 in/sec was determined from the analysis. Rotational results quantities are shown in Figures B10 and B11, where the maximum rotation of 0.7 radians and a maximum rotational velocity of 12 rad/sec were found respectively. This shows a much higher rotational affect of the oblique impact. Displacement of the lander center-of-gravity (c.g.) during the impact is shown in Figure B12, and a maximum penetration of 46 in was determined.

Tendon forces found for the four airbags were 2200 lb for the bottom or impacting airbag; 3100 lb, 1800 lb, and 1700 lb were determined for bags 2 to 4, respectively, and the time-histories of these tendon forces are shown in Figures B13 to B16. Latch forces during the event are shown in Figure B17, and a maximum of 5500 lb was determined. For the hinges on the baseplate, a maximum force of 5700 lb was found. This time-history is shown in Figure B18.

The stress distribution in the bottom surface of the impacting airbag 1 is shown in Figure B19. A very high stress is found but a closer view of the maximum stress zone, Figure B20, shows that a contact-induced hourglass condition exists that nullifies the result local to this element. Moving one element away from this hourglass zone produces the force time-history shown in Figure B21, where a maximum fabric force of 550 lb/in is found. This fabric tear force is slightly lower than the rough impacting plane shown next.

Mars 3 - Rocky Oblique Impact

The plots of the deformed mesh (outside view and an inside view of the system using a clipping plane) during the normal impact onto a smooth plane are shown in Figures C1 - C10. These figures, which again show external and internal views of the Pathfinder, are snapshots of the mesh at 37.5 msec increments from 0 to 375 msec. The acceleration time-history is shown in Figure C11. A 30 g maximum acceleration normal, and 23 g acceleration tangentially were found from the analysis, giving a total of 38 g. The velocity time history for this event is shown in Figure C12, where a rebound velocity of 280 in/sec was determined from the analysis. Rotational results quantities are shown in Figures C13 and C14, where the maximum rotation of -0.5 radians and a maximum rotational velocity of 10 rad/sec were found, respectively. Displacement of the lander center-of-gravity (c.g.) during the impact is shown in Figure C15, and a maximum penetration of 50 in was determined.

Tendon forces found for the four airbags were 2900 lb for the bottom or impacting airbag; 2800 lb, 1700 lb, and 3100 lb were determined for bags 2 to 4, respectively, and the time-histories of these tendon forces are shown in Figures C16 to C19. Latch forces during the event are shown in Figure C20, where a maximum of 7600 lb and a norm of 4900 lb were determined. For the hinges on the baseplate, a maximum force of 5800 lb and a norm of 2700 lb were found. This time-history is shown in Figure C21.

This event experienced the highest fabric forces, caused by the affect of the rocks. For the bottom airbag, the top view of lander penetration effect is shown in Figure C22. A maximum force of 300 lb/in is found in the vicinity of this penetration. This force is caused during the early portion of the impact, as is shown by the force time-history of this higher stress region in Figure C23. As this bottom airbag is inverted to allow viewing of the bottom surface, the influence of the rocks is readily visible as the distribution of maximum principal stress in the fabric is shown in Figure C24. Again the force time-history of a high stress region of the airbag shows that a force of approximately 600 lb is evident during the impact, shown in Figure C25. This is the highest fabric force found in any of the analyses.

Mars 4 - Oblique Impact Onto Inclined Plane

The plots of the deformed mesh (outside view and an inside view of the system using a clipping plane) during the normal impact onto a smooth plane are shown in Figures D1 - D7. These figures are snapshots of the mesh at 37.5 msec increments from 0 to 225 msec and again show the external and internal view side-by-side. This analysis showed the greatest penetration of the lander into the airbags, resulting in the highest tendon loads from all the impact cases studied. This penetration is visible in the figures. The acceleration time-history is shown in Figure D8, and a 40 g maximum normal acceleration and a 26 g tangential acceleration were found from the analysis. The velocity time-history for this event is shown in Figure D9, where a rebound velocity of 470 in/sec was determined from the analysis. Rotational results quantities are shown in Figures D10 and D11, where the maximum rotation of 0.02 radians and a maximum rotational velocity of 11 rad/sec were found, respectively. Displacement of the lander center-of-gravity (c.g.) during the impact is shown in Figure D12, and a maximum penetration of 42 in. in the Y direction and 44 in. in the Z direction were determined.

Tendon forces found for the four airbags were 1500 lb for the bottom or impacting airbag; 3700 lb, 3800 lb, and 3700 lb were determined for bags 2 to 4, and the time-histories of these tendon forces are shown in Figures D13 to D16, respectively. Latch forces during the event are shown in Figure D17, and a maximum of 6100 lb was determined. For the hinges on the baseplate, a maximum force of 8200 lb was found. This time-history is shown in Figure D18.

The stress distribution of maximum principal stress is shown in Figure D19. The region of influence of the flat impacting surface is visible in the plot. At this point in time, the maximum force in the fabric was 270 lb/in, but the plot is used to identify the zones of maximum stress. The greatest force time-history in one of these zones is shown in Figure D20, where a maximum force of 390 lb/in was found.

Summary of Results

The goal of preventing the lander from experiencing greater than 50 g's was met; the inclined plane scenario produces 48 g's net.

The maximum fabric force experienced by the airbags was 600 lb/in during the rocky impact plane. The nominal fabric force without the influence of the rocks was 390 lb/in. The kevlar fabric generally available is in the 1000 lb/in capacity range, with higher capacity from custom weaves.

The maximum force experienced by the tendons was 3800 lb, during the oblique/flat plane, where the tendons assist the lander in rolling over.

The maximum hinge force of 8200 lb was found during the oblique impact which corresponds with the highest tendon load. The hinge force of 8200 lb could be considered a shock loading, and 2700 lb was the maximum determined as a longer duration vibration load. The latches were found to have a maximum force of 7600 lb as a shock loading and 4900 lb as a longer duration vibration load. These loads provide the basis for JPL to design this specific equipment with the appropriate mission specific factors-of-safety.

In no case did the lander come close to contacting the impact surface.

Discussion of Results

Two interesting points have been learned from this analysis. First, the initial overlapped geometry produces zones where excess fabric exists, and membrane action for load transfer is therefore not very efficient. It essentially takes more fabric, and weight, to produce a shape that is less structurally efficient. Designing the airbags to reflect these zones of interference would make the system lighter and more efficient for load transfer.

Secondly, the internal tethers cause a high stress zone to exist where the bags are pulled into the center. If the tethers were longer, the airbags would be allowed to expand, thereby reducing the membrane load required to pull them to their present position. This would reduce the current stress state in the fabric. Also, the pulling of fabric into the middle causes more airbag area to be encountered in a shorter period of time, thereby raising the deceleration of the lander. Allowing the airbags to contact over a greater distance would reduce the deceleration, while adding to the distance between the impact plane and the lander.

References

1. ABAQUS/Explicit User's Manual, Version 5.4, Hibbitt, Karlsson & Sorensen, Inc., Pawtucket, RI, 1994.

2. Patran Plus User Manual, Version 2.5, PDA Engineering, Costa Mesa, CA, 1994.

3. High Strain-Rate Testing of Parachute Materials, K. Gwinn, J. Totten, D. Waye, Sandia National Laboratories, 13th AIAA Aerodynamic Decelerator Systems Technology Conference, May, 1994.

4. Mars Pathfinder Airbag Impact Attenuation System, D. E. Waye, J. K. Cole, Sandia National Laboratories, T. P. Rivellini, JPL, to be presented at the AIAA 13th Aerodynamic Decelerator Systems Technology Conference, May, 1994.

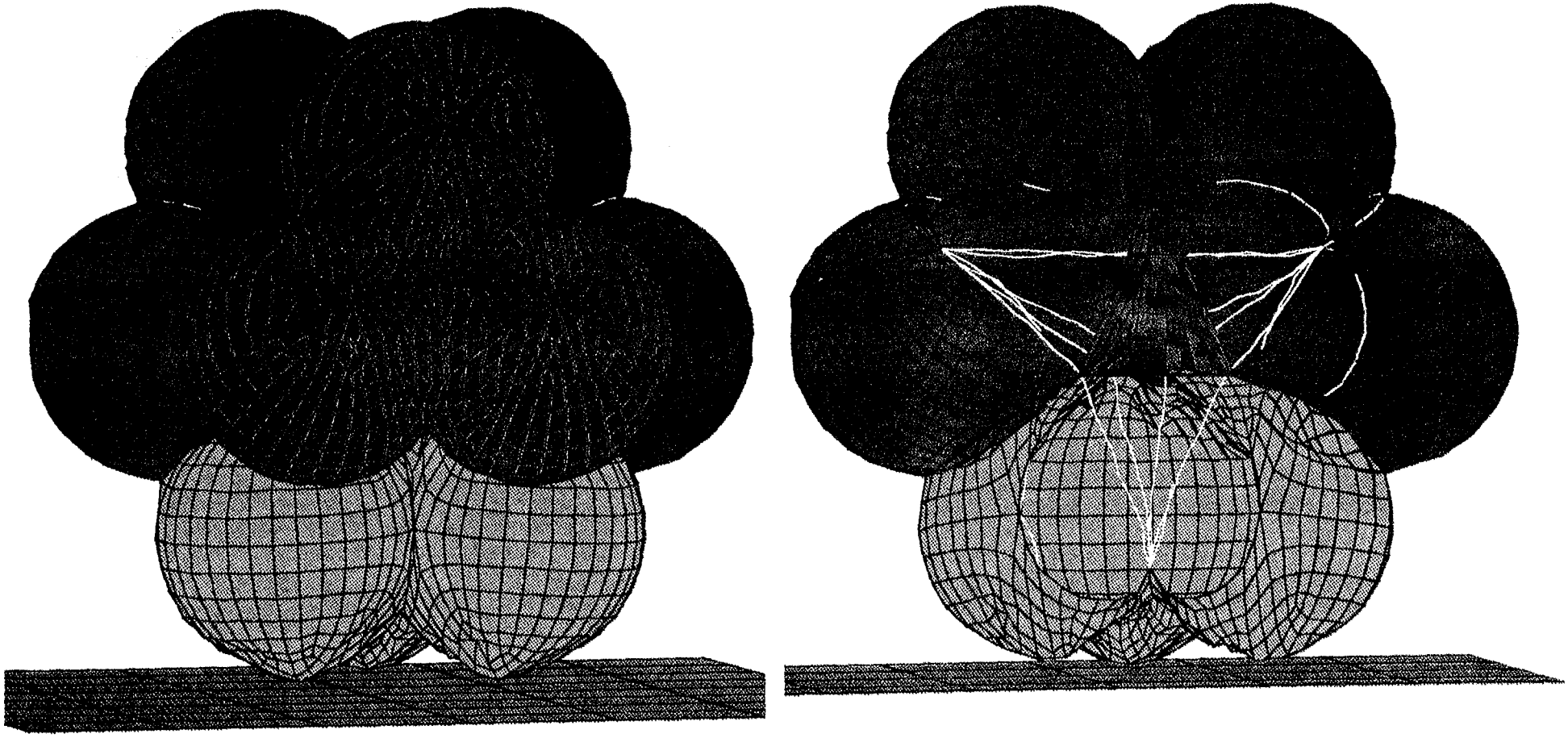

Figure A1. Deformed Mesh at 0 msec Into Impact 1

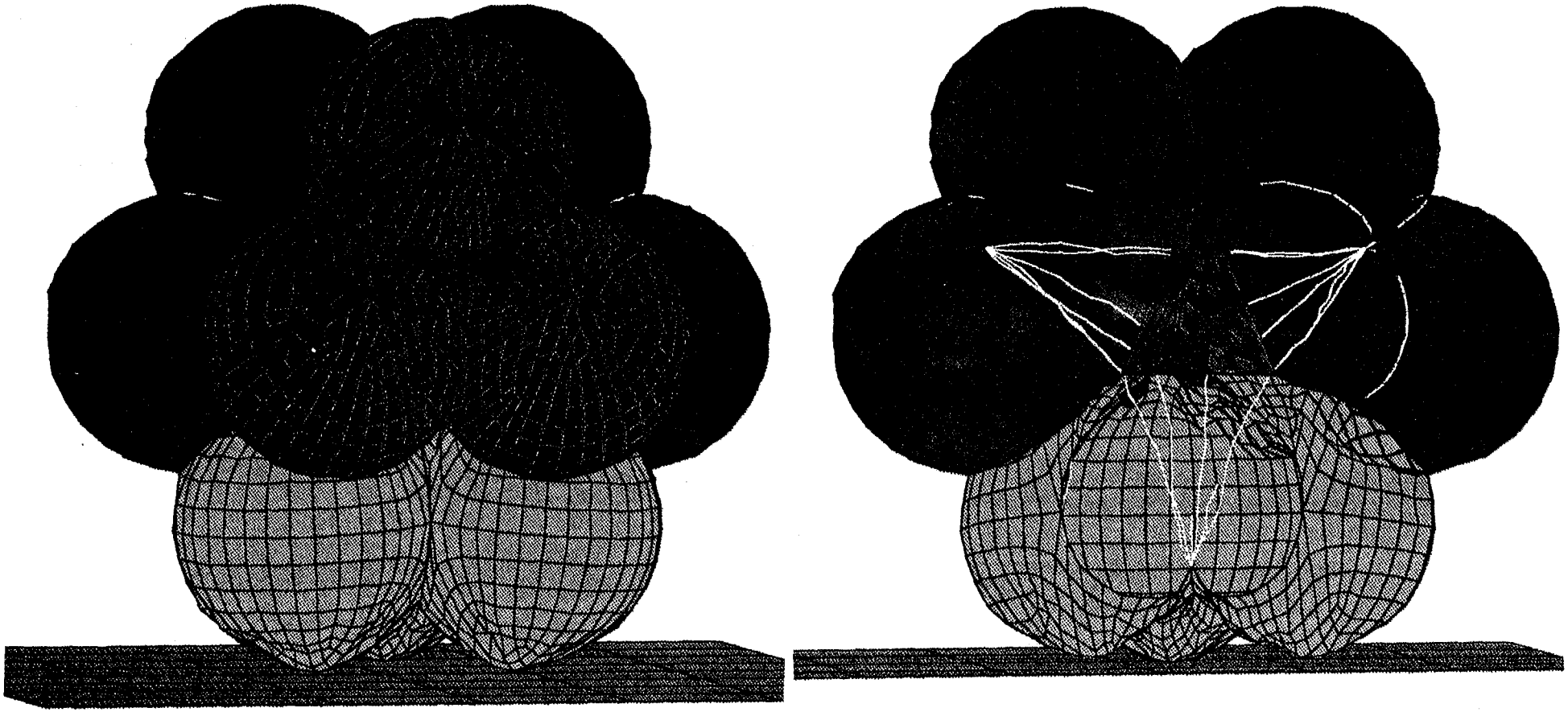

Figure A2. Deformed Mesh at 37.5 msec Into Impact 1

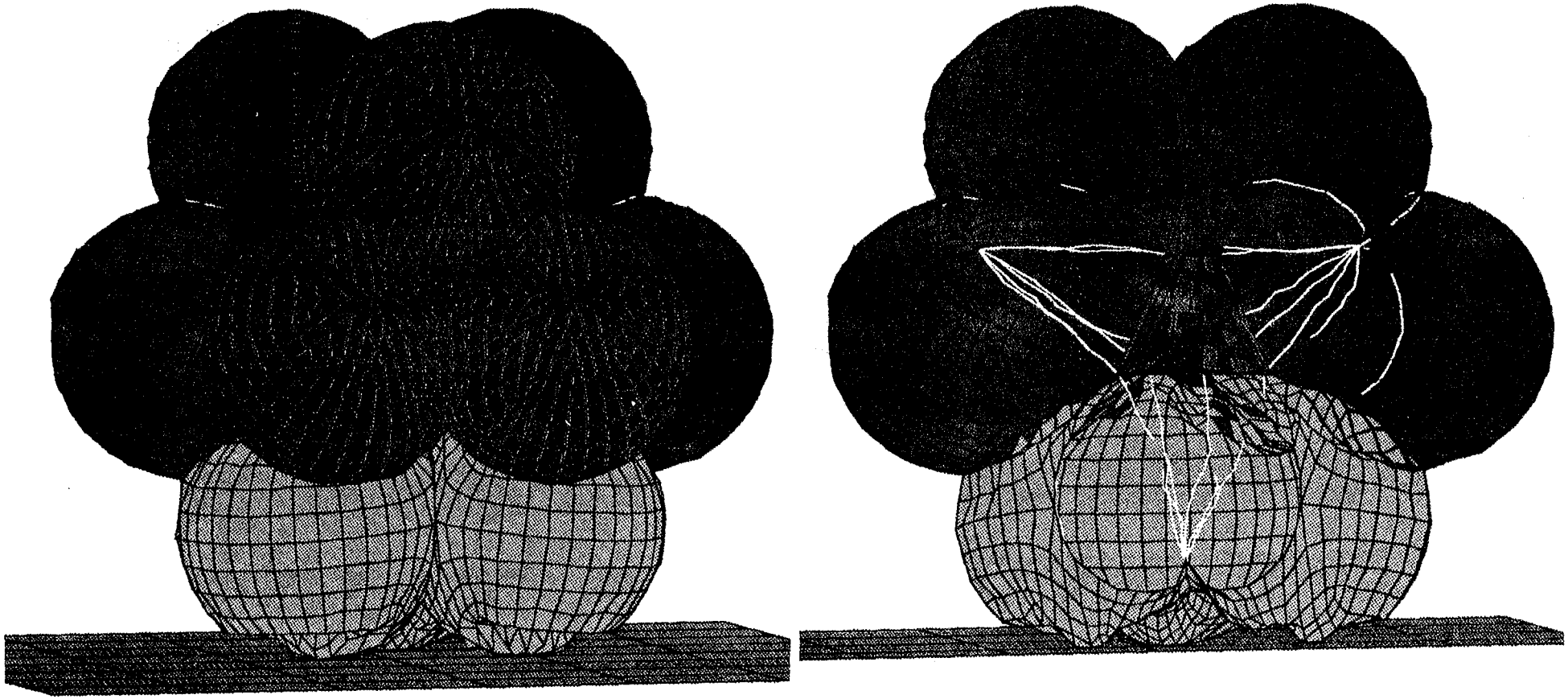

Figure A3. Deformed Mesh at 75 msec Into Impact 1

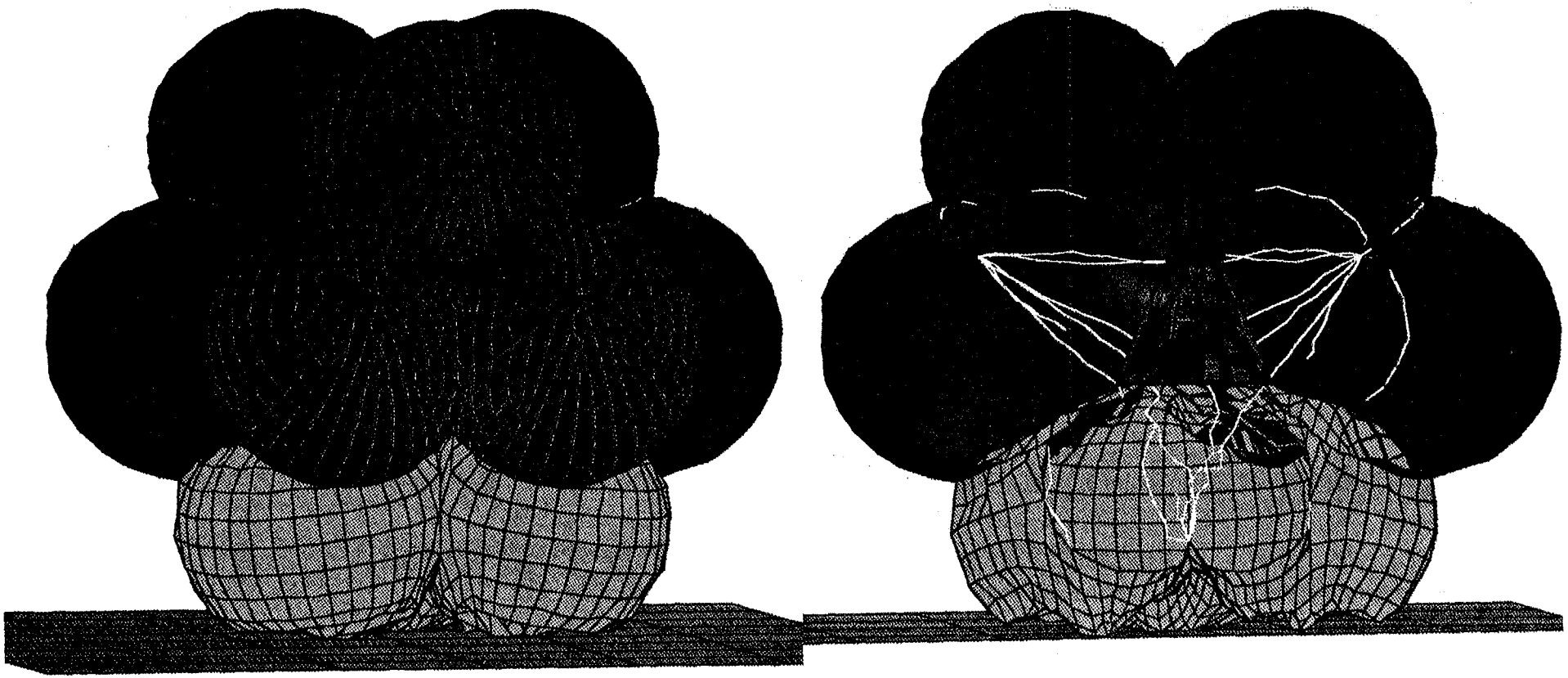

Figure A4. Deformed Mesh at 112.5 msec Into Impact 1

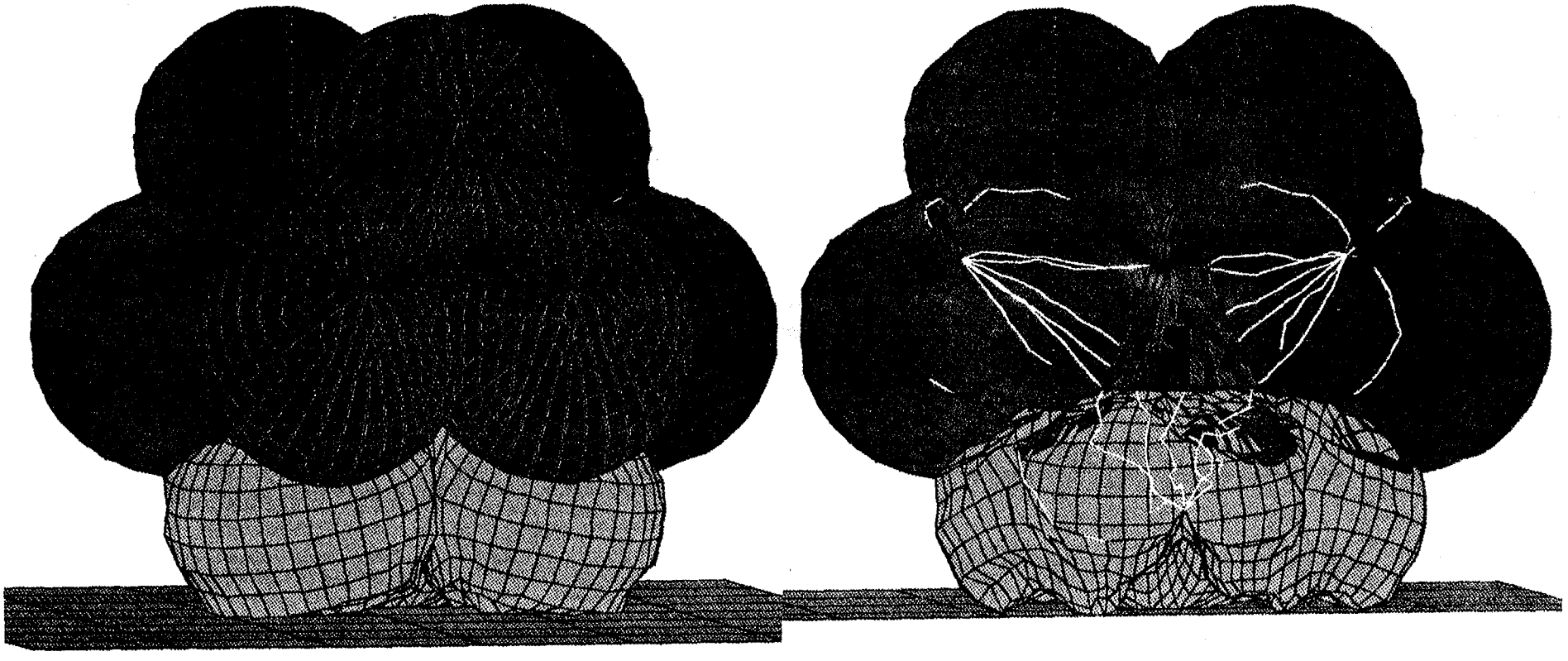

Figure A5. Deformed Mesh at 150 msec Into Impact 1

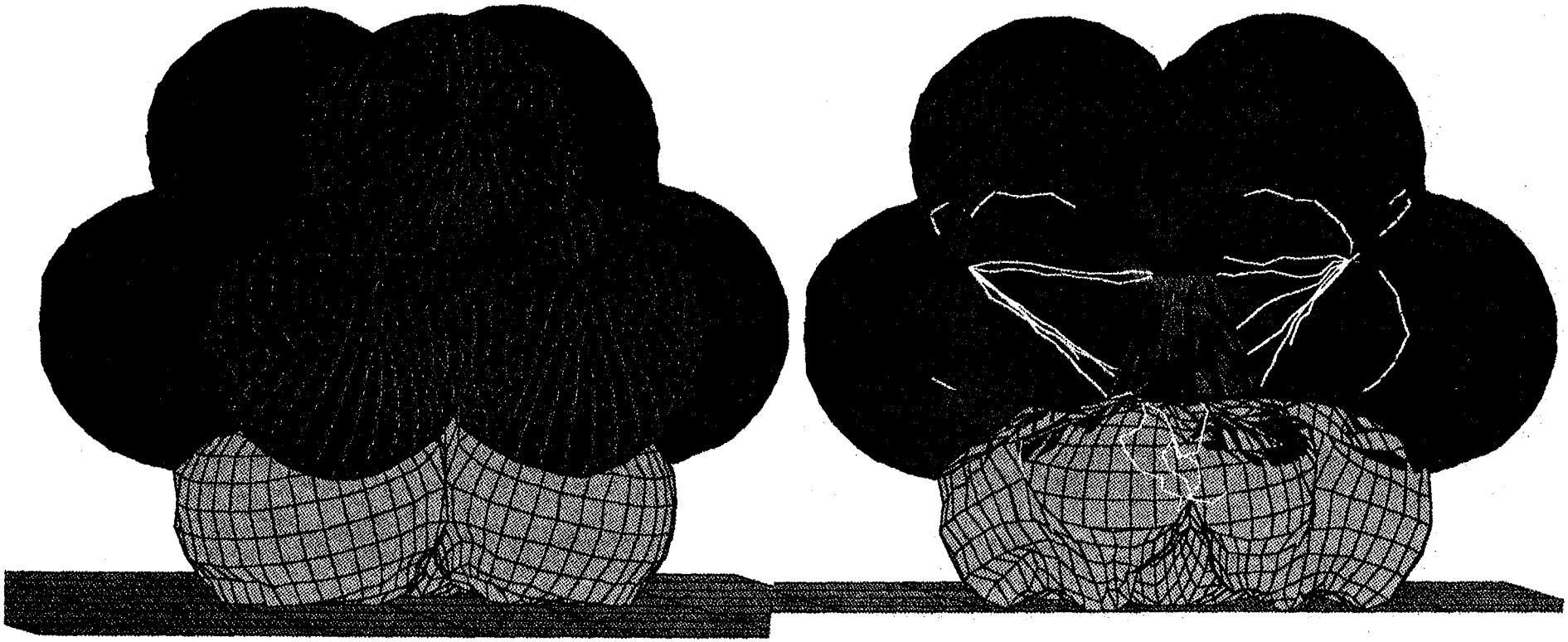

Figure A6. Deformed Mesh at 187.5 msec Into Impact 1

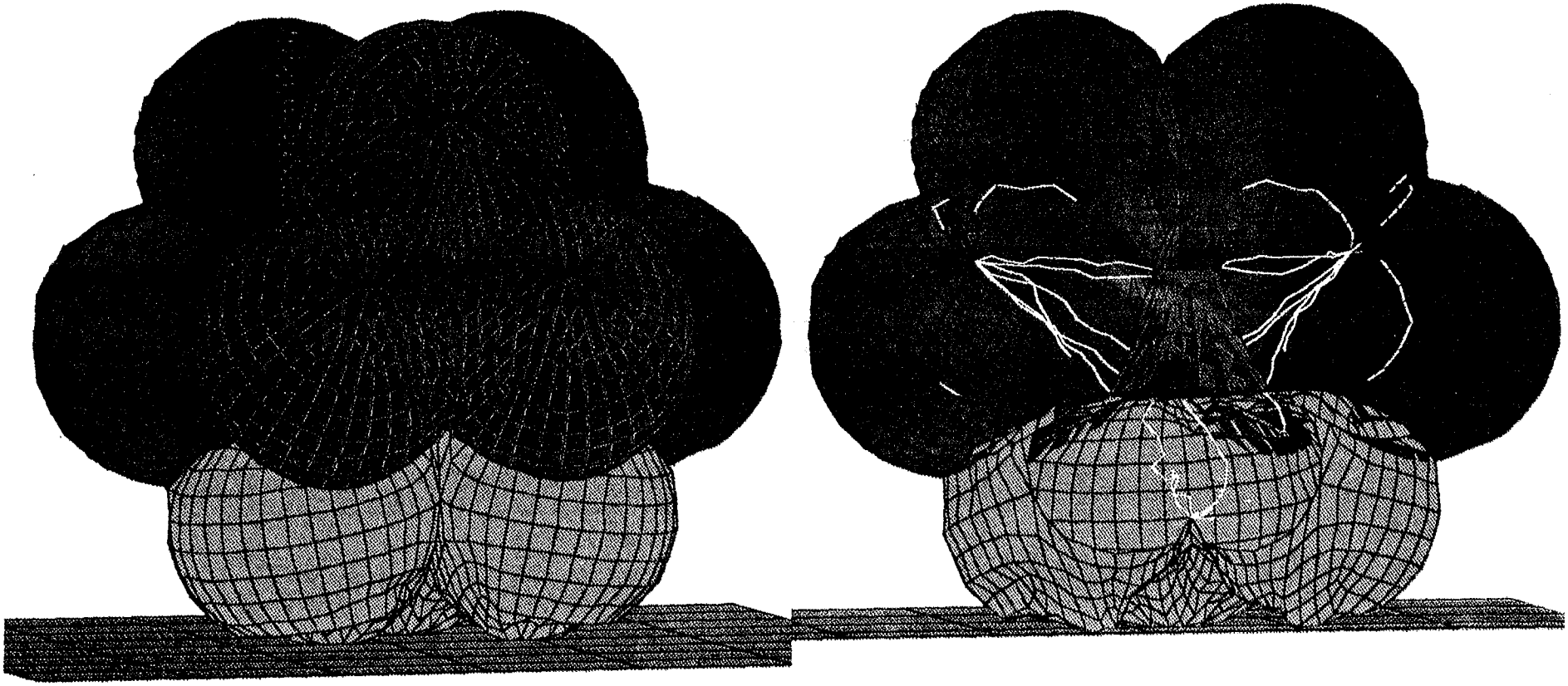

Figure A7. Deformed Mesh at 225 msec Into Impact 1

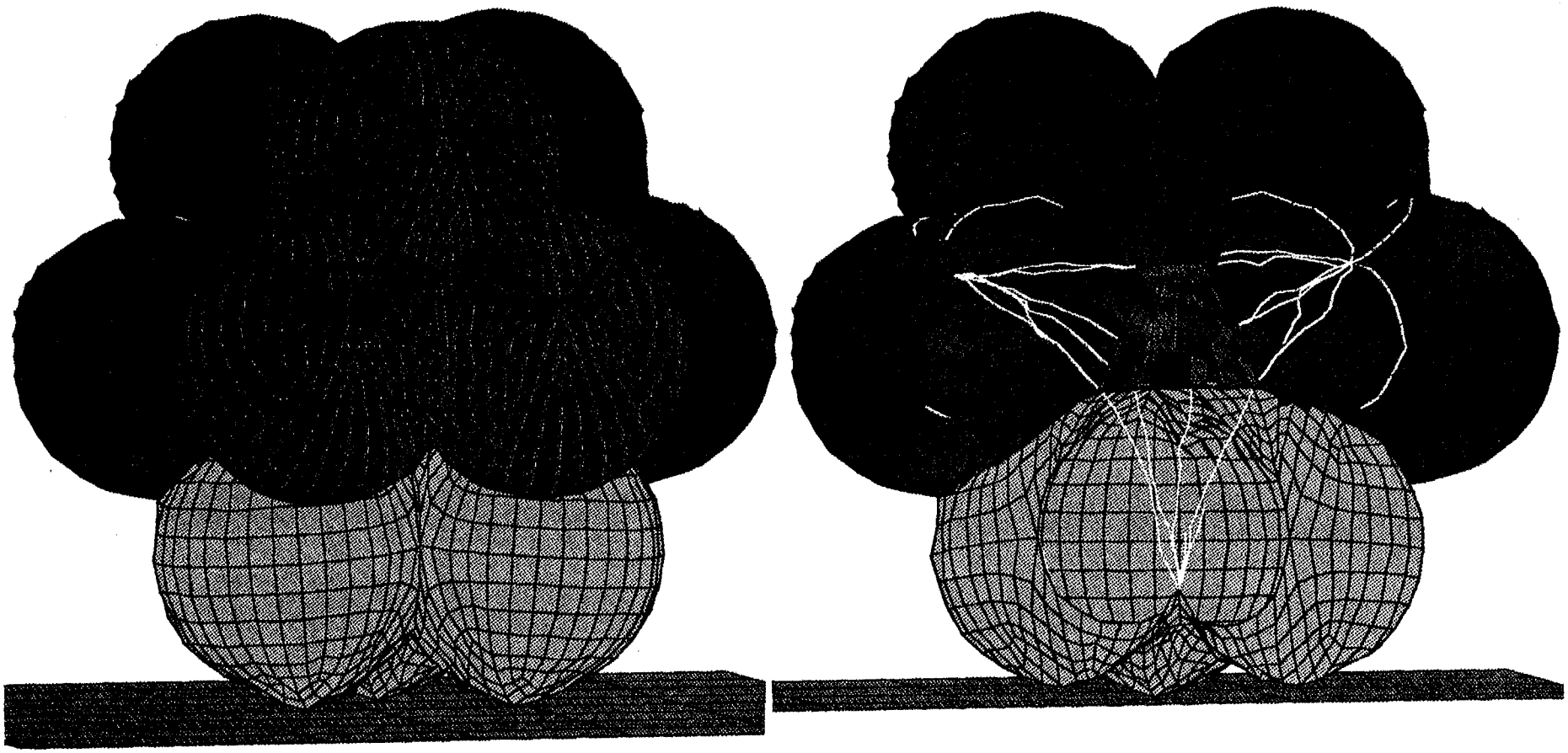

Figure A8. Deformed Mesh at 262.5 msec Into Impact 1

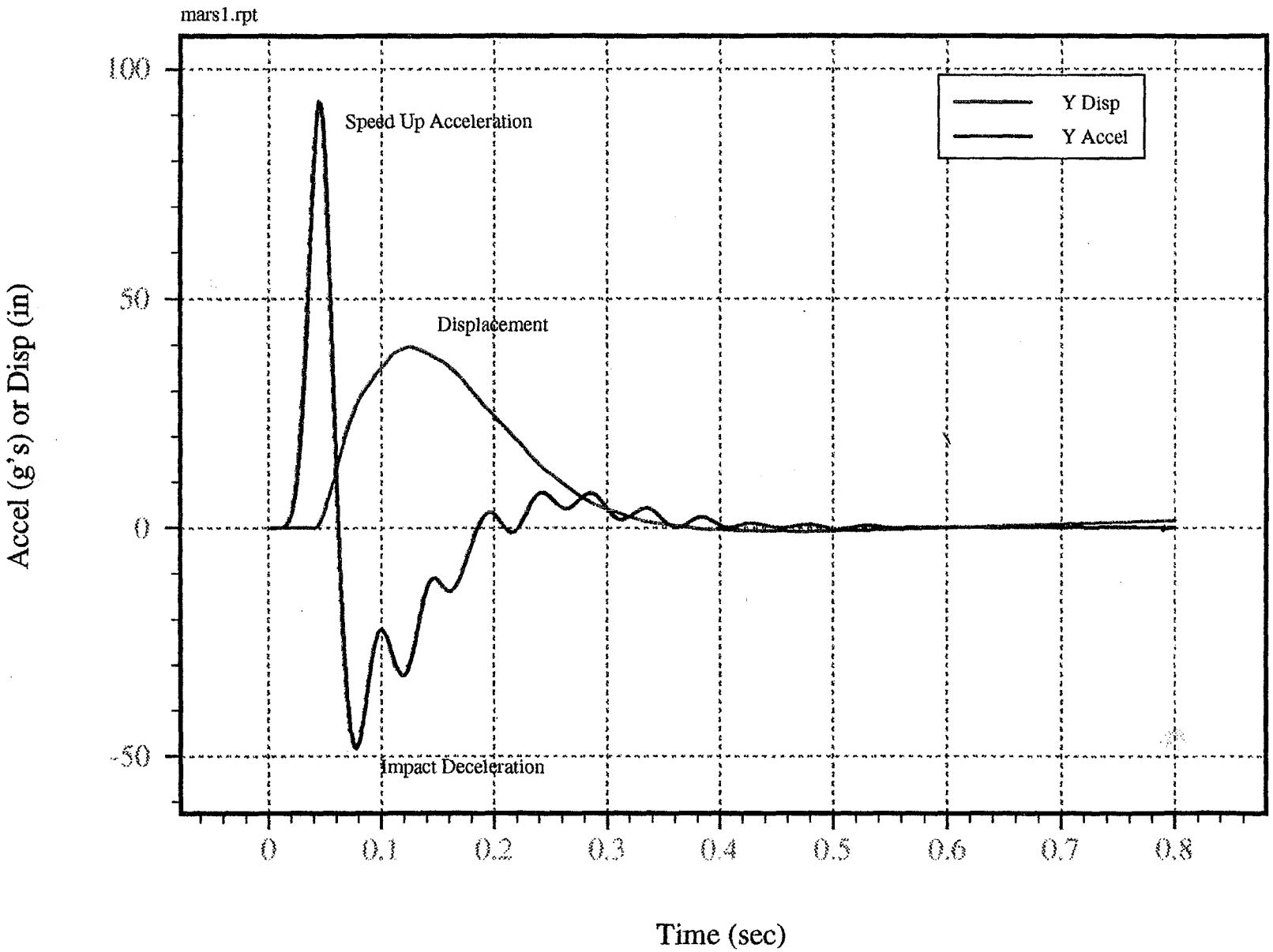

Figure A9. Lander C.G. Acceleration Time-History for Impact 1

MARS1, Normal Impact, Smooth Surface

LINE	VARIABLE	SCALE FACTOR
1	lander x vel	+1.00E+00
2	lander y vel	+1.00E+00
3	lander z vel	+1.00E+00

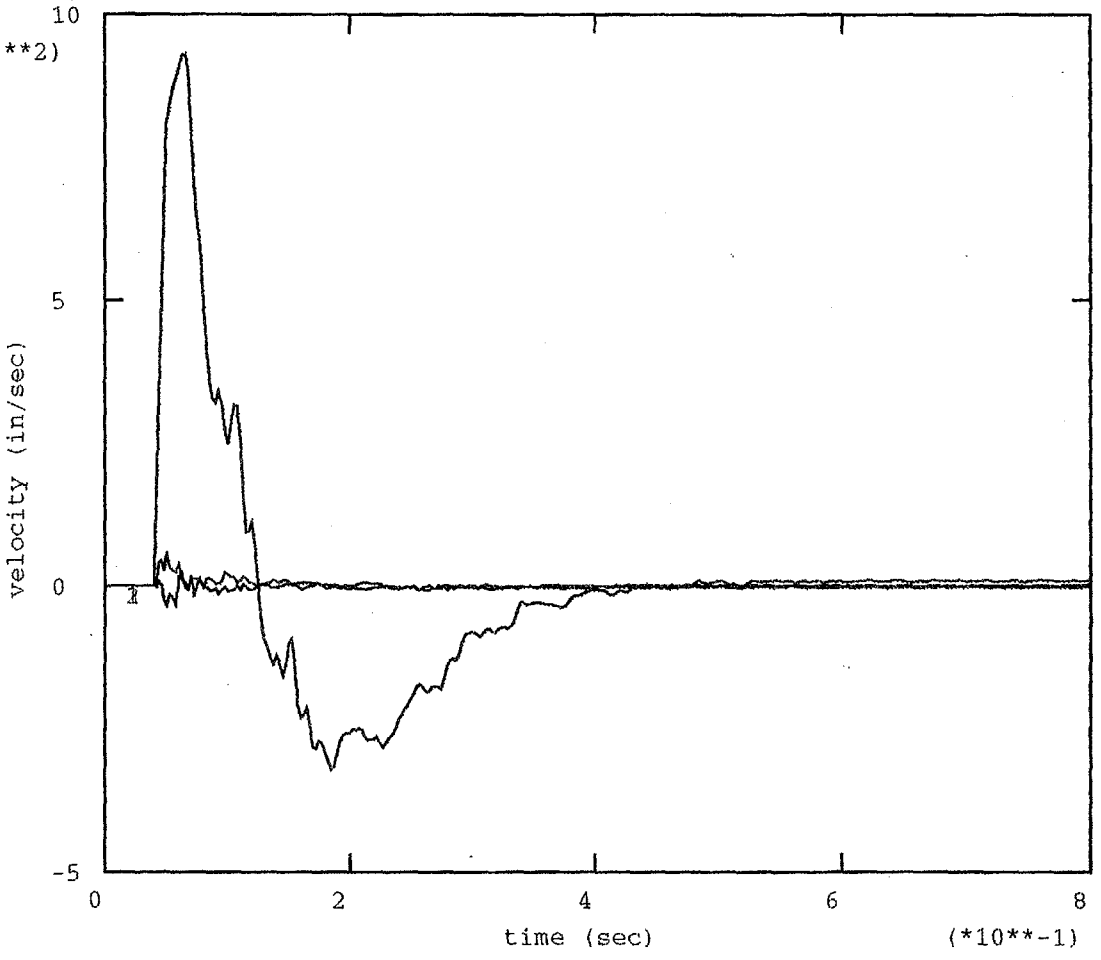

Figure A10. Lander C.G. Velocity Time-History for Impact 1

MARS1, Normal Impact, Smooth Surface

LINE	VARIABLE	SCALE FACTOR
1	lander x rot	+1.00E+00
2	lander y rot	+1.00E+00
3	lander z rot	+1.00E+00

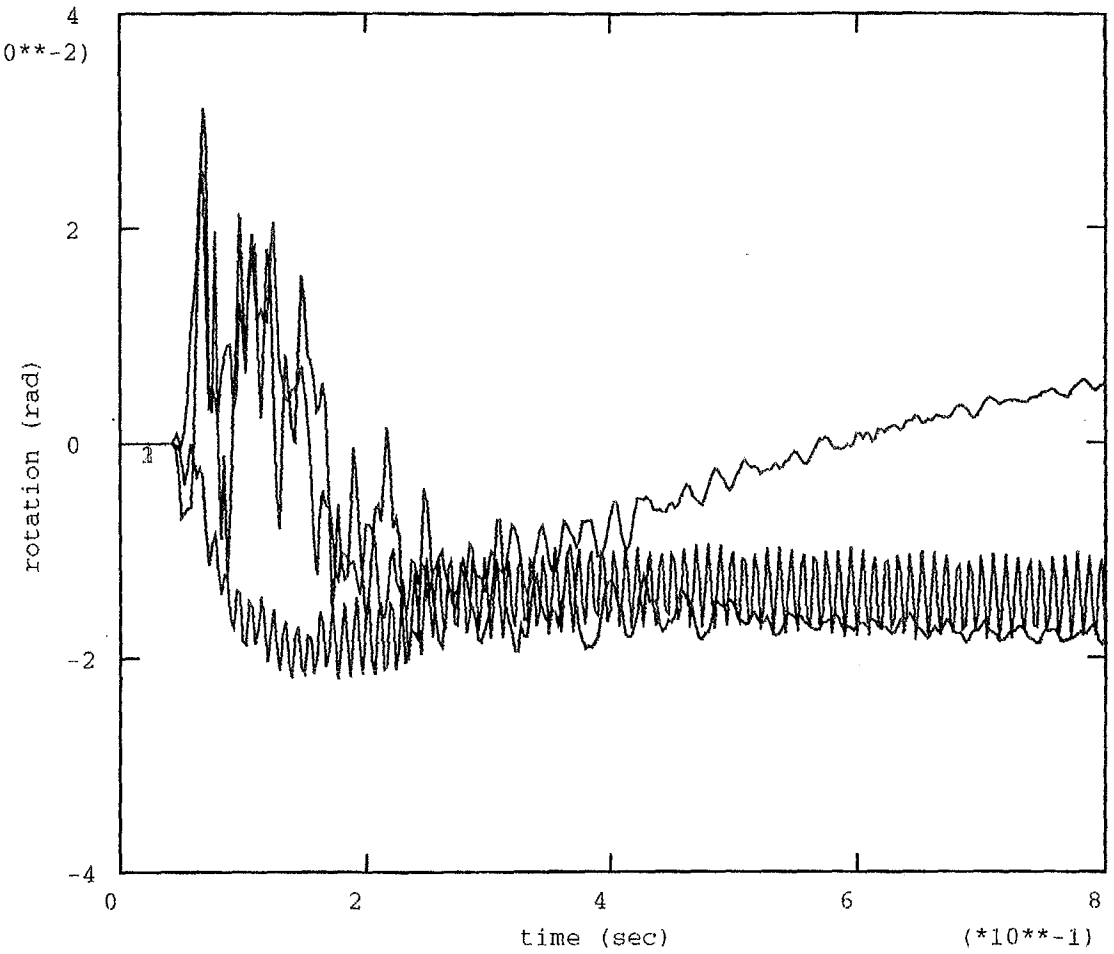

Figure A11. Lander C.G. RotationTime-History for Impact 1

MARS1, Normal Impact, Smooth Surface

LINE	VARIABLE	SCALE FACTOR
1	land x rot vel	+1.00E+00
2	land y rot vel	+1.00E+00
3	land z rot vel	+1.00E+00

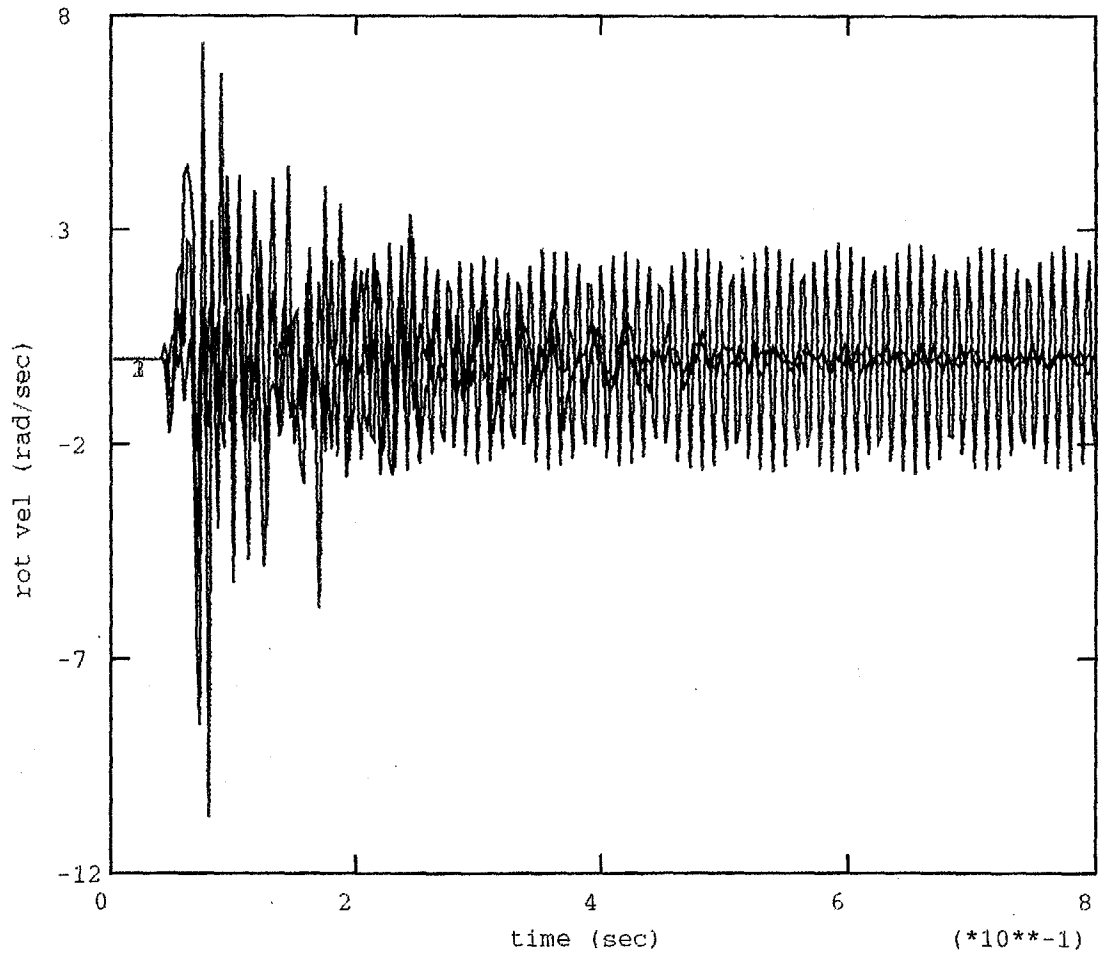

Figure A12. Lander C.G. Rotational Velocity Time-History for Impact 1

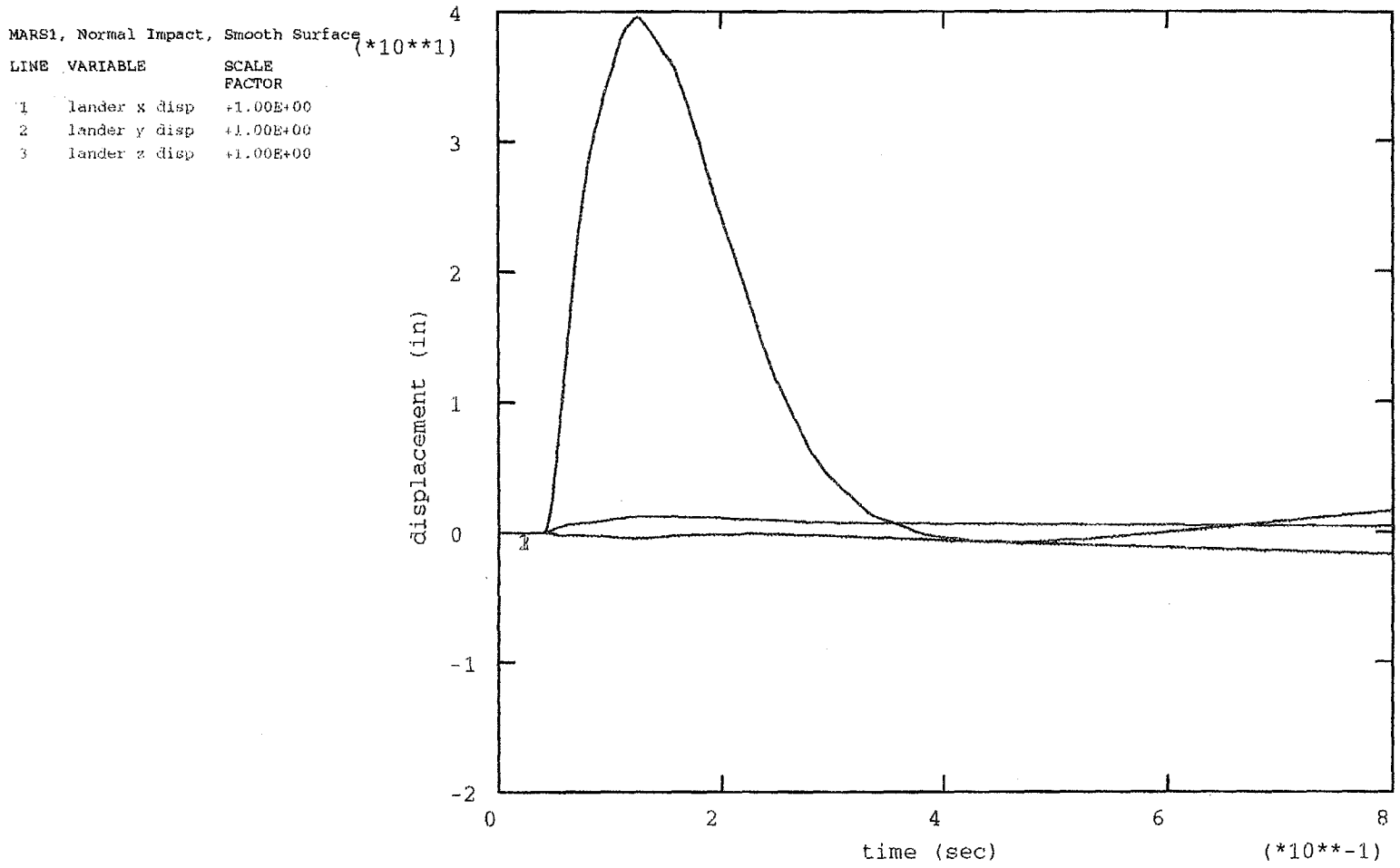

Figure A13. Lander C.G. Displacement Time-History for Impact 1

MARS1, Normal Impact, Smooth Surface

LINE	VARIABLE	SCALE FACTOR
1	bag 1 tendon 1	+1.00E-01
2	bag 1 tendon 2	+1.00E-01
3	bag 1 tendon 4	+1.00E-01
4	bag 1 tendon 5	+1.00E-01
5	bag 1 tendon 6	+1.00E-01

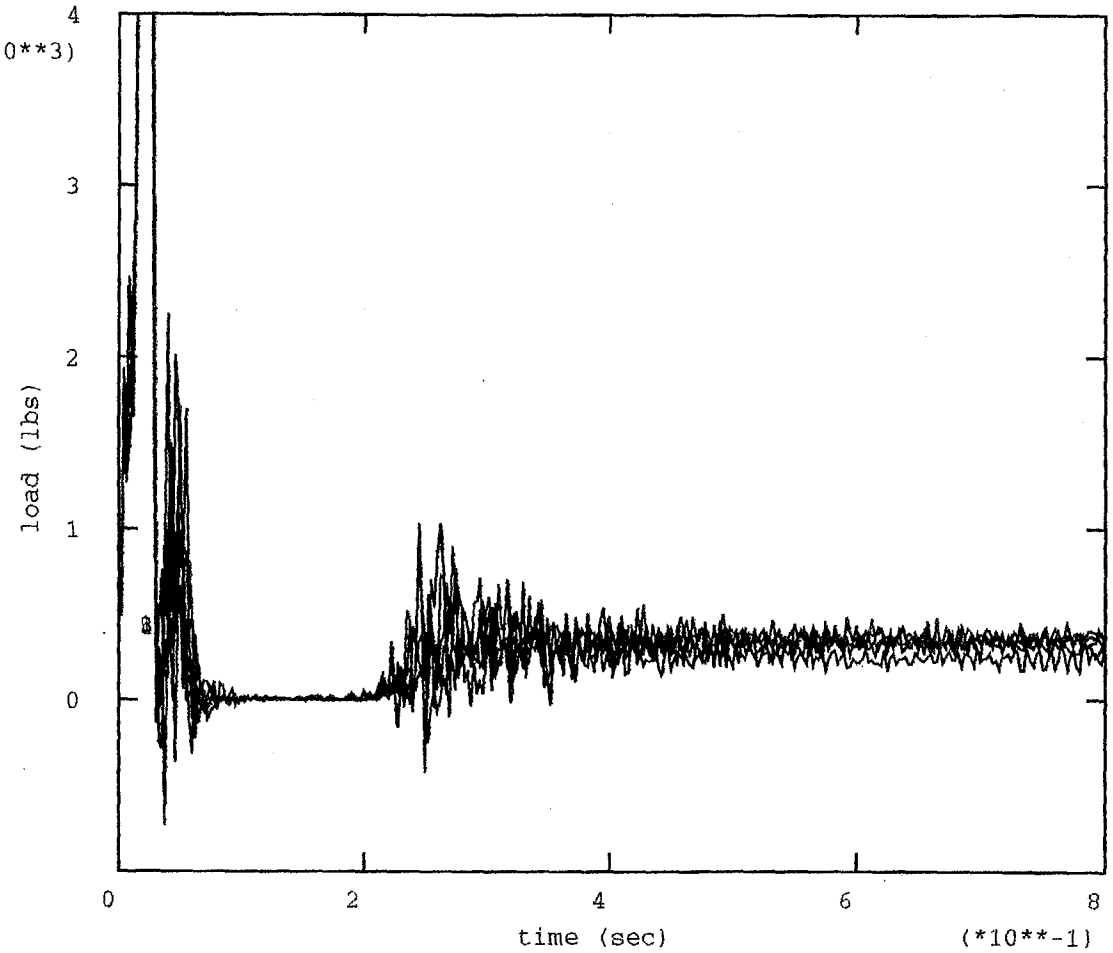

Figure A14. Bag 1 Tendon Force Time-History for Impact 1

MARS1, Normal Impact, Smooth Surface

LINE	VARIABLE	SCALE FACTOR
1	bag 2 tendon 1	+1.00E-01
2	bag 2 tendon 2	+1.00E-01
3	bag 2 tendon 3	+1.00E-01
4	bag 2 tendon 4	+1.00E-01
5	bag 2 tendon 5	+1.00E-01
6	bag 2 tendon 6	+1.00E-01

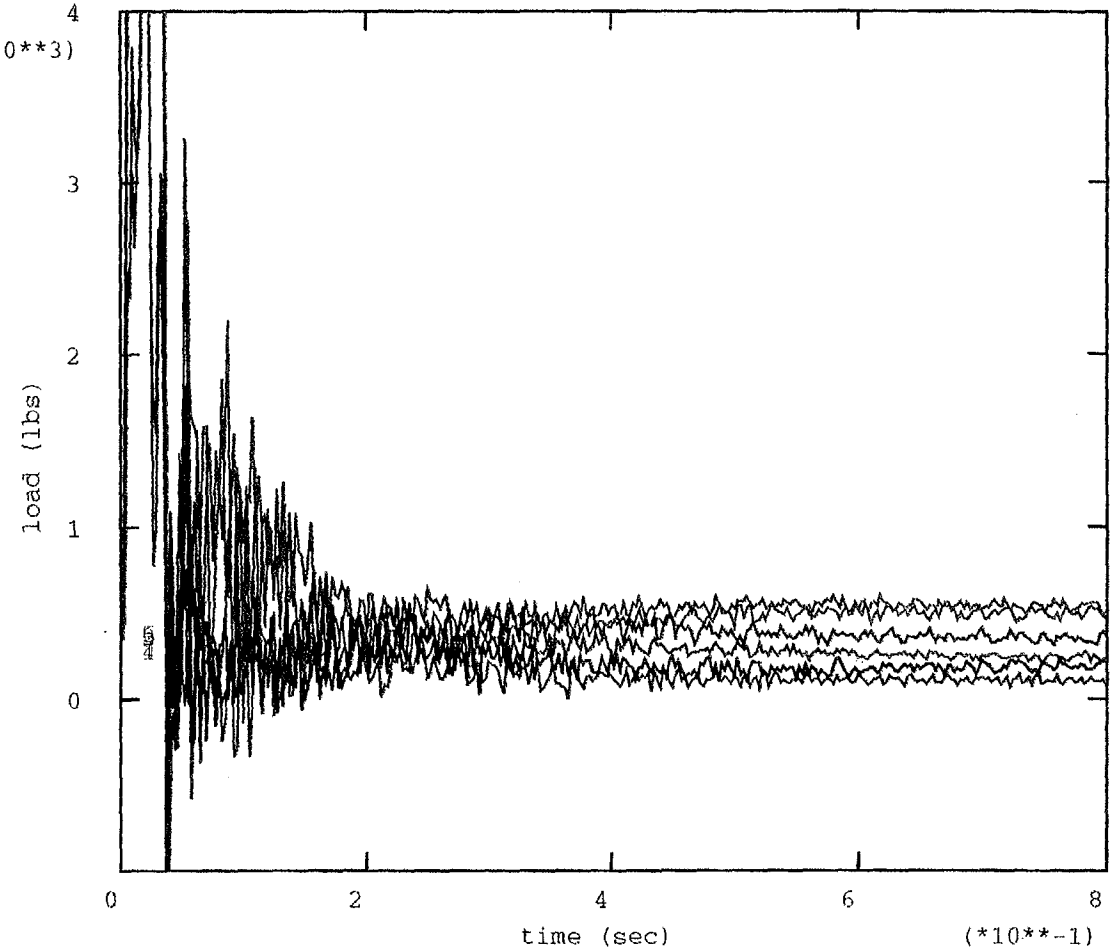

Figure A15. Bag 2 Tendon Force Time-History for Impact 1

MARS1, Normal Impact, Smooth Surface

LINE	VARIABLE	SCALE FACTOR
1	bag 3 tendon 1	+1.00E-01
2	bag 3 tendon 2	+1.00E-01
3	bag 3 tendon 3	+1.00E-01
4	bag 3 tendon 4	+1.00E-01
5	bag 3 tendon 5	+1.00E-01
6	bag 3 tendon 6	+1.00E-01

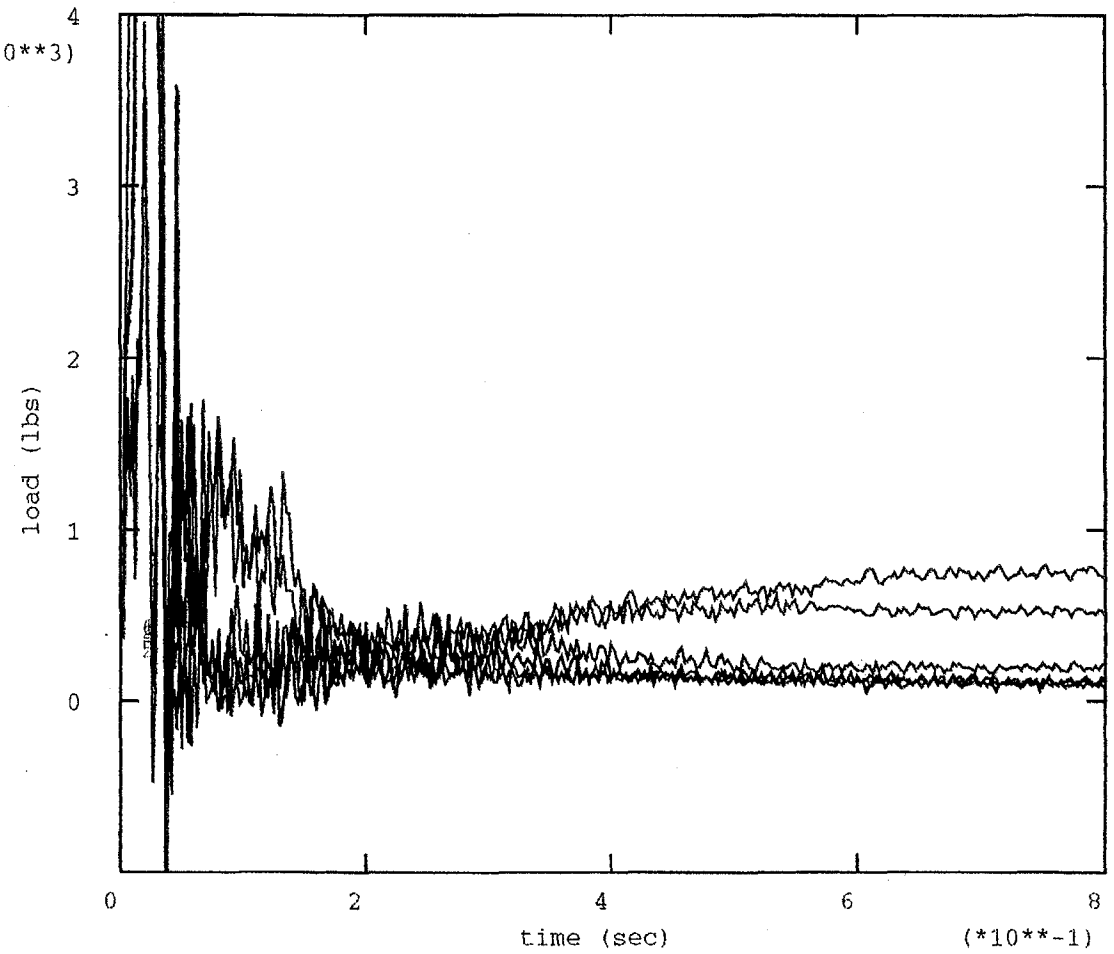

Figure A16. Bag 3 Tendon Force Time-History for Impact 1

MARS1, Normal Impact, Smooth Surface

LINE	VARIABLE	SCALE FACTOR
1	bag 4 tendon 1	+1.00E-01
2	bag 4 tendon 2	+1.00E-01
3	bag 4 tendon 3	+1.00E-01
4	bag 4 tendon 4	+1.00E-01
5	bag 4 tendon 5	+1.00E-01
6	bag 4 tendon 6	+1.00E-01

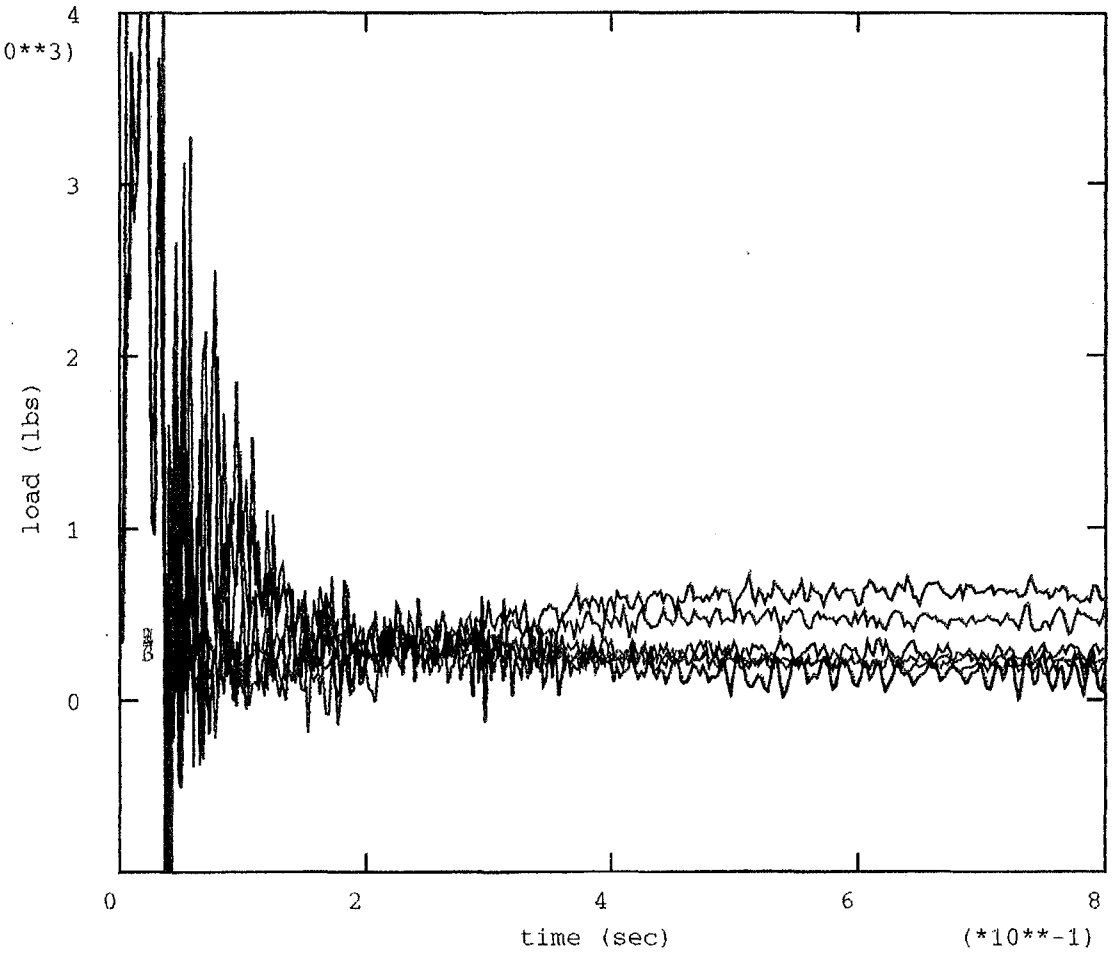

Figure A17. Bag 4 Tendon Force Time-History for Impact 1

MARS1, Normal Impact, Smooth Surface

LINE	VARIABLE	SCALE FACTOR
1	2-4 in-line	+2.47E+00
2	2-4 norm	+1.58E+00
3	2-3 in-line	+2.47E+00
4	2-3 norm	+1.58E+00
5	3-4 in-line	+2.47E+00
6	3-4 norm	+1.58E+00

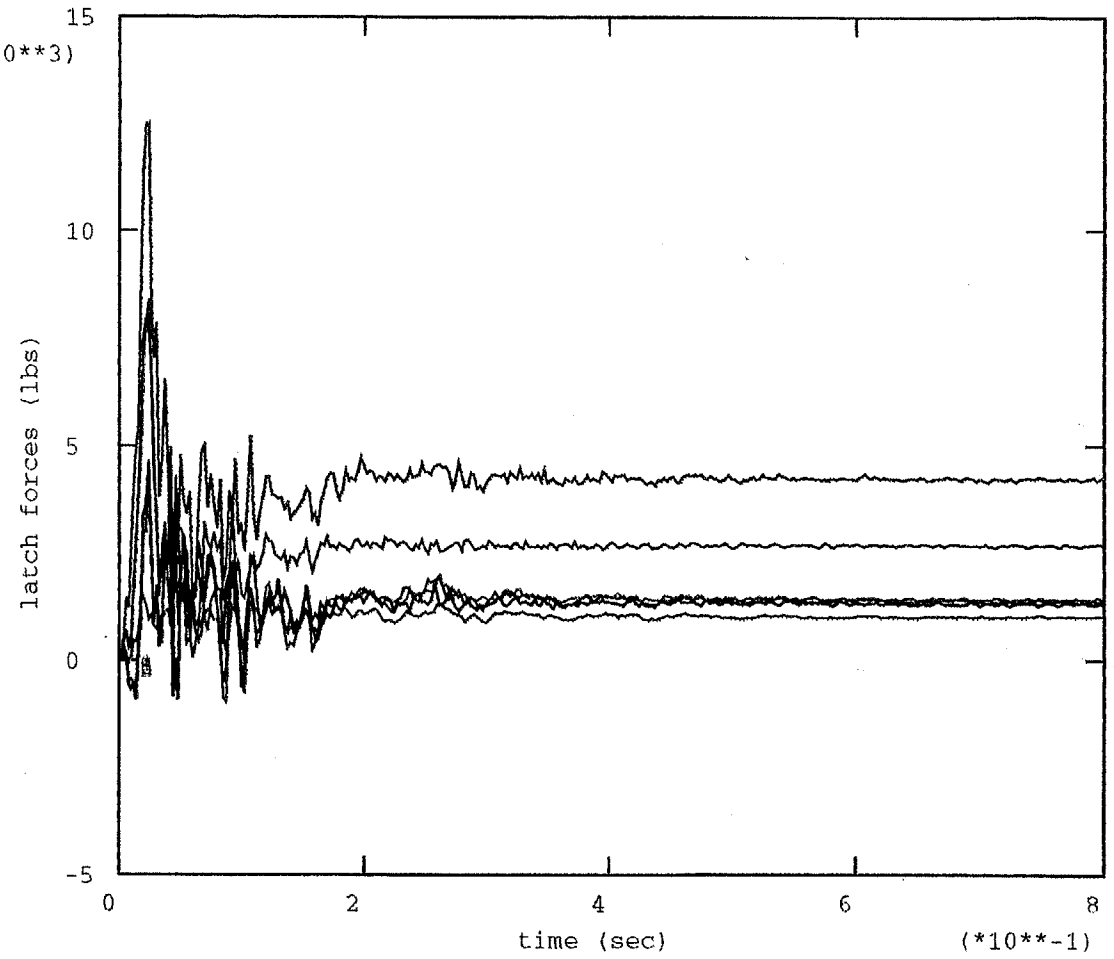

Figure A18. Latch Force Time-History for Impact 1

MARS1, Normal Impact, Smooth Surface

LINE	VARIABLE	SCALE FACTOR
1	p4 in-line	+2.71E+00
2	p4 norm	+2.38E+00
3	p4 in-line	+2.71E+00
4	p4 norm	+2.23E+00
5	p2 in-line	+2.71E+00
6	p2 norm	+2.23E+00
7	p2 in-line	+2.71E+00
8	p2 norm	+2.07E+00
9	p3 norm	+3.05E+00
10	p3 norm	+3.05E+00
11	p3 in-line	+2.07E+00
12	p3 norm	+3.05E+00

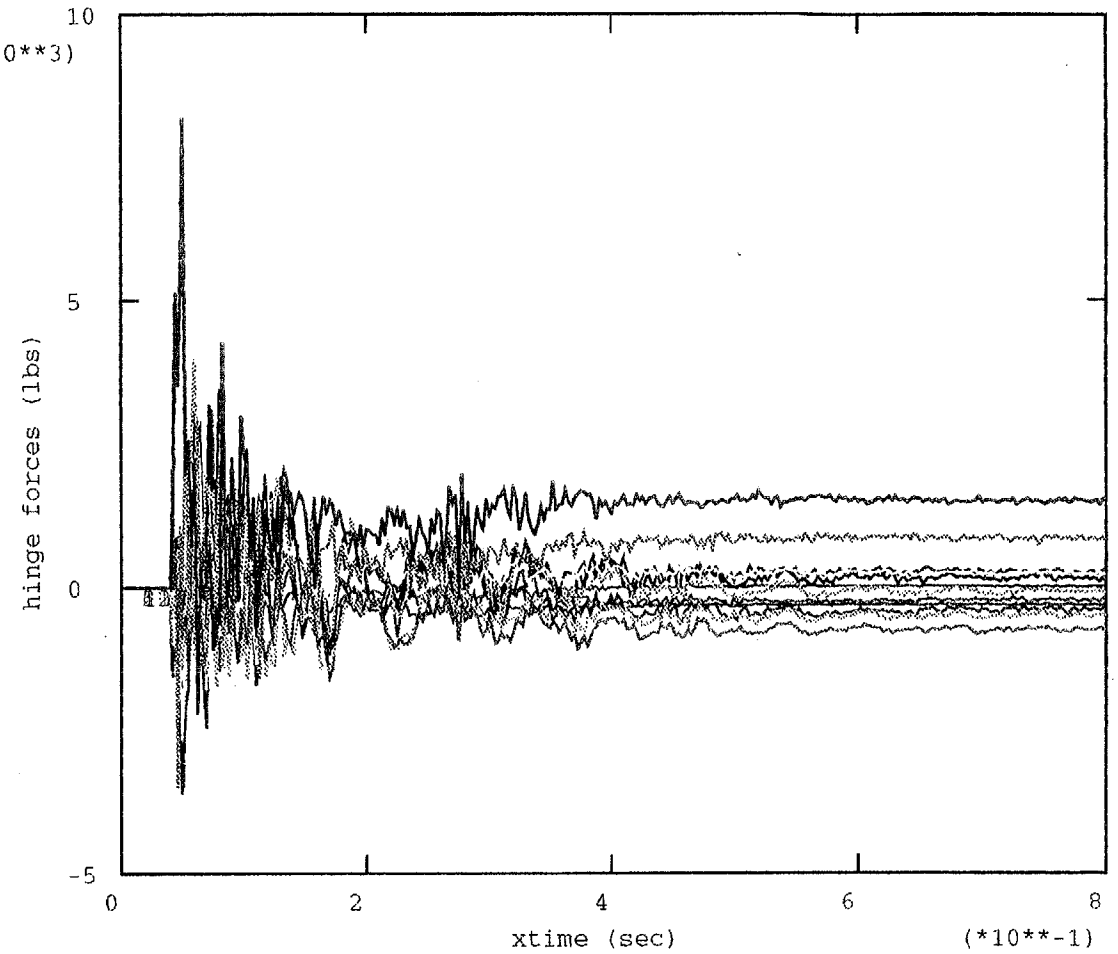

Figure A19. Hinge Force Time-History for Impact 1

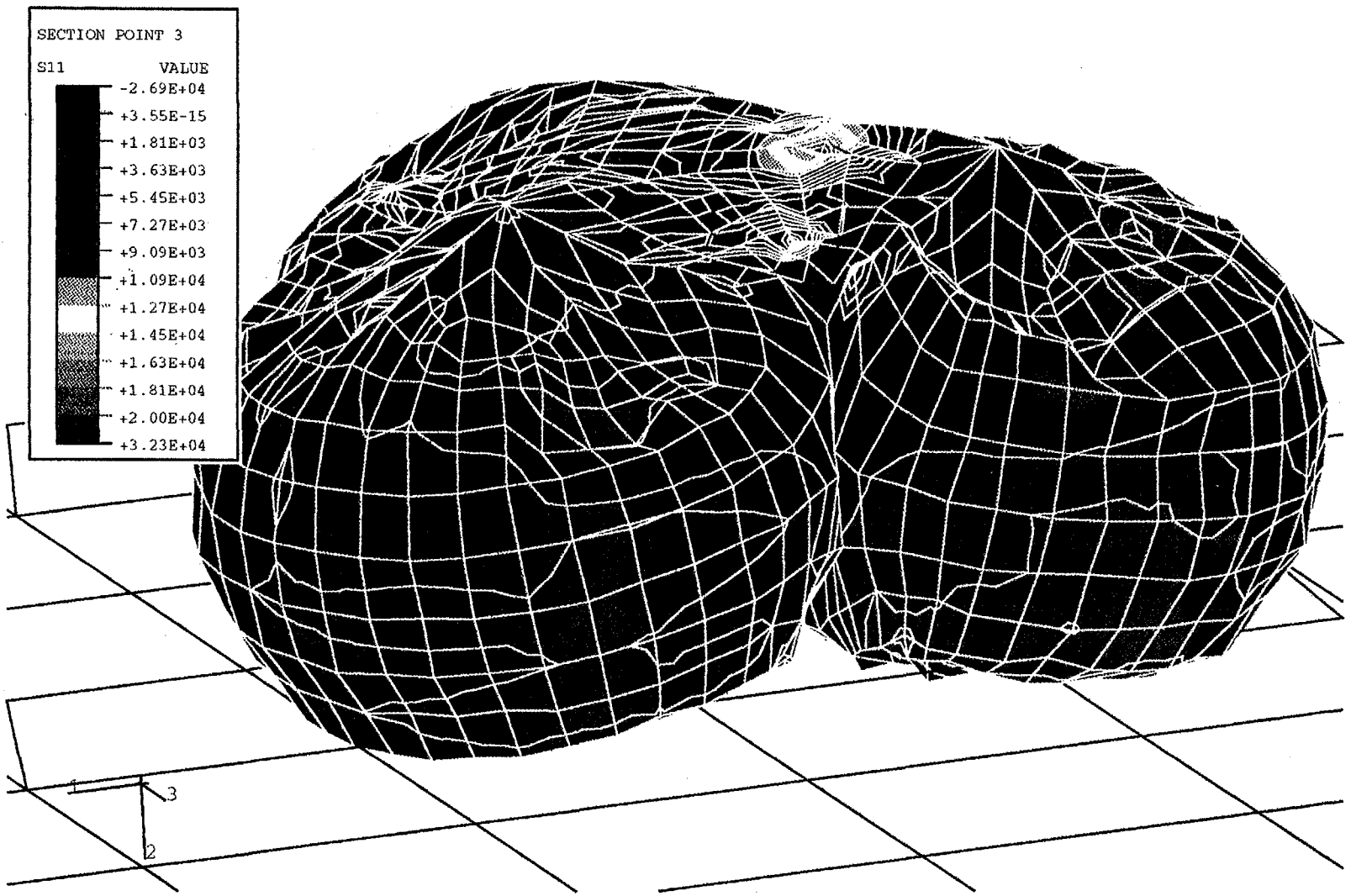

Figure A20. Maximum Principal Stress Distribution Example for Impact 1

Appendix B

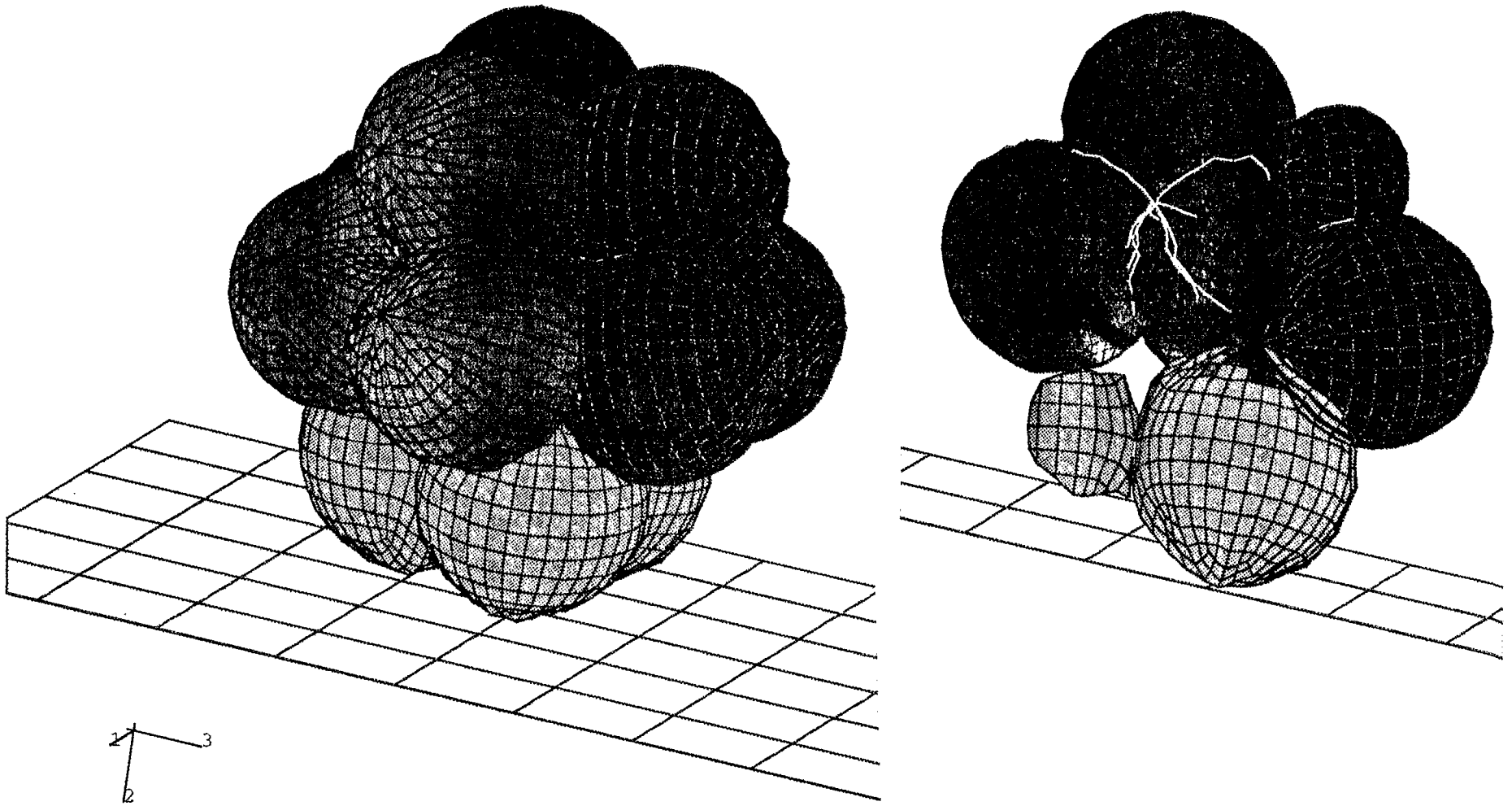

Figure B1. Deformed Mesh at 0 msec Into Impact 2

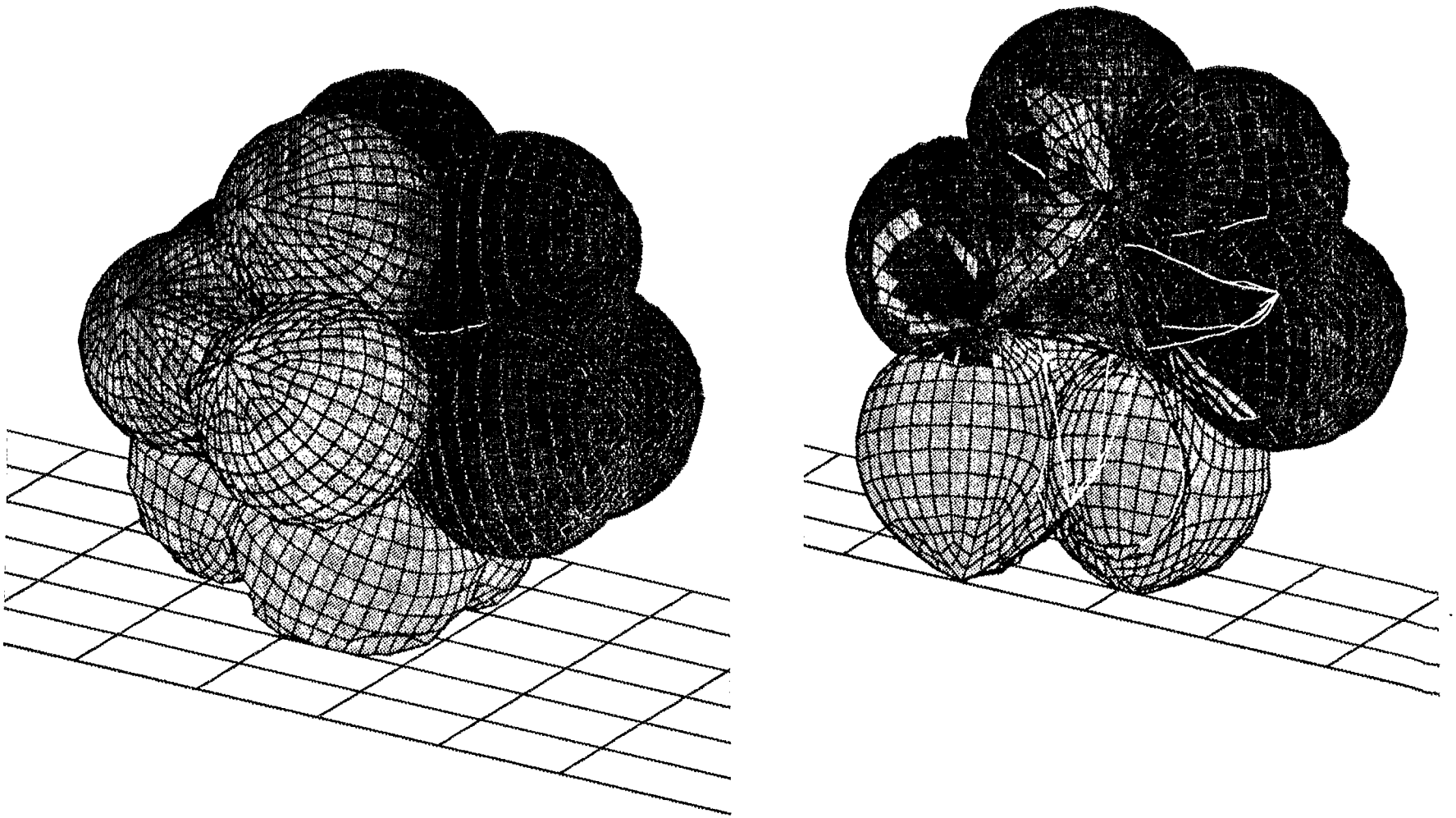

Figure B2. Deformed Mesh at 37.5 msec Into Impact 2

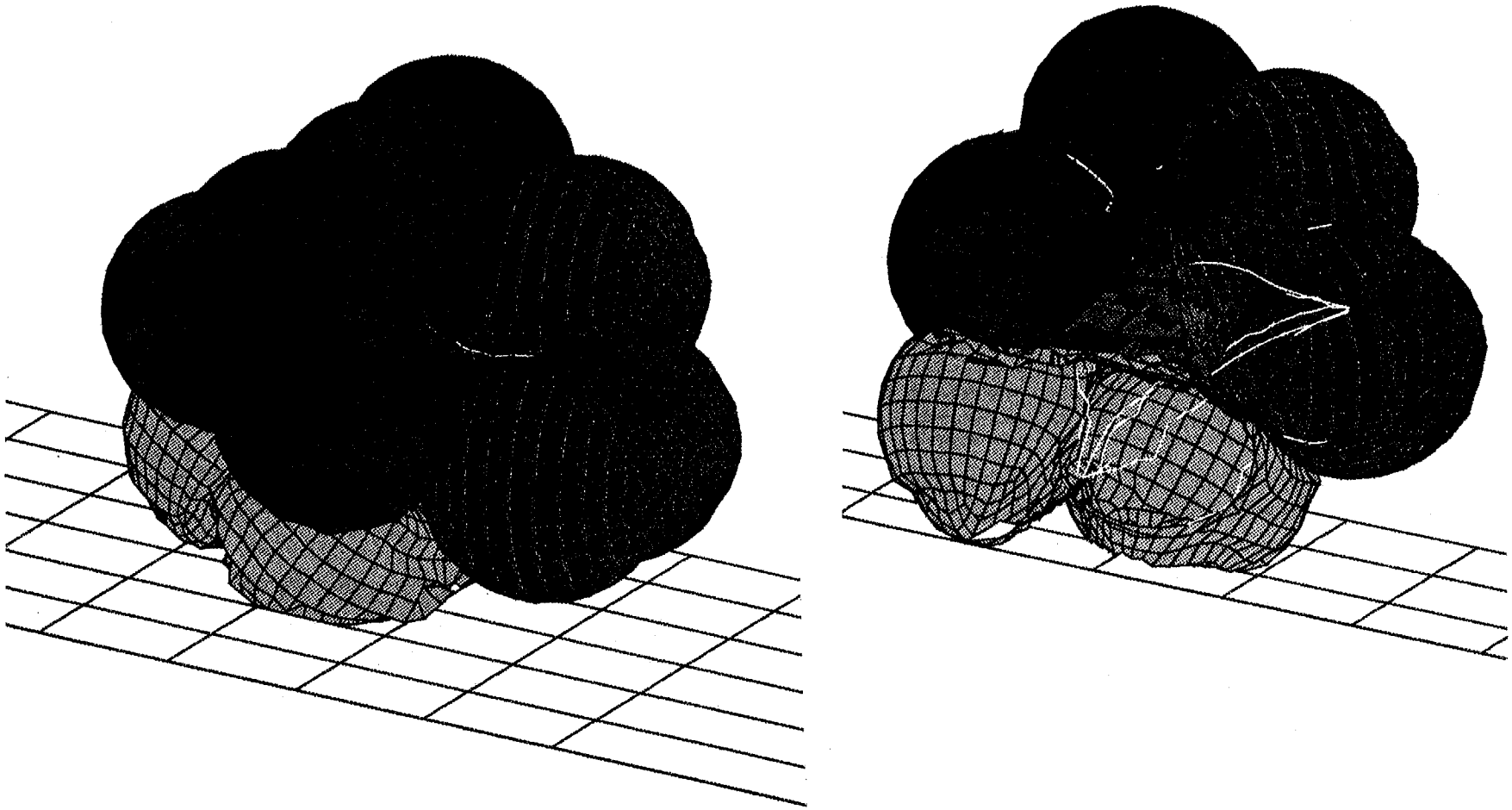

Figure B3. Deformed Mesh at 75 msec Into Impact 2

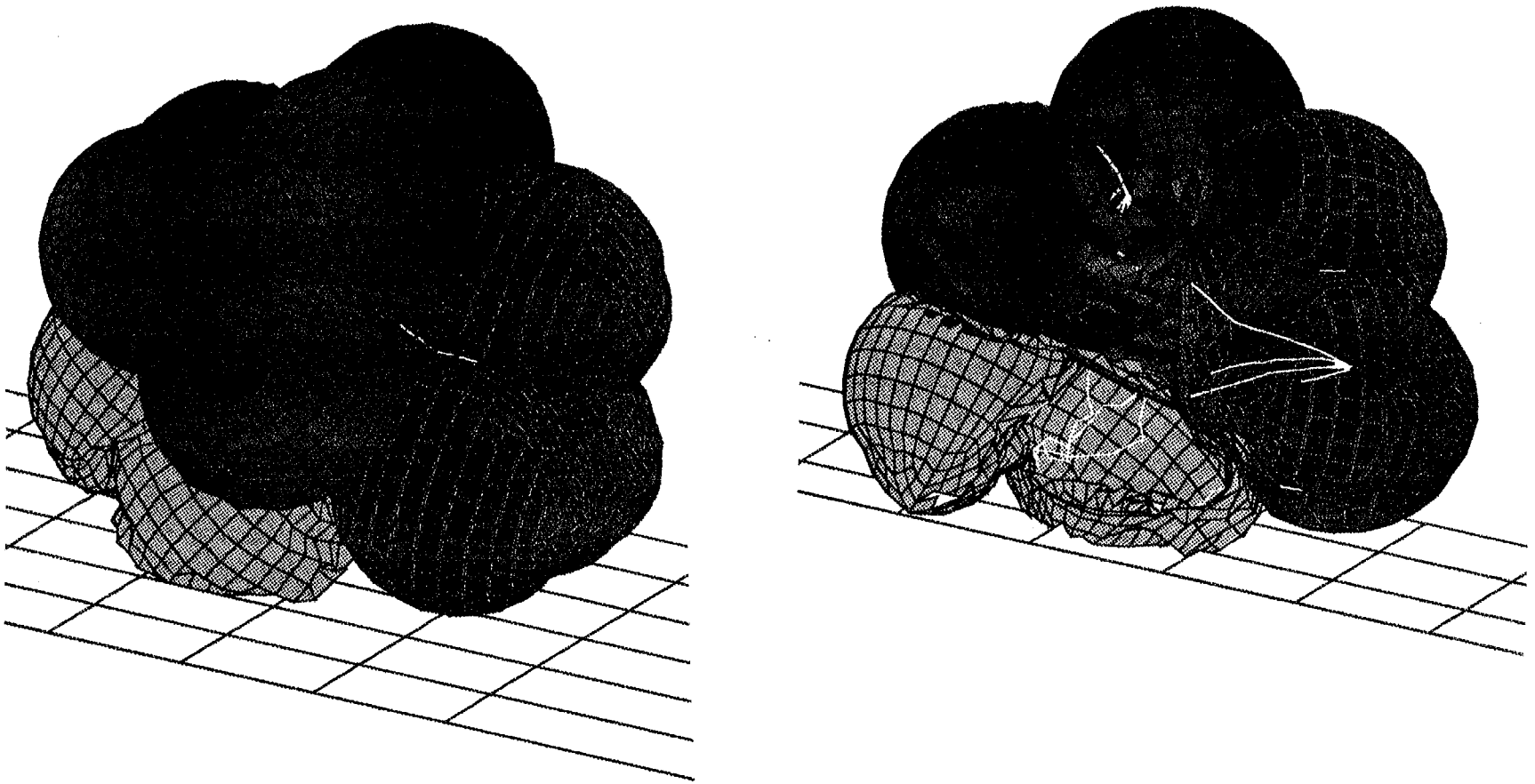

Figure B4. Deformed Mesh at 112.5 msec Into Impact 2

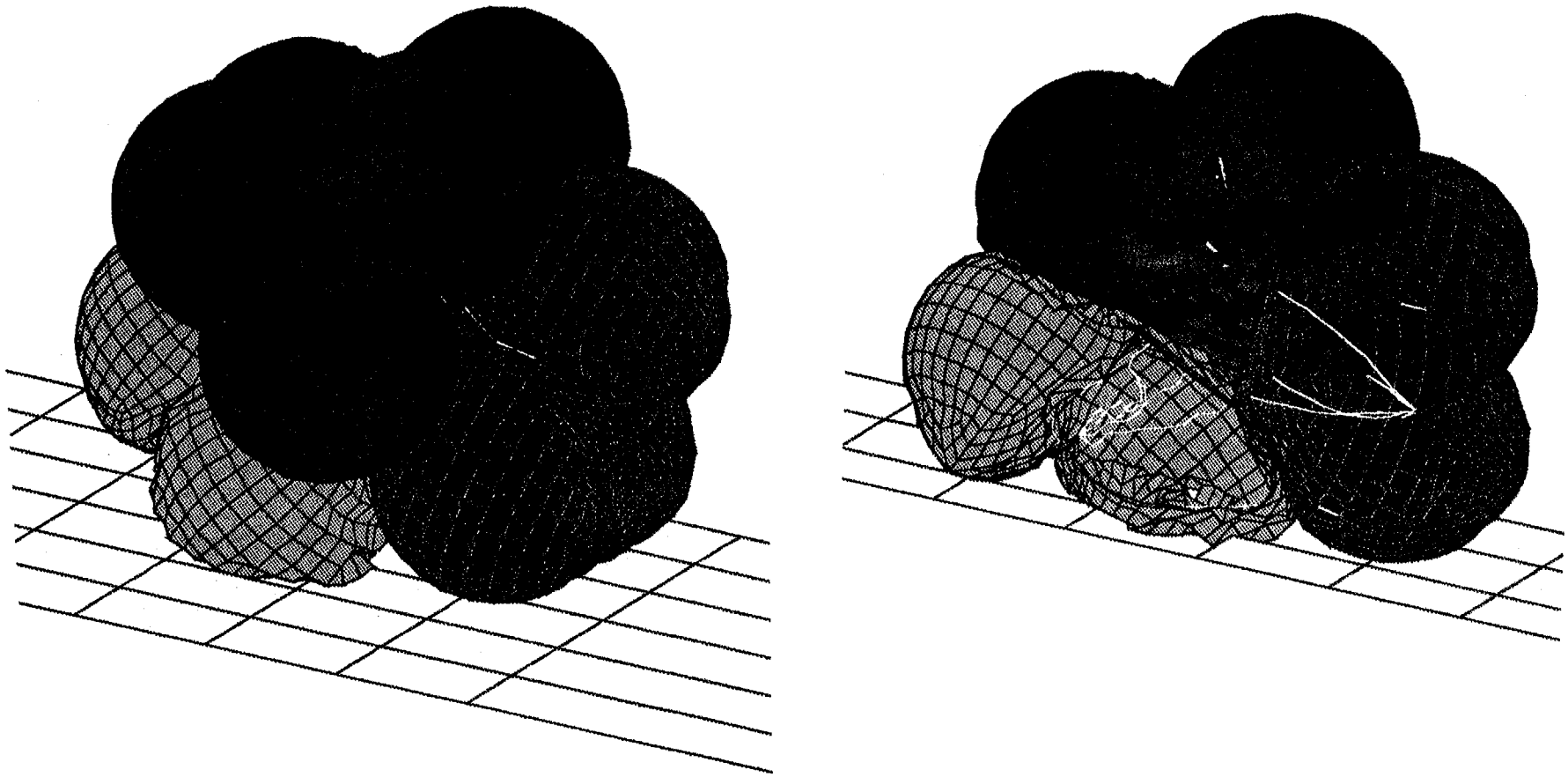

Figure B5. Deformed Mesh at 150 msec Into Impact 2

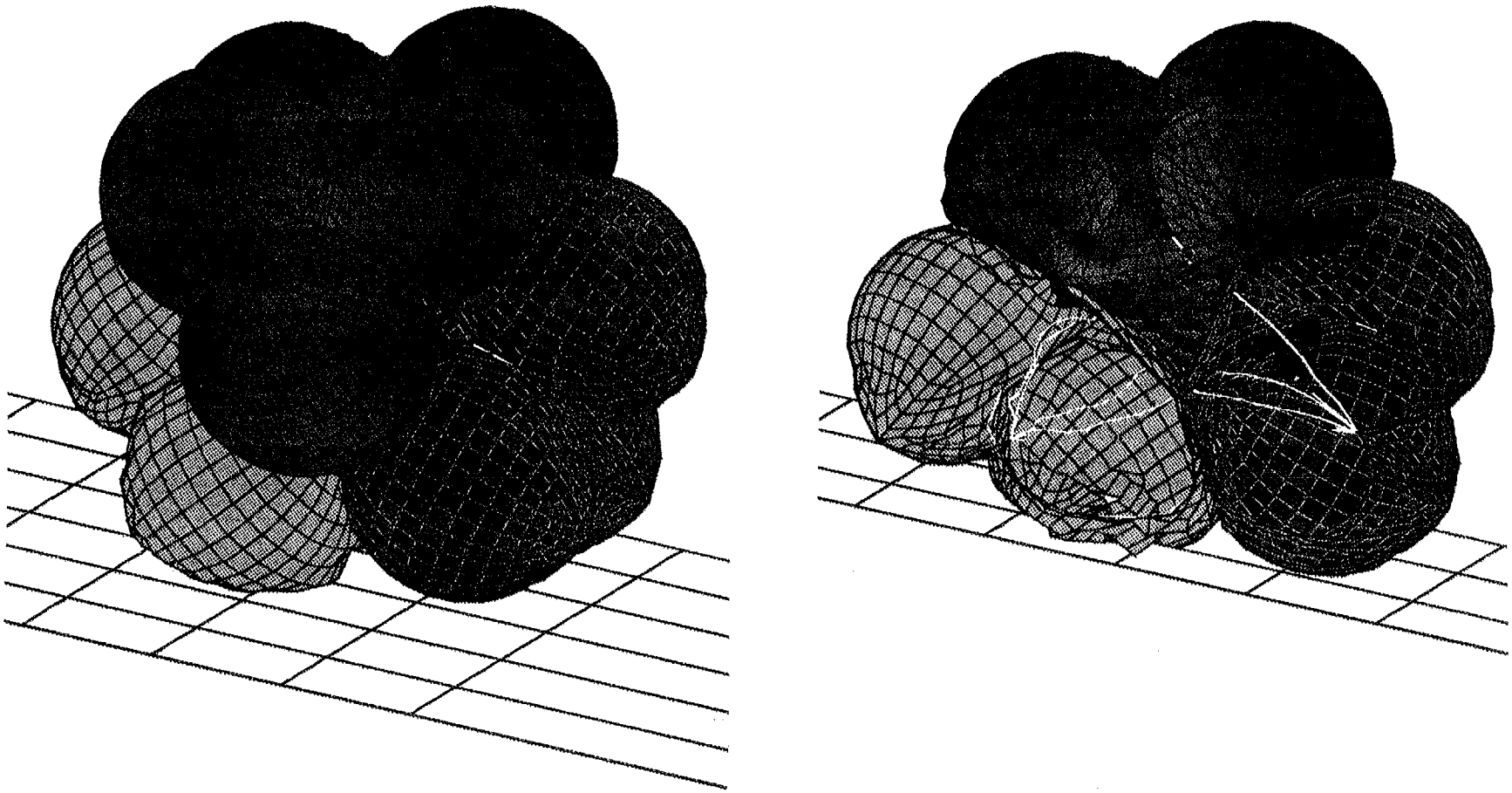

FiBure B6. Deformed Mesh at 187.5 msec Into Impact 2

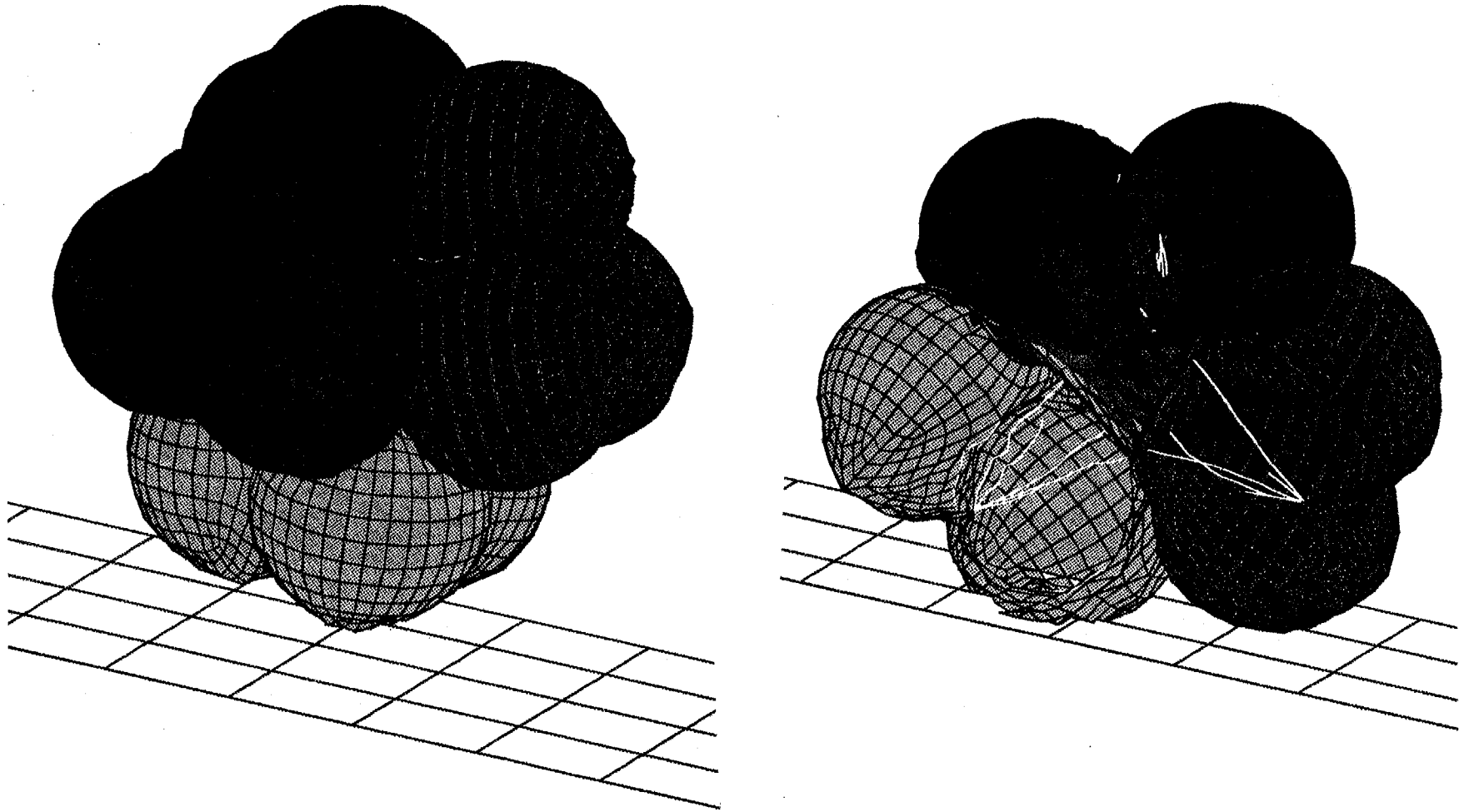

Figure B7. Deformed Mesh at 225 msec Into Impact 2

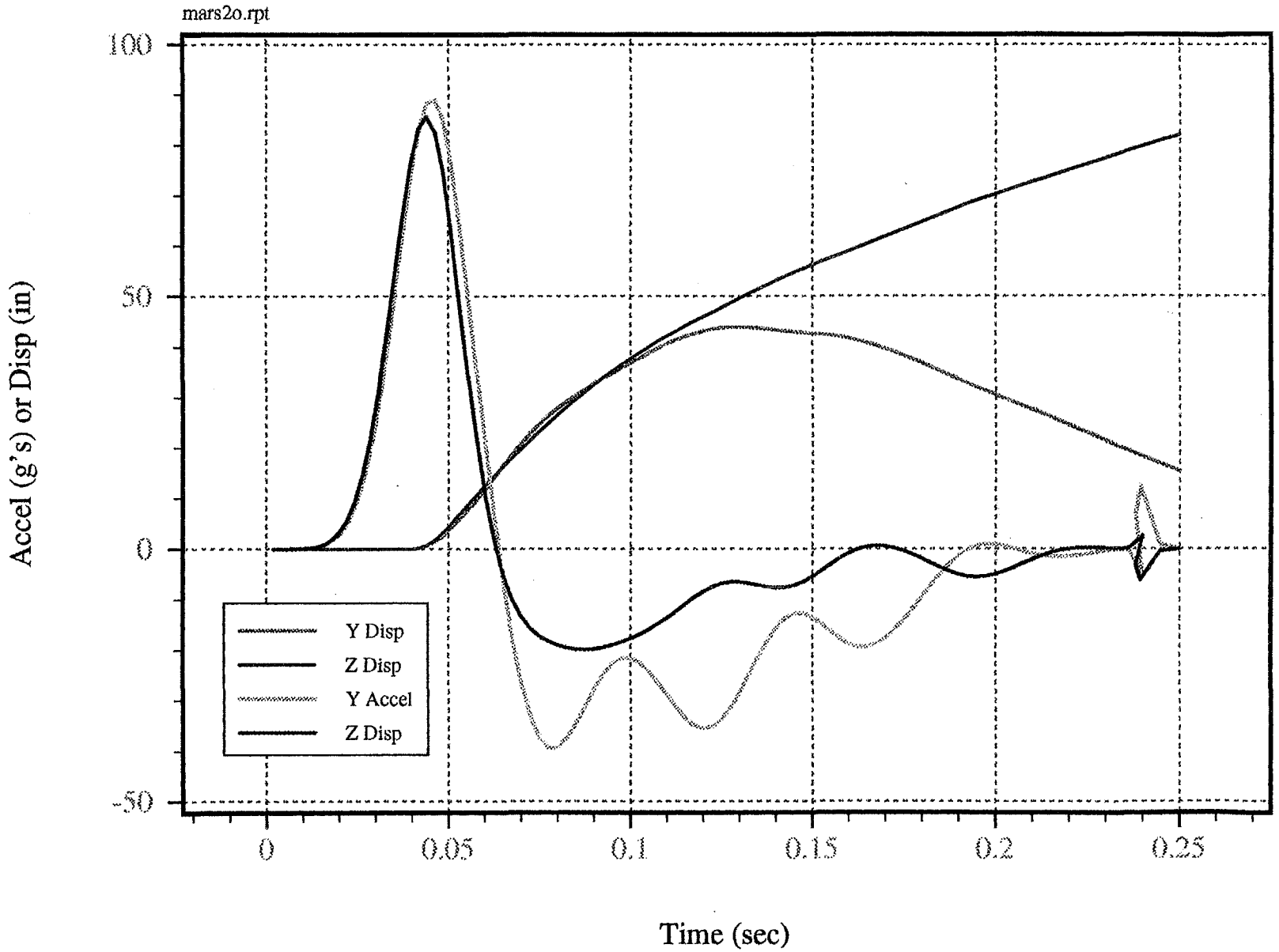

Figure B8. Lander C.G. Acceleration Time-History for Impact 2

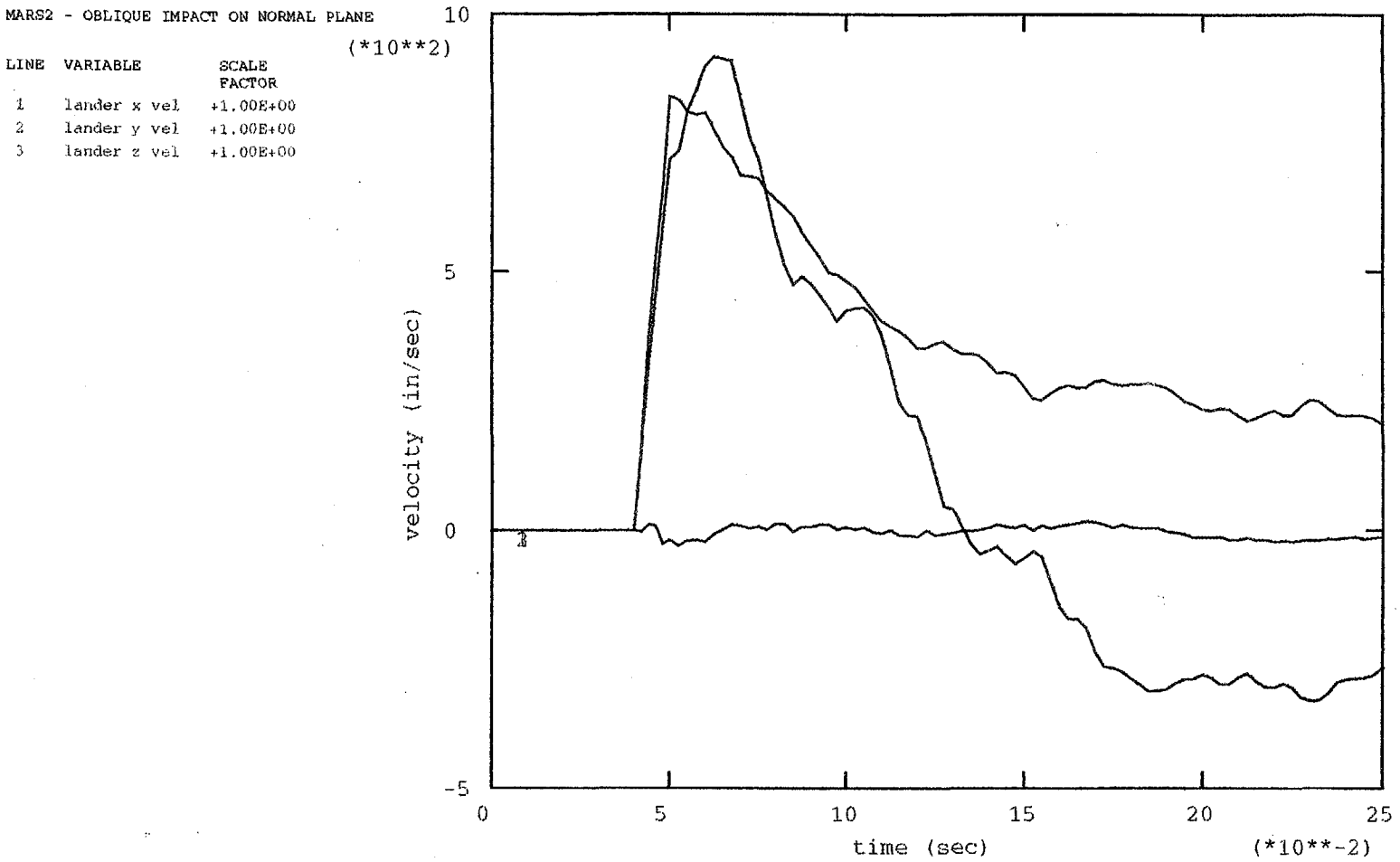

Figure B9. Lander C.G. Velocity Time-History for Impact 2

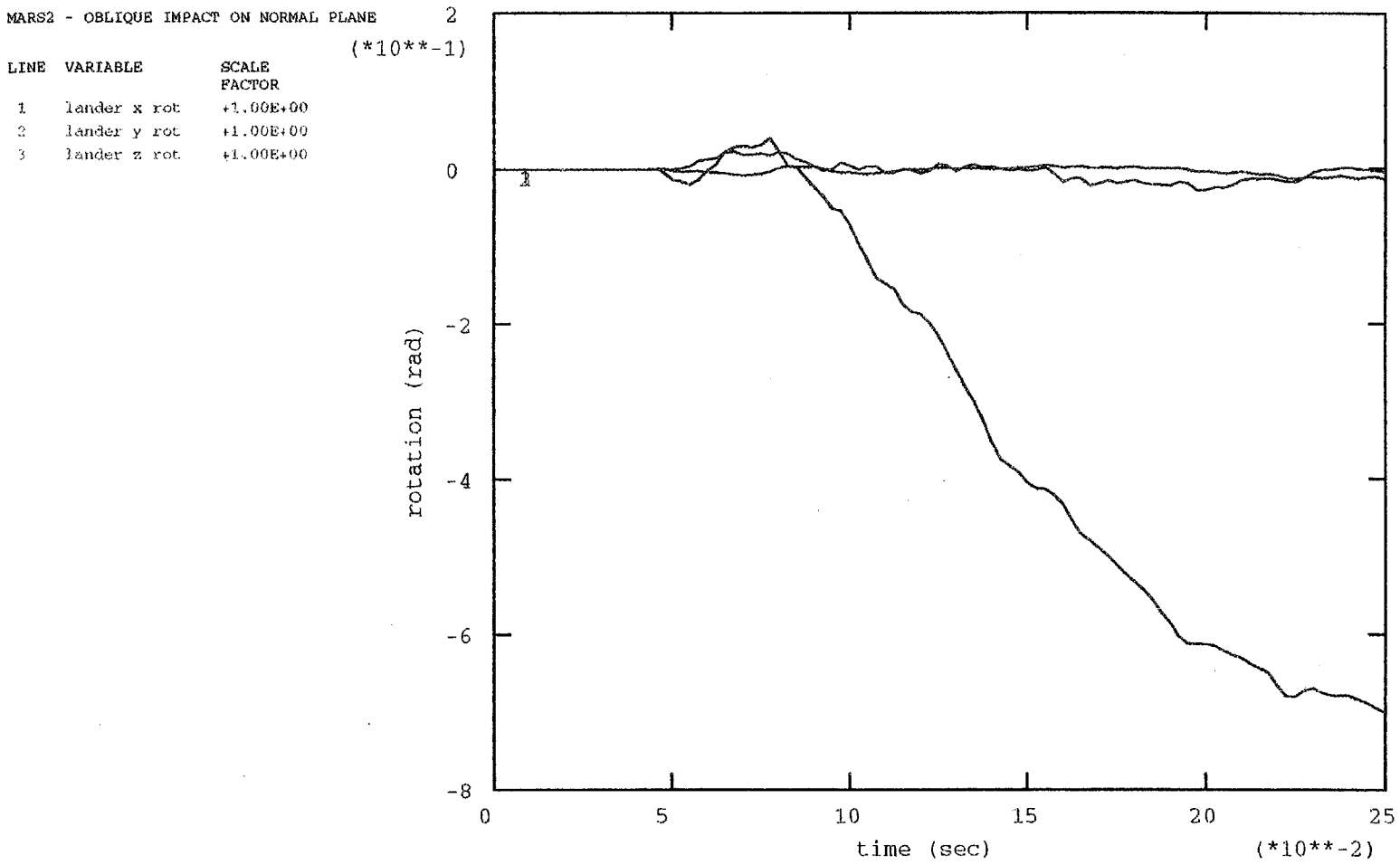

Figure B10. Lander C.G. RotationTime-History for Impact 2

MARS2 - OBLIQUE IMPACT ON NORMAL PLANE

LINE	VARIABLE	SCALE FACTOR
1	land x rot vel	+1.00E+00
2	land y rot vel	+1.00E+00
3	land z rot vel	+1.00E+00

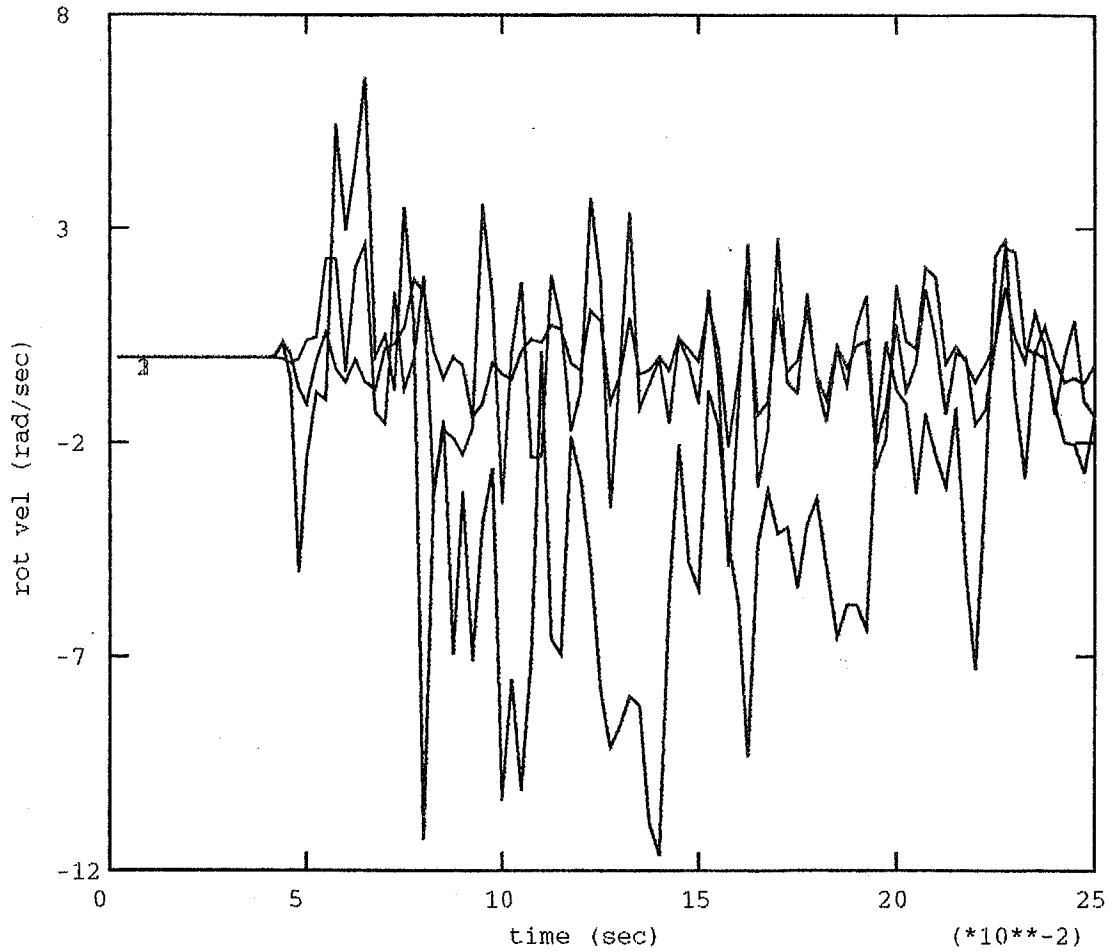

Figure B11. Lander C.G. Rotational Velocity Time-History for Impact 2

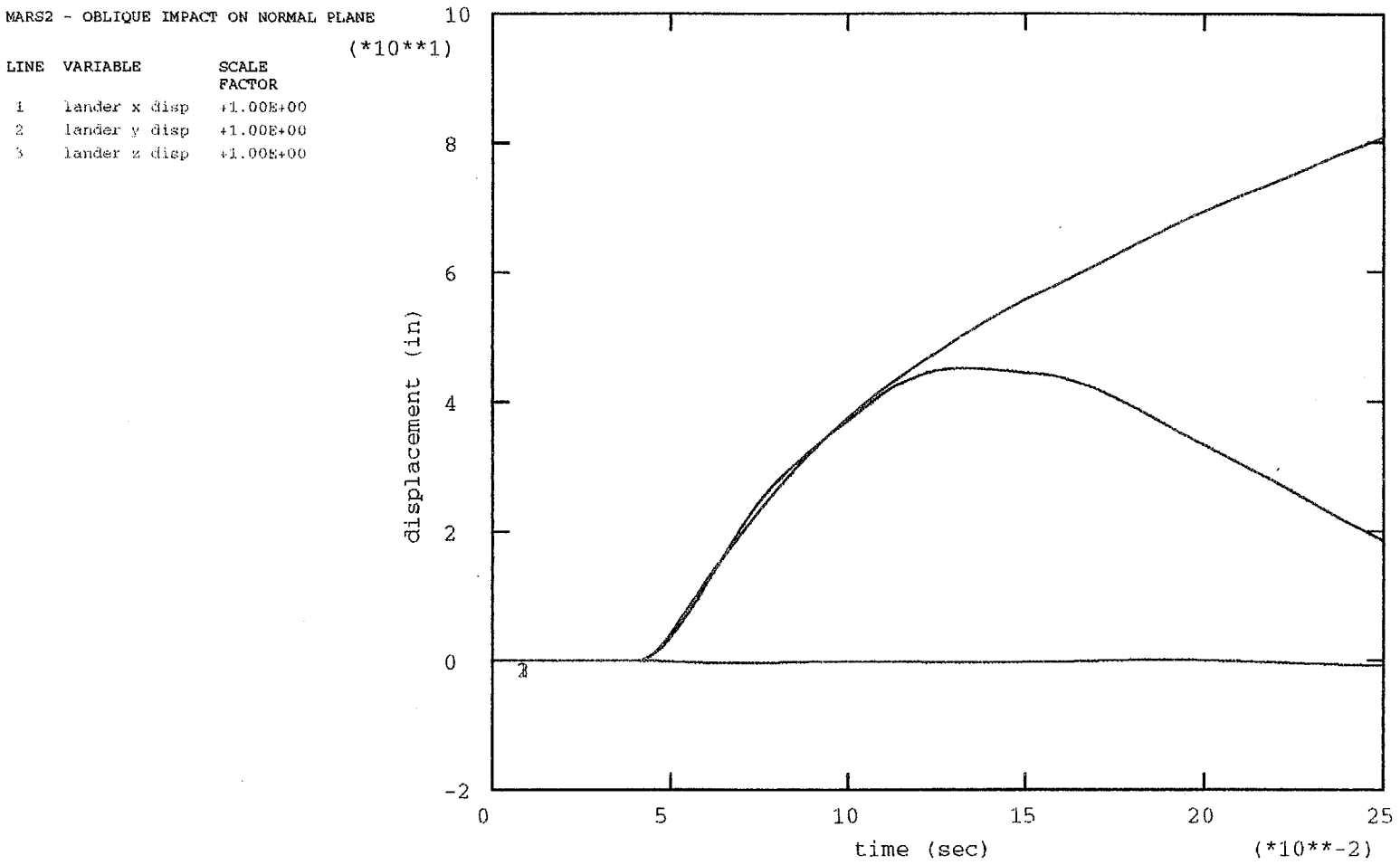

Figure B12. Lander C.G. Displacement Time-History for Impact 2

MARS2 - OBLIQUE IMPACT ON NORMAL PLANE

LINE	VARIABLE	SCALE FACTOR
1	bag 1 tendon 1	+1.00E-01
2	bag 1 tendon 2	+1.00E-01
3	bag 1 tendon 4	+1.00E-01
4	bag 1 tendon 5	+1.00E-01
5	bag 1 tendon 6	+1.00E-01

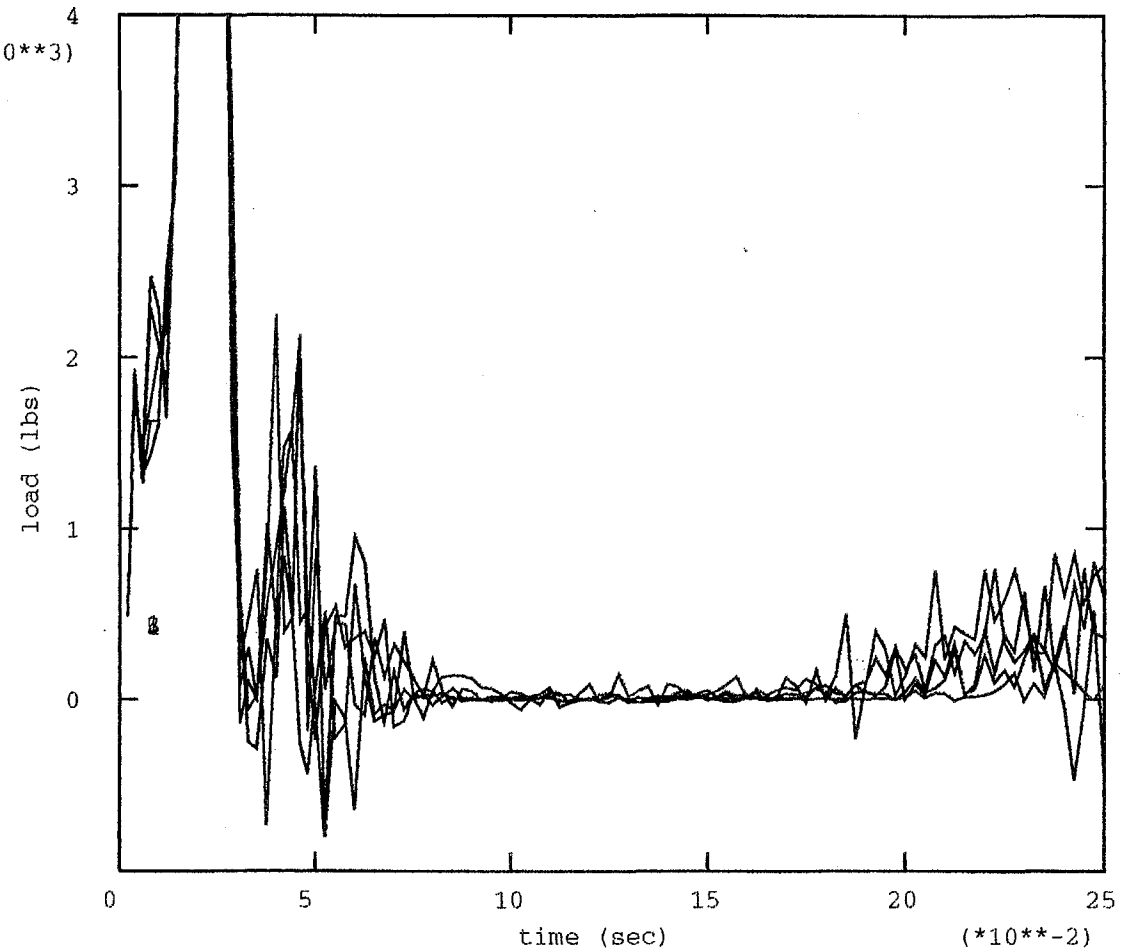

Figure B13. Bag 1 Tendon Force Time-History for Impact 2

MARS2 - OBLIQUE IMPACT ON NORMAL PLANE

LINE	VARIABLE	SCALE FACTOR
1	bag 2 tendon 1	+1.00E-01
2	bag 2 tendon 2	+1.00E-01
3	bag 2 tendon 3	+1.00E-01
4	bag 2 tendon 4	+1.00E-01
5	bag 2 tendon 5	+1.00E-01
6	bag 2 tendon 6	+1.00E-01

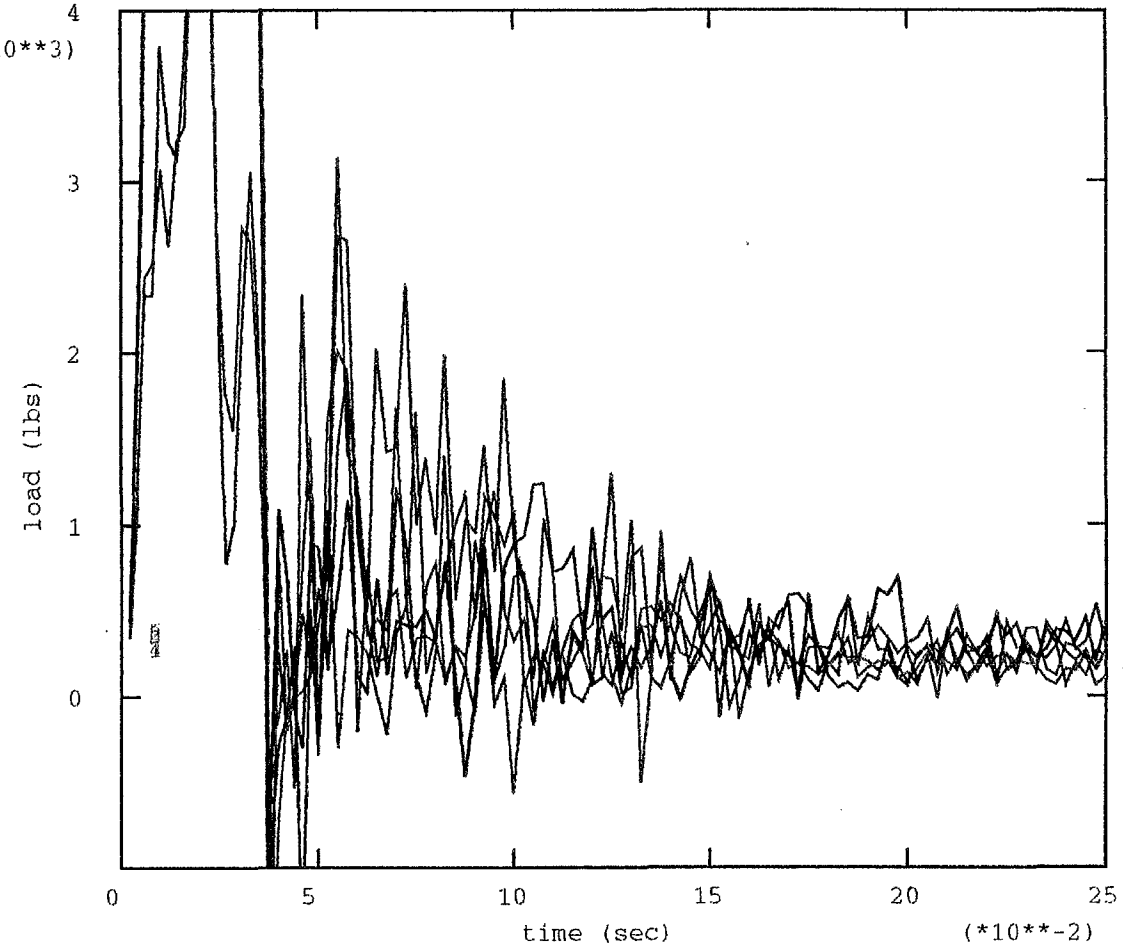

Figure B14. Bag 2 Tendon Force Time-History for Impact 2

MARS2 - OBLIQUE IMPACT ON NORMAL PLANE

LINE	VARIABLE	SCALE FACTOR
1	bag 3 tendon 1	+1.00E-01
2	bag 3 tendon 2	+1.00E-01
3	bag 3 tendon 3	+1.00E-01
4	bag 3 tendon 4	+1.00E-01
5	bag 3 tendon 5	+1.00E-01
6	bag 3 tendon 6	+1.00E-01

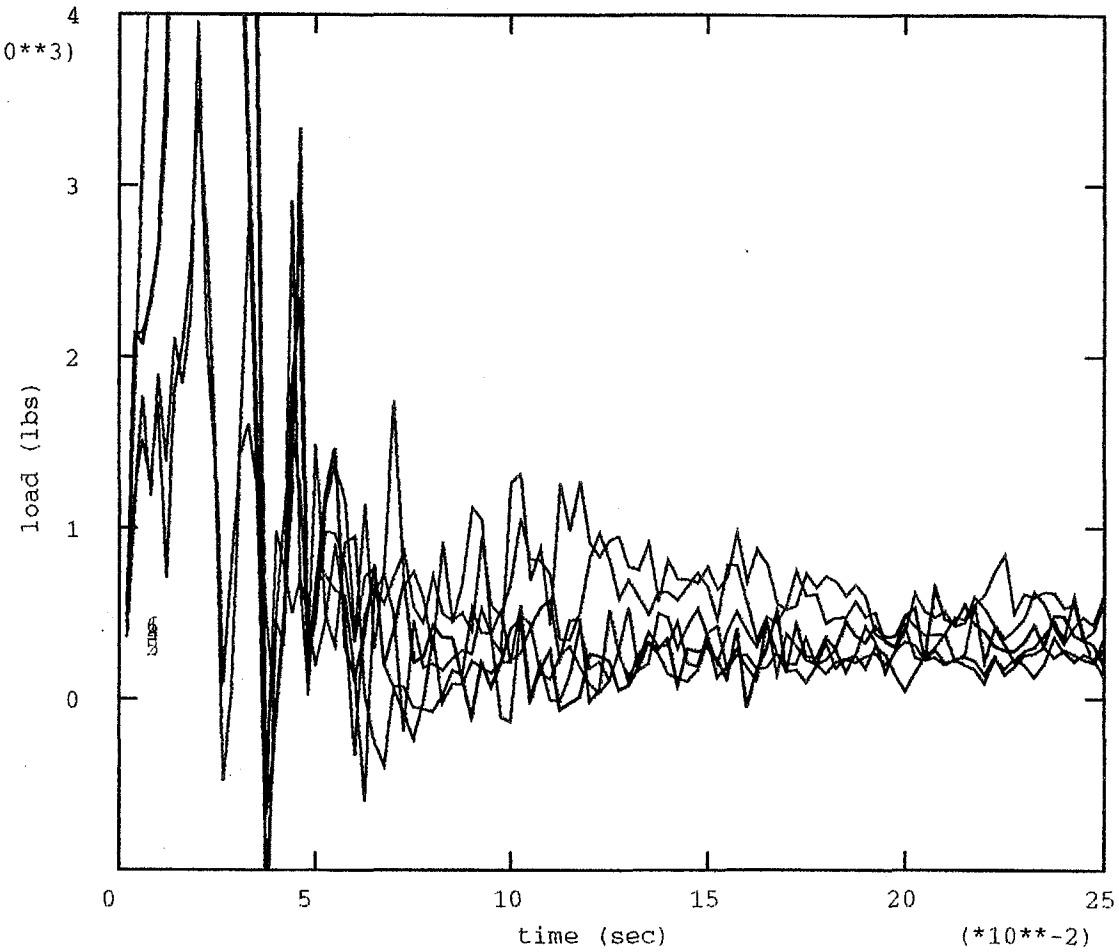

Figure B15. Bag 3 Tendon Force Time-History for Impact 2

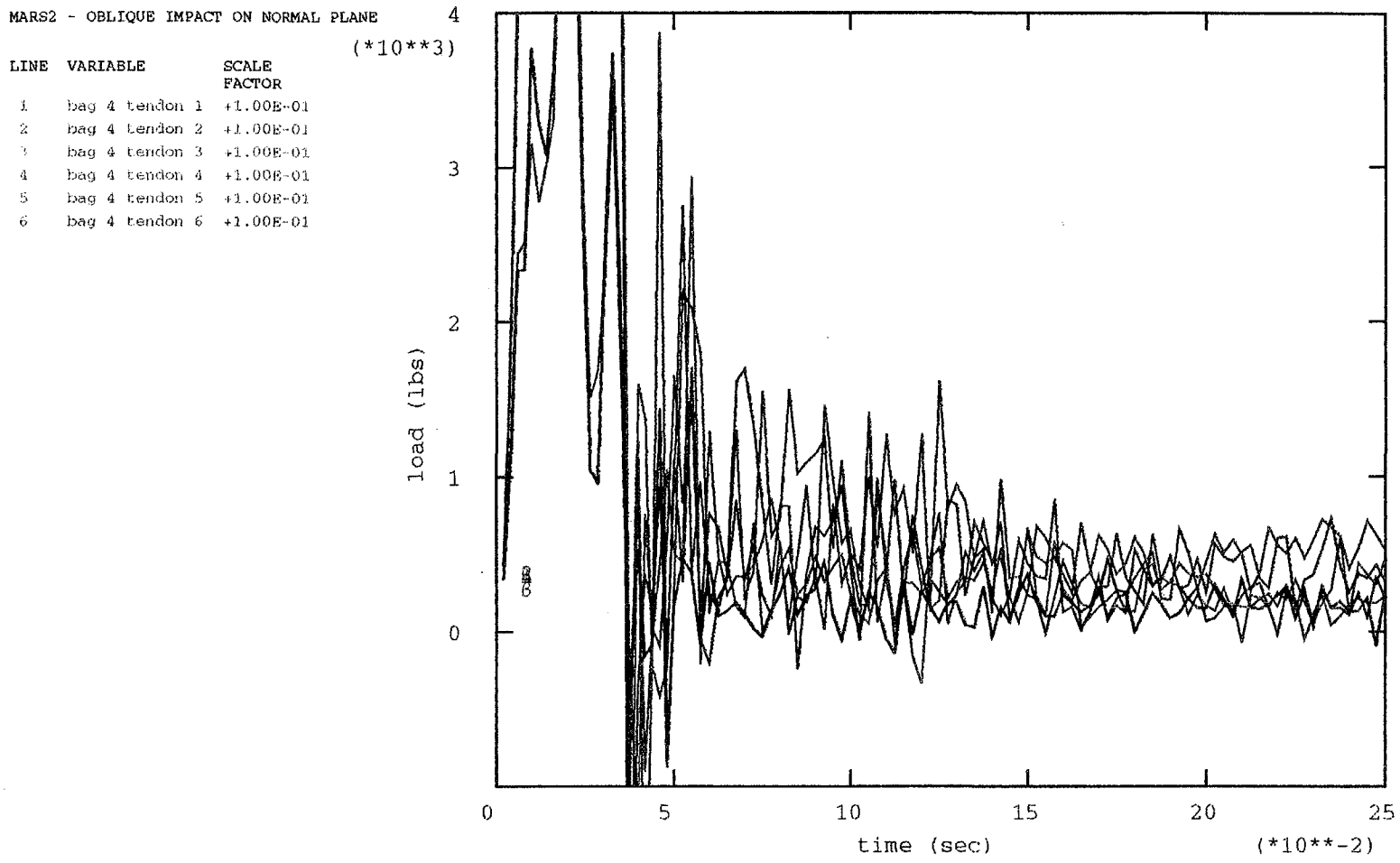

Figure B16. Bag 4 Tendon Force Time-History for Impact 2

MARS2 - OBLIQUE IMPACT ON NORMAL PLANE

LINE	VARIABLE	SCALE FACTOR
1	2-4 in-line	+2.47E+00
2	2-4 norm	+1.58E+00
3	2-3 in-line	+2.47E+00
4	2-3 norm	+1.58E+00
5	3-4 in-line	+2.47E+00
6	3-4 norm	+1.58E+00

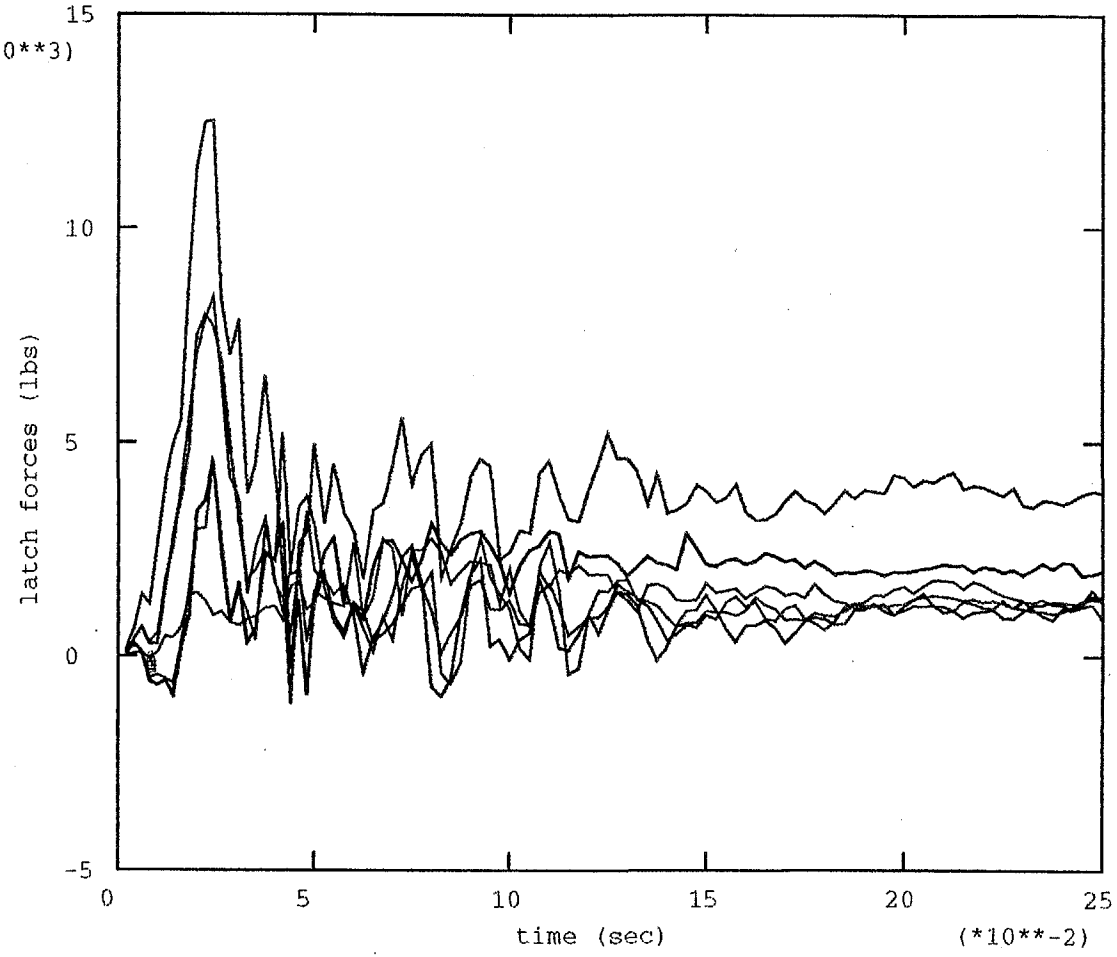

Figure B17. Latch Force Time-History for Impact 2

MARS2 - OBLIQUE IMPACT ON NORMAL PLANE

LINE	VARIABLE	SCALE FACTOR
1	p4 in-line	+2.71E+00
2	p4 norm	+2.38E+00
3	p4 in-line	+2.71E+00
4	p4 norm	+2.23E+00
5	p2 in-line	+2.71E+00
6	p2 norm	+2.23E+00
7	p2 in-line	+2.71E+00
8	p2 norm	+2.67E+00
9	p3 norm	+3.35E+00
10	p3 in-line	+2.07E+00
11	p3 in-line	+2.07E+00
12	p3 norm	+3.05E+00

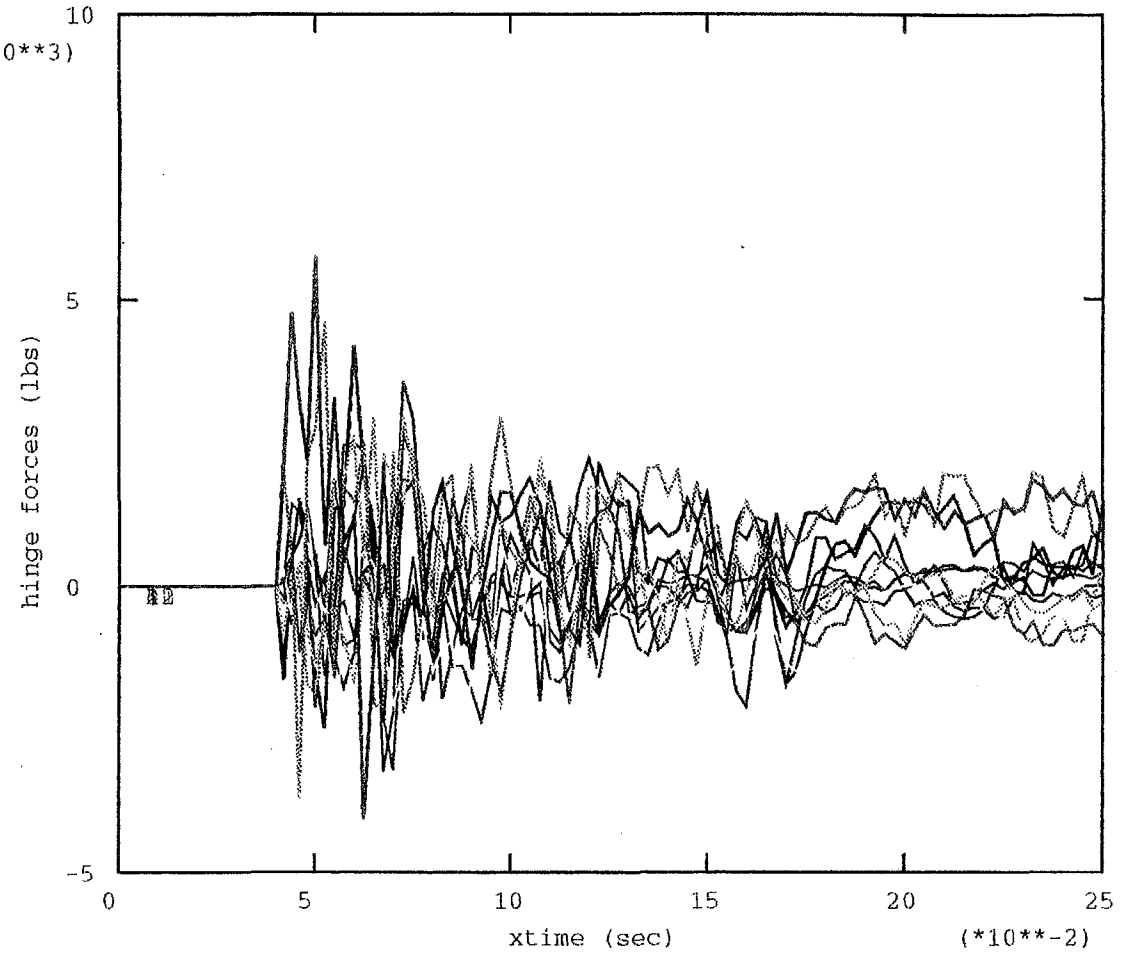

Figure B18. Hinge Force Time-History for Impact 2

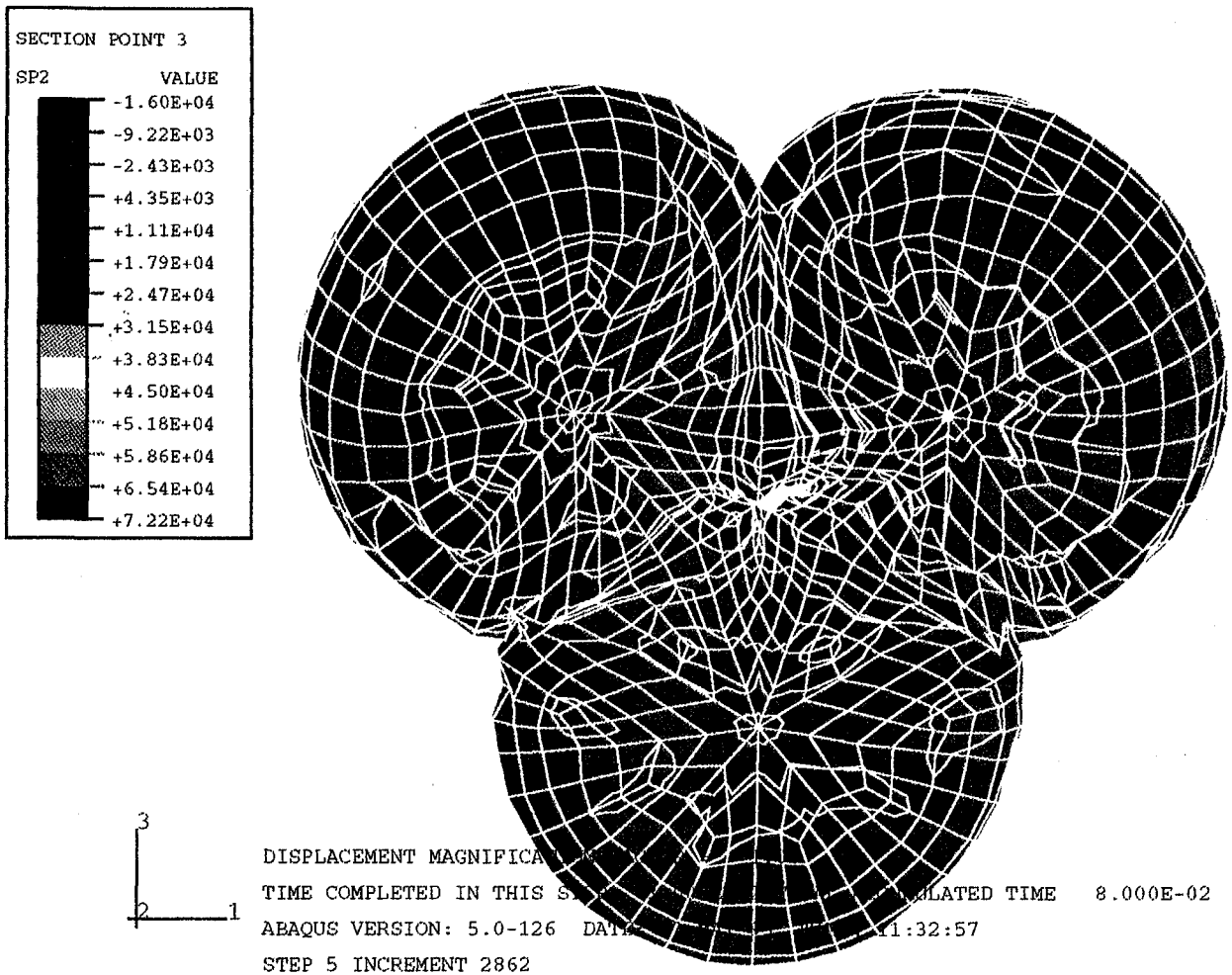

Figure B19. Maximum Principal Stress Distribution, Bottom Airbag, for Impact 2

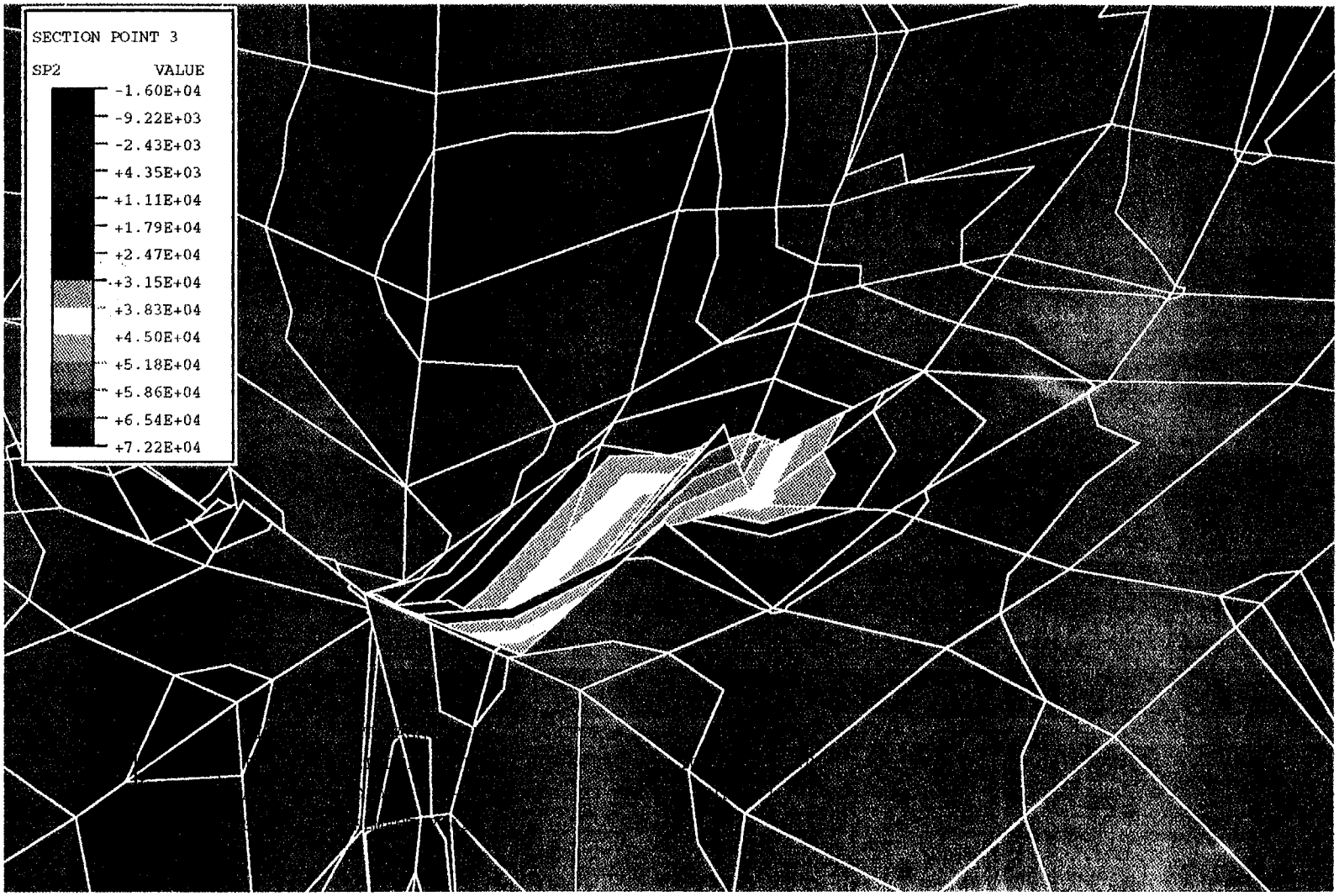

Figure B20. Closeup View of High Stress Region for Impact 2

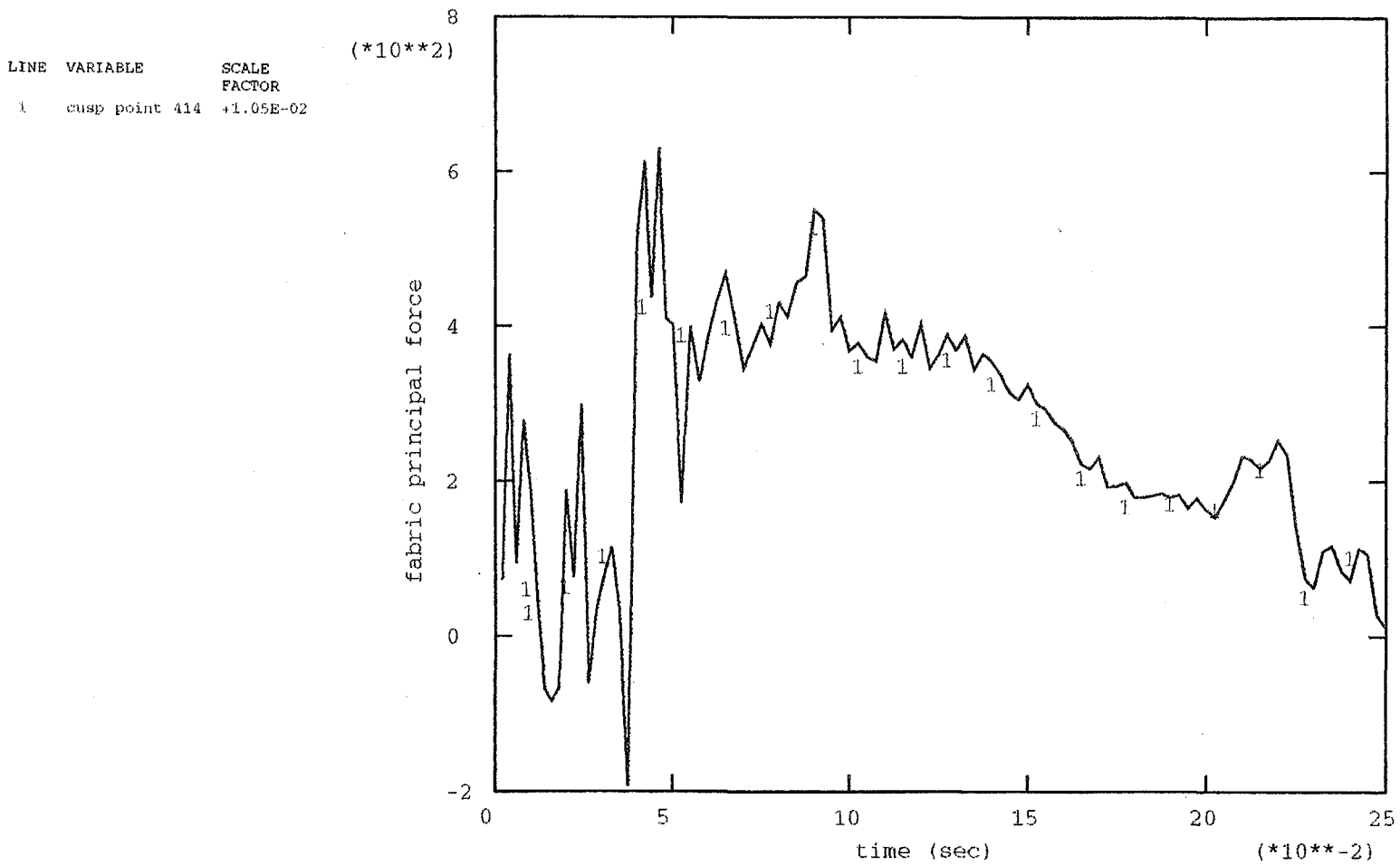

Fibure B21. Maximum Fabric Force Time-History for Impact 2

Appendix C

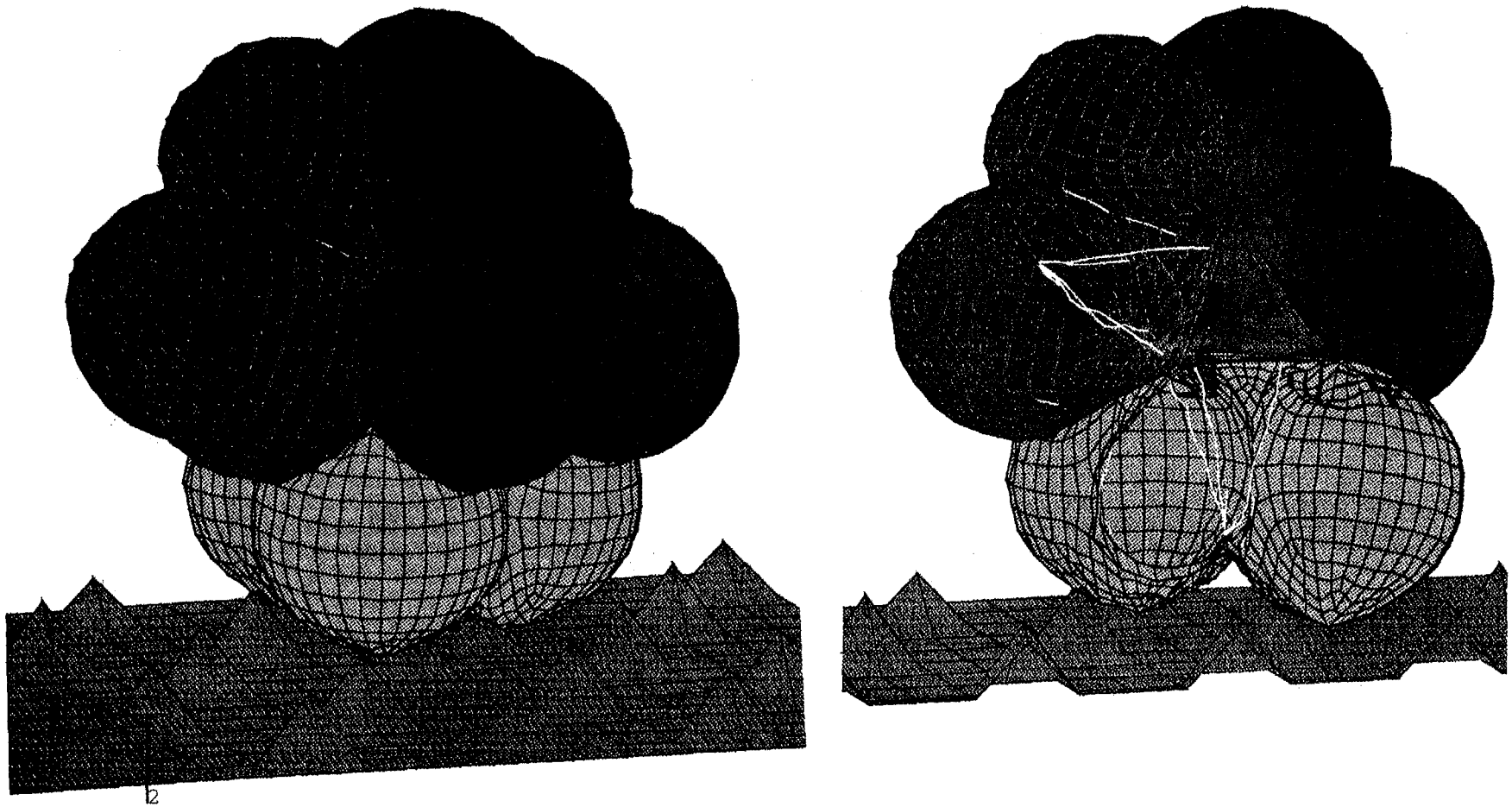

Figure C1. Deformed Mesh at 0 msec Into Impact 3

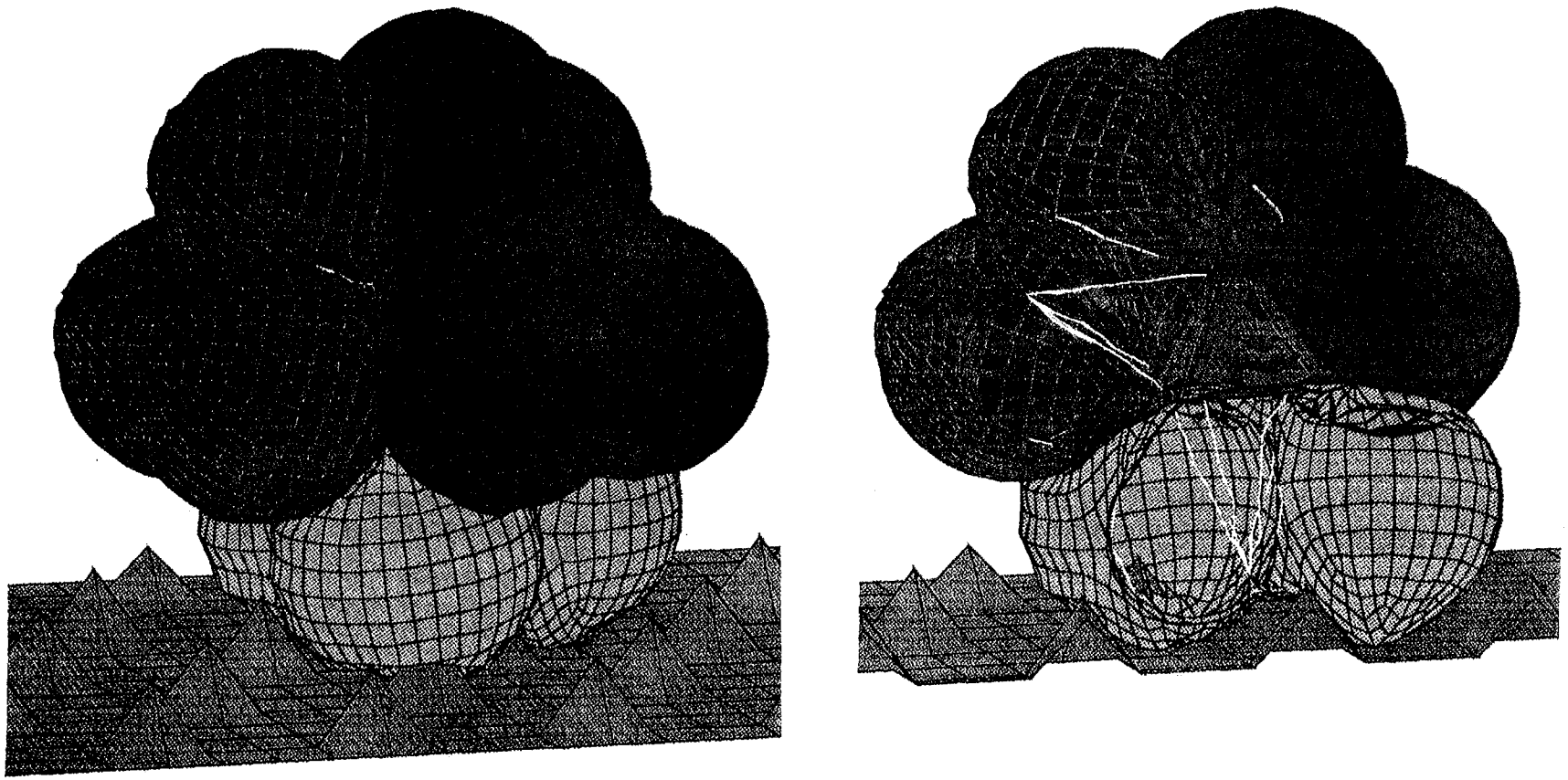

Figure C2. Deformed Mesh at 37.5 msec Into Impact 3

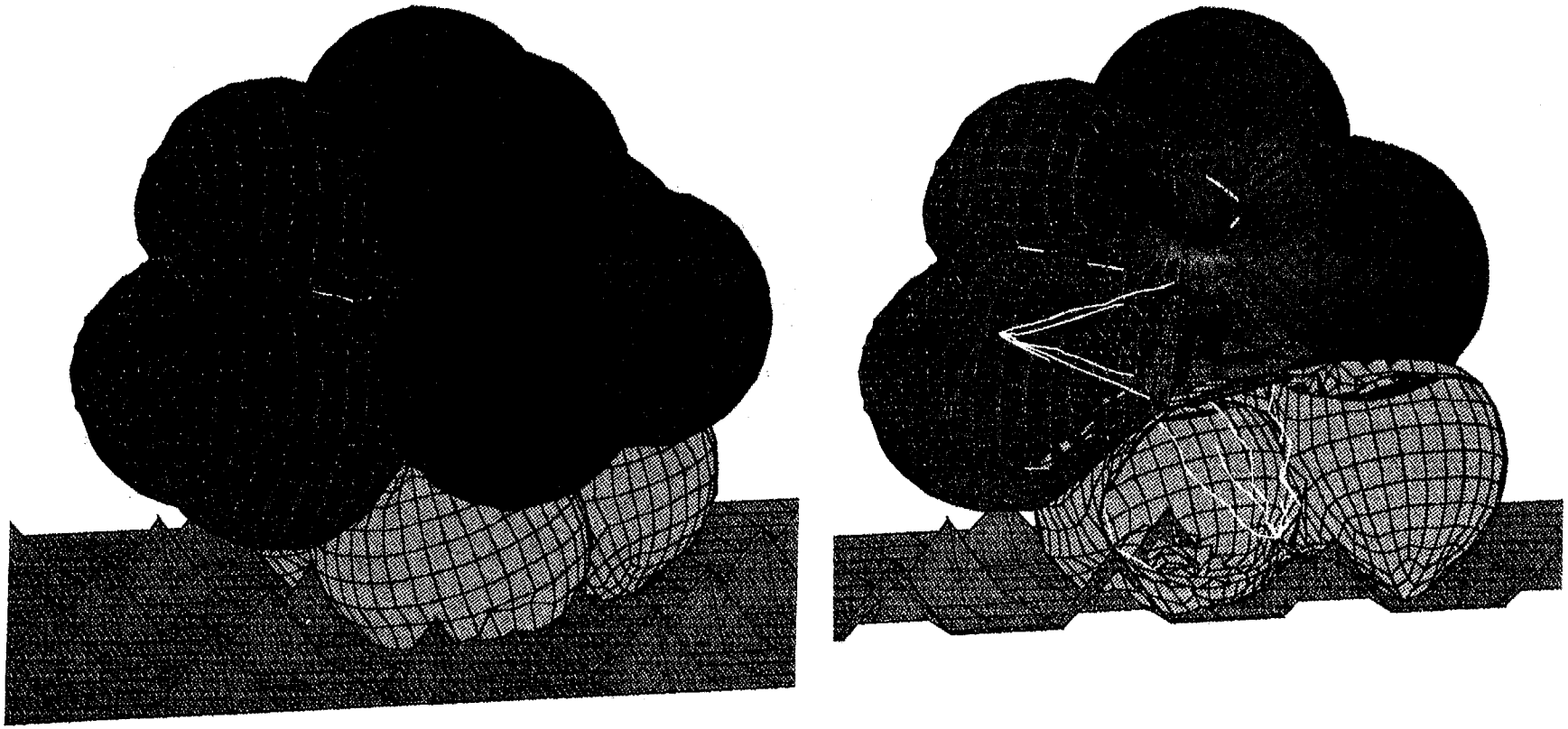

Figure C3. Deformed Mesh at 75 msec Into Impact 3

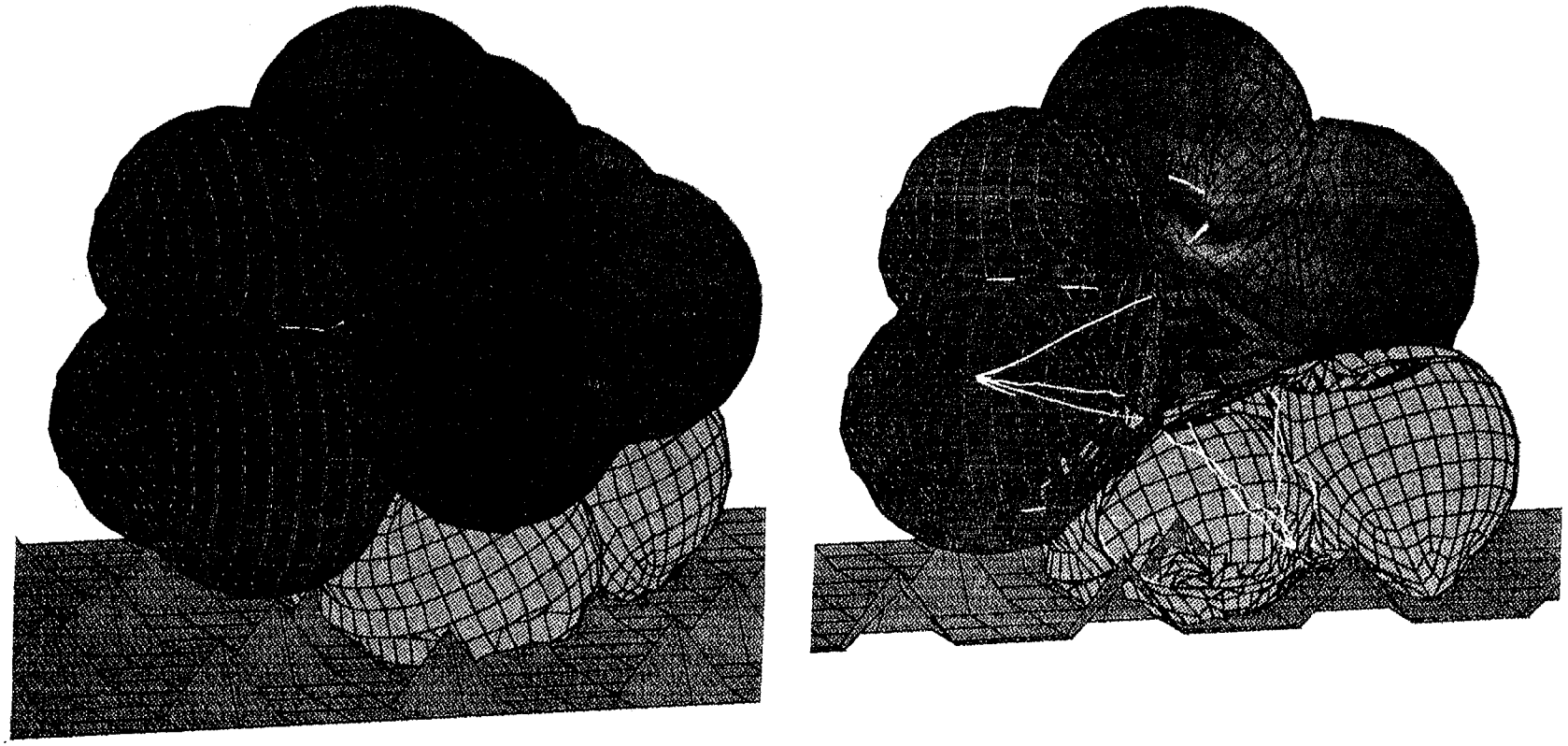

Figure C4. Deformed Mesh at 112.5 msec Into Impact 3

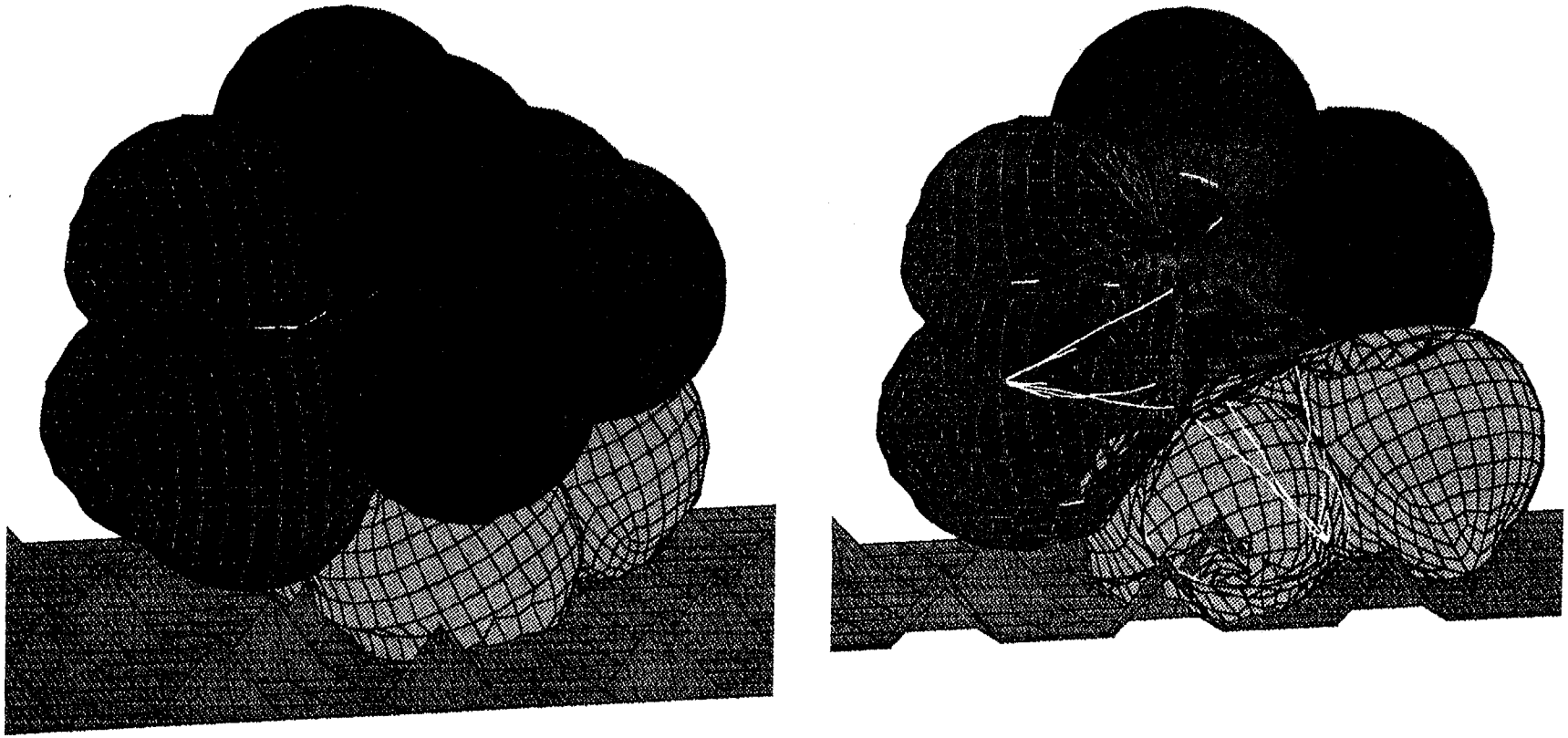

Figure C5. Deformed Mesh at 150 msec Into Impact 3

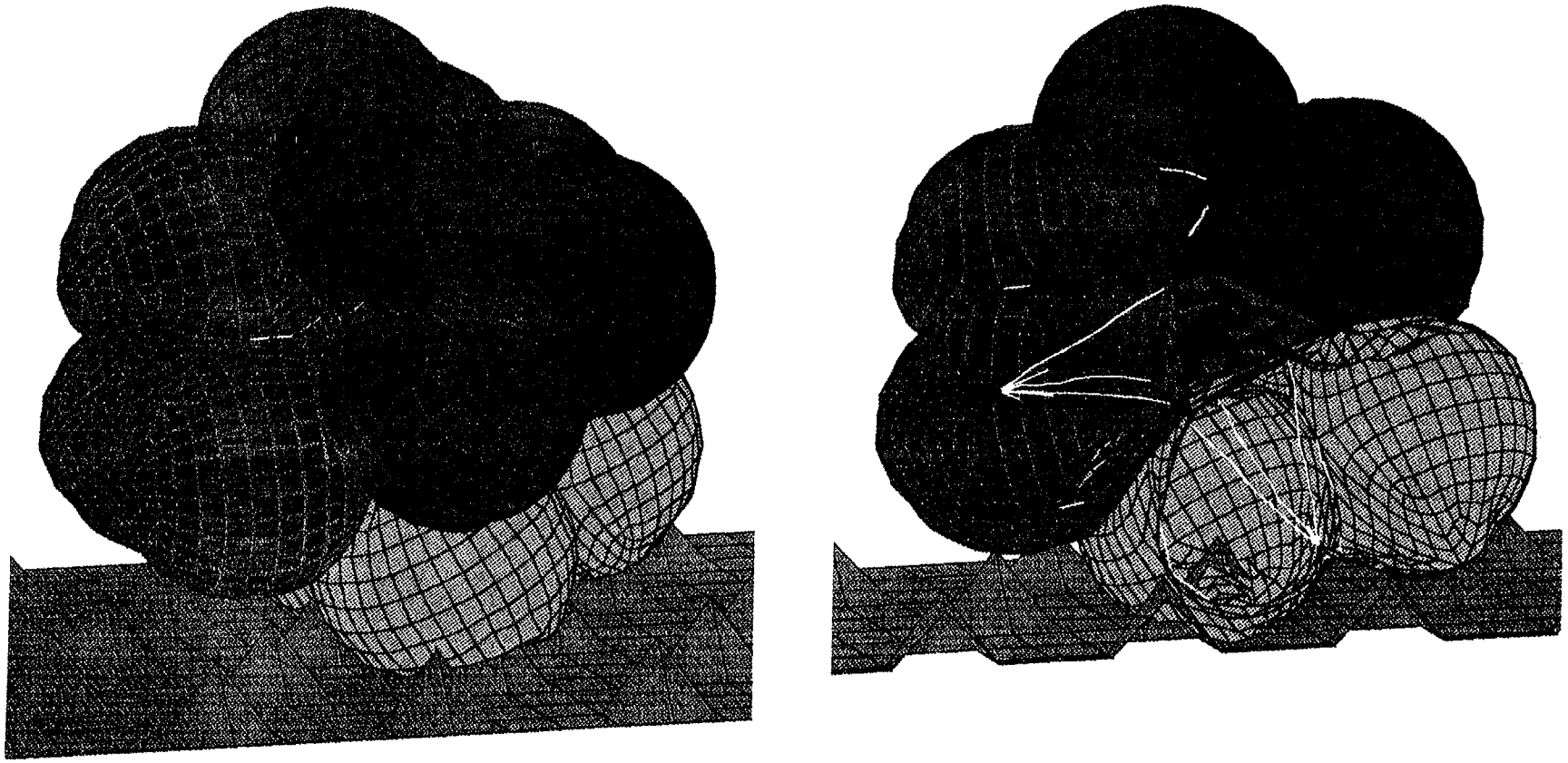

Figure C6. Deformed Mesh at 187.5 msec Into Impact 3

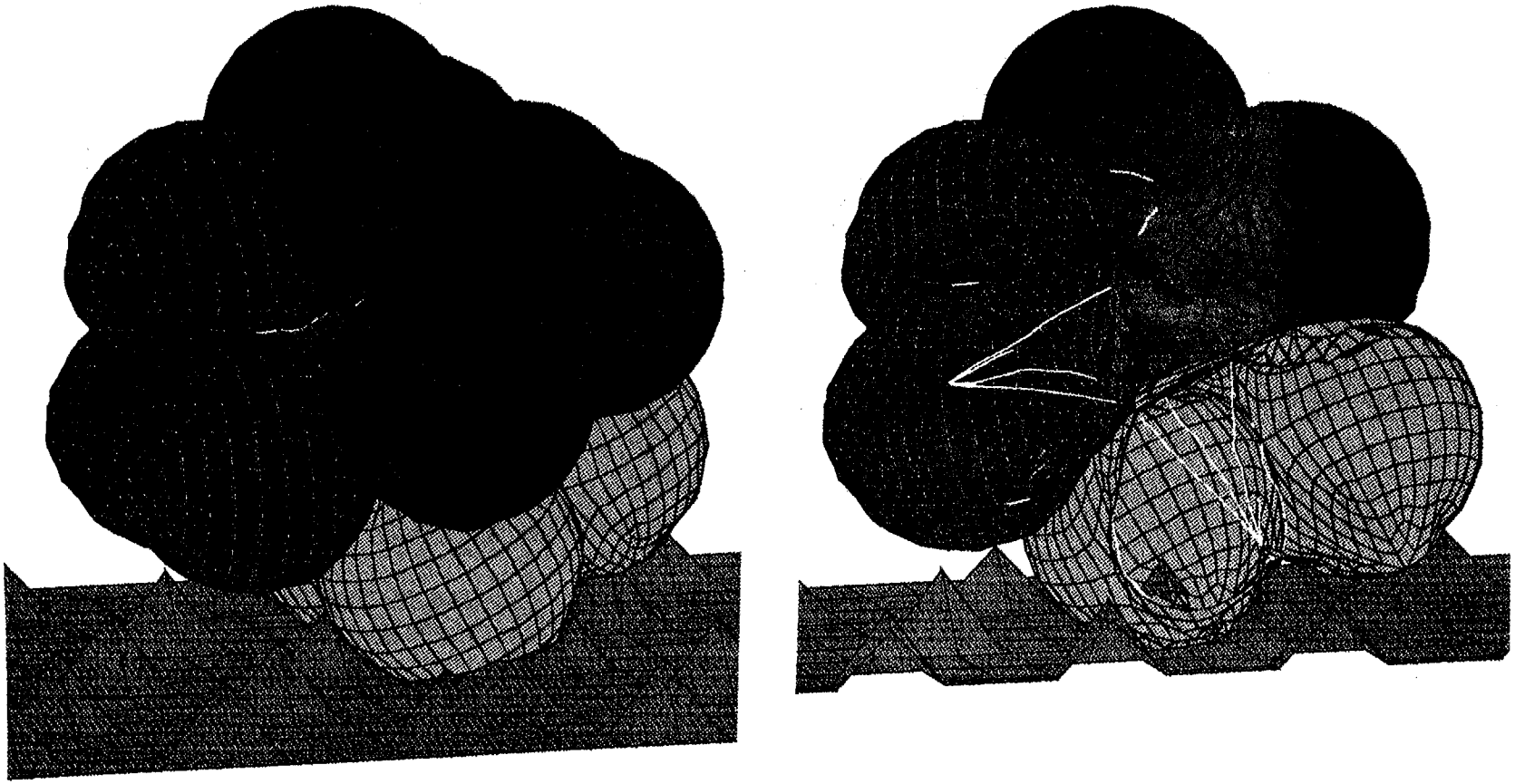

Figure C7. Deformed Mesh at 225 msec Into Impact 3

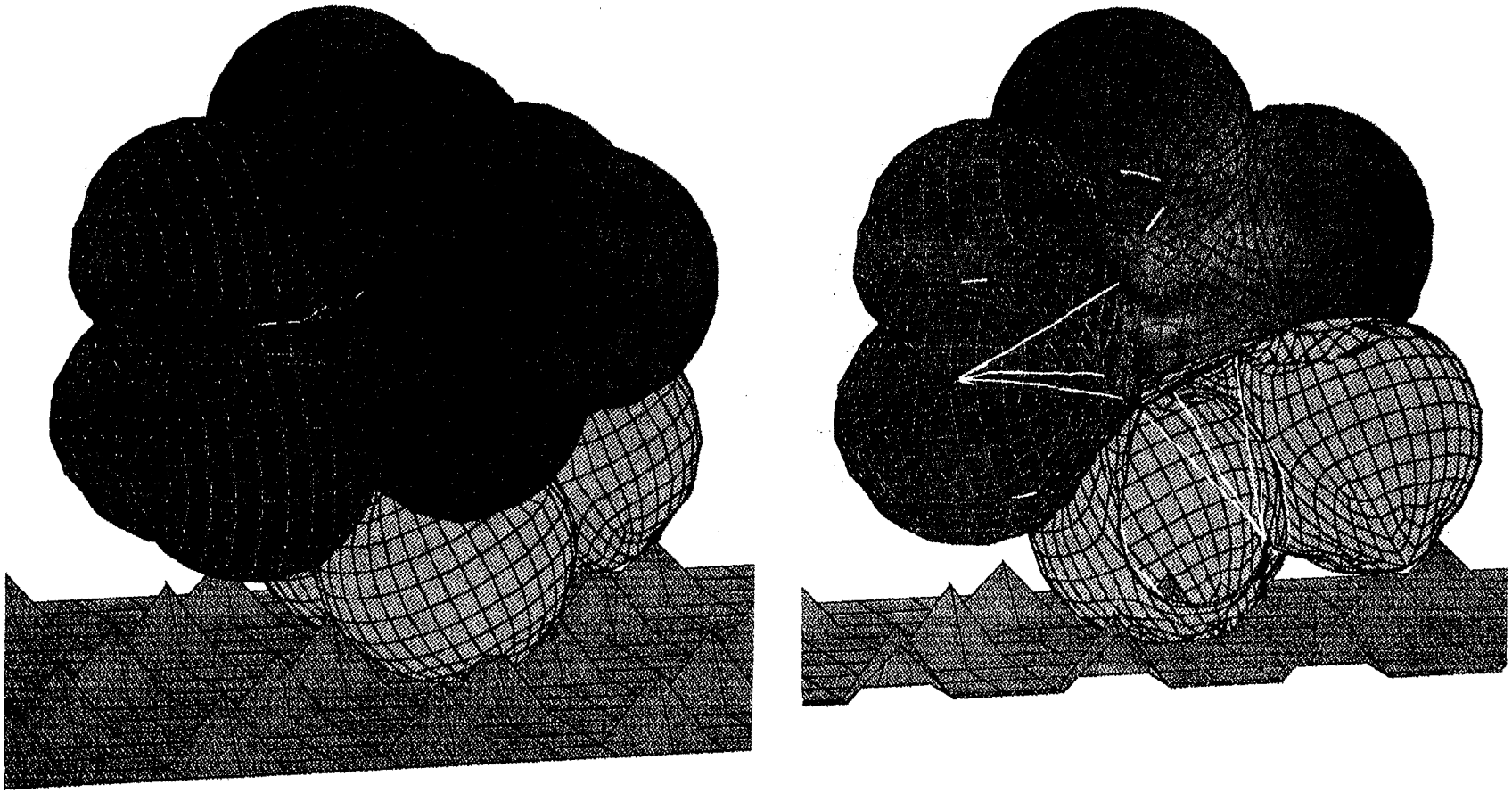

Figure C8. Deformed Mesh at 262.5 msec Into Impact 3

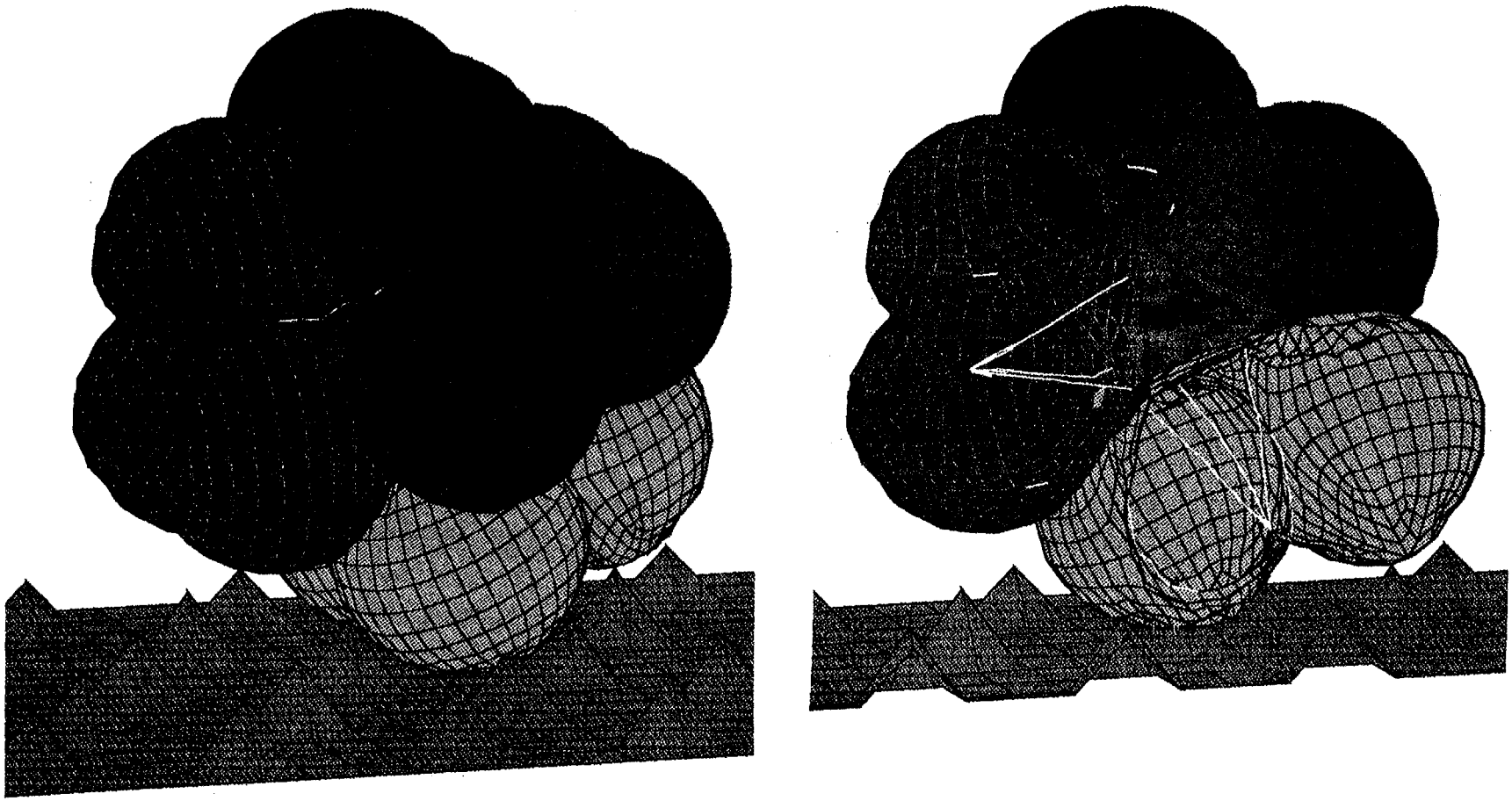

Figure C9. Deformed Mesh at 300 msec Into Impact 3

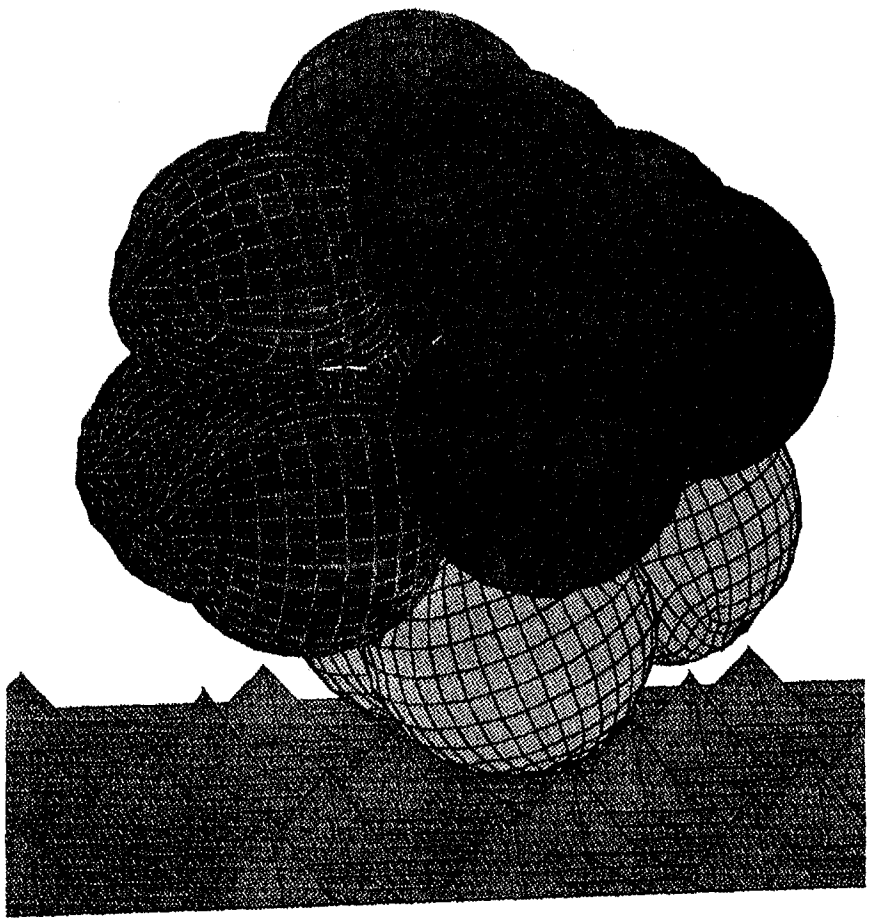

Figure C10. Deformed Mesh at 337.5 msec Into Impact 3

Mars 3 - Oblique impact at 20m/sec, Rough Surface

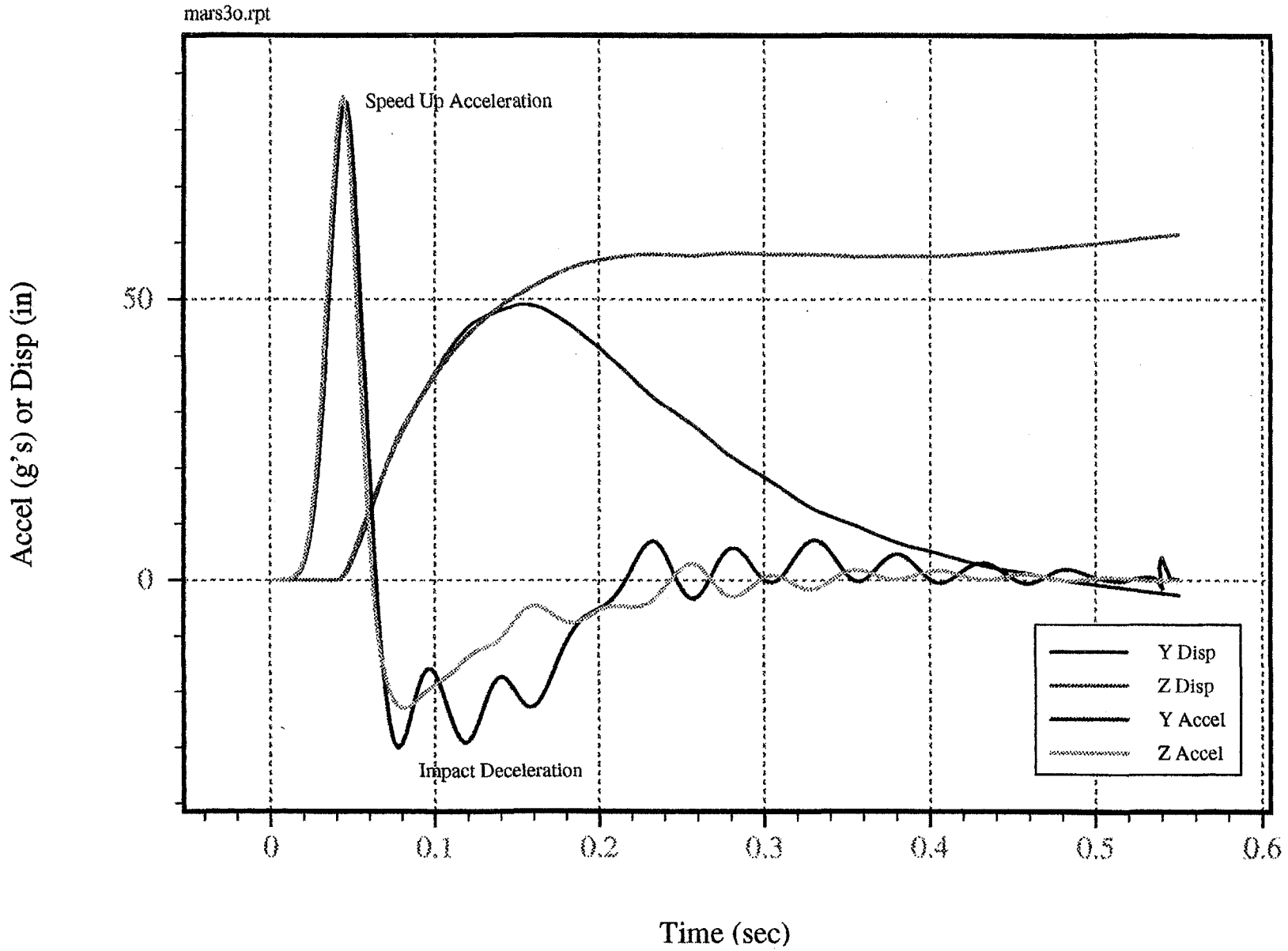

Figure C11. Lander C.G. Acceleration Time-History for Impact 3

OBLIQUE IMPACT ON ROCKS, MARS3

LINE	VARIABLE	SCALE FACTOR
1	lander x vel	+1.00E+00
2	lander y vel	+1.00E+00
3	lander z vel	+1.00E+00

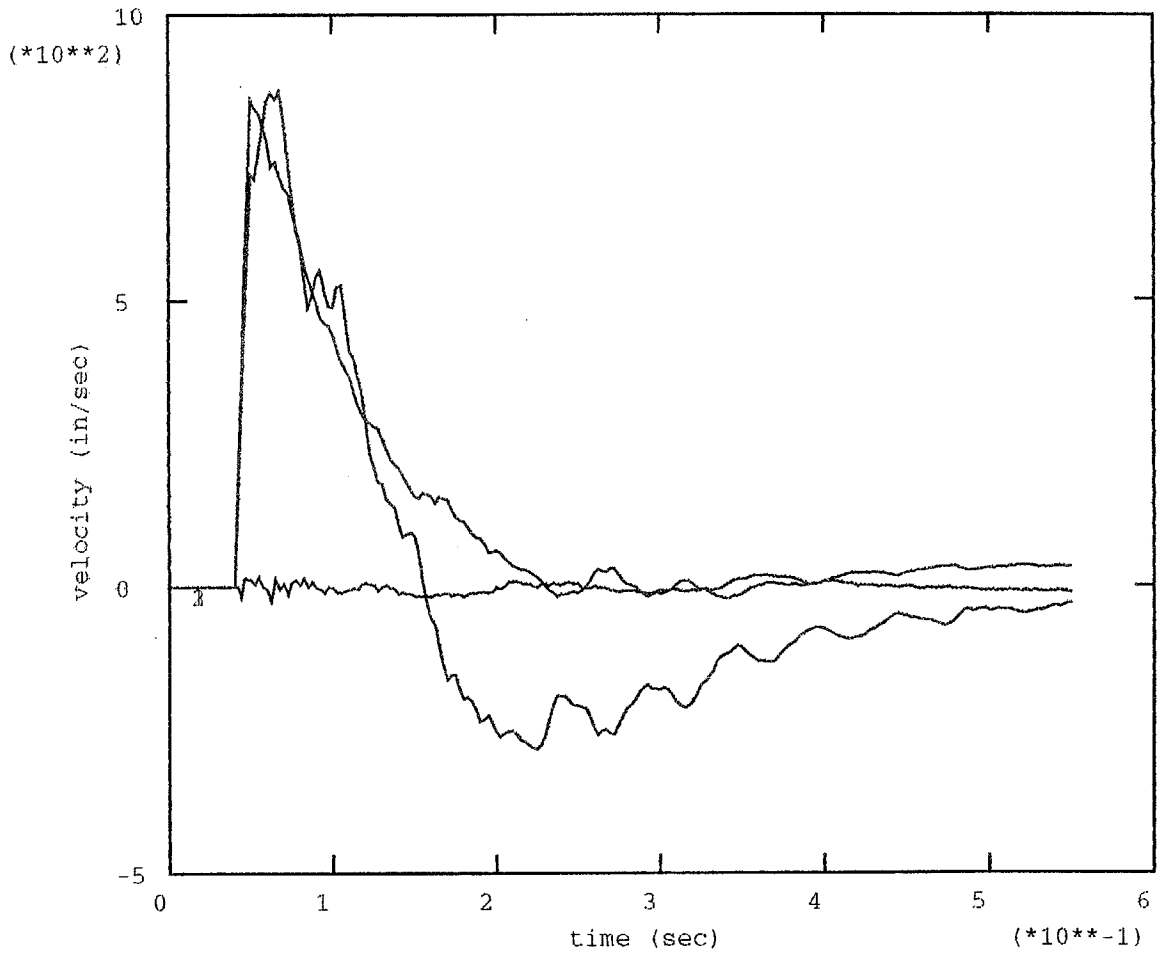

Figure C12. Lander C.G. Velocity Time-History for Impact 3

OBLIQUE IMPACT ON ROCKS, MARS3

LINE	VARIABLE	SCALE FACTOR
1	lander x rot	+1.00E+00
2	lander y rot	+1.00E+00
3	lander z rot	+1.00E+00

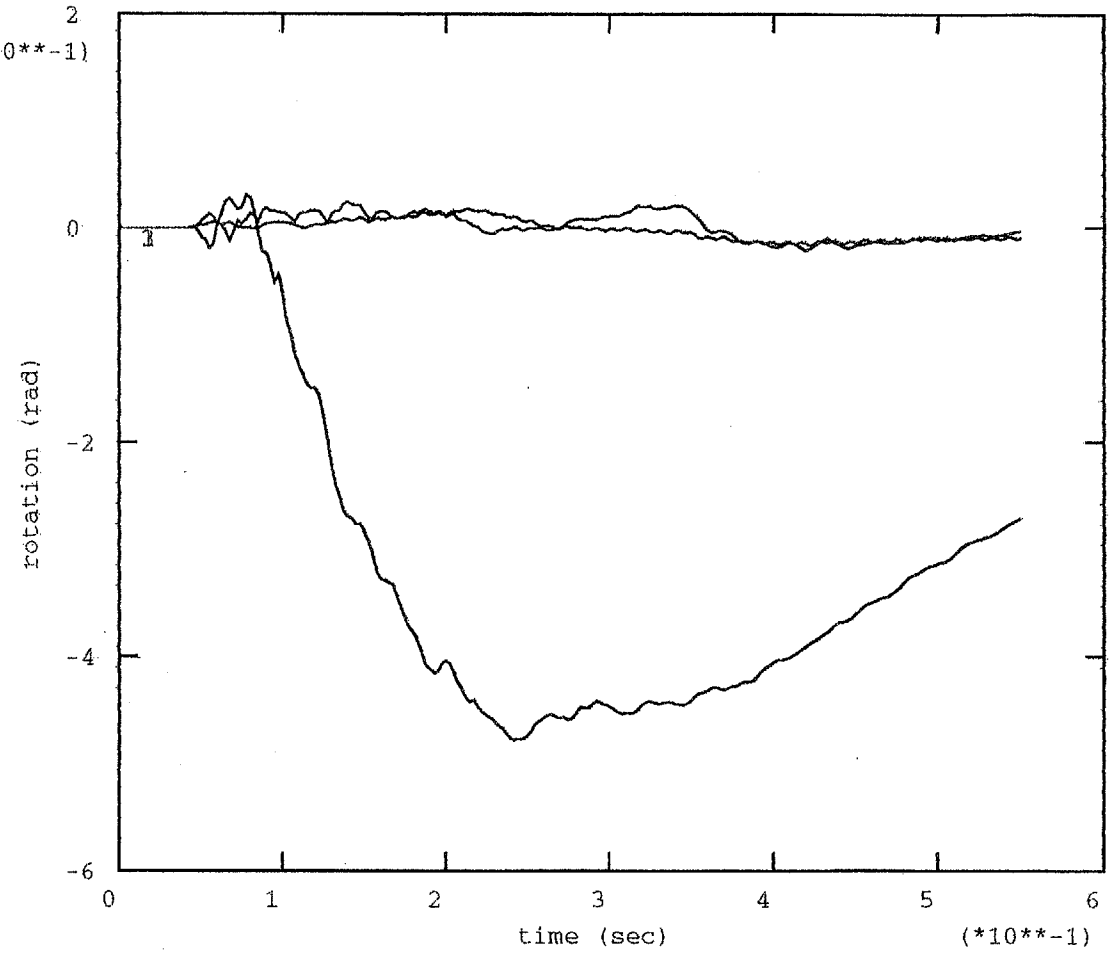

Figure C13. Lander C.G. RotationTime-History for Impact 3

OBLIQUE IMPACT ON ROCKS, MARS3

LINE	VARIABLE	SCALE FACTOR
1	land x rot vel	+1.00E+00
2	land y rot vel	+1.00E+00
3	land z rot vel	+1.00E+00

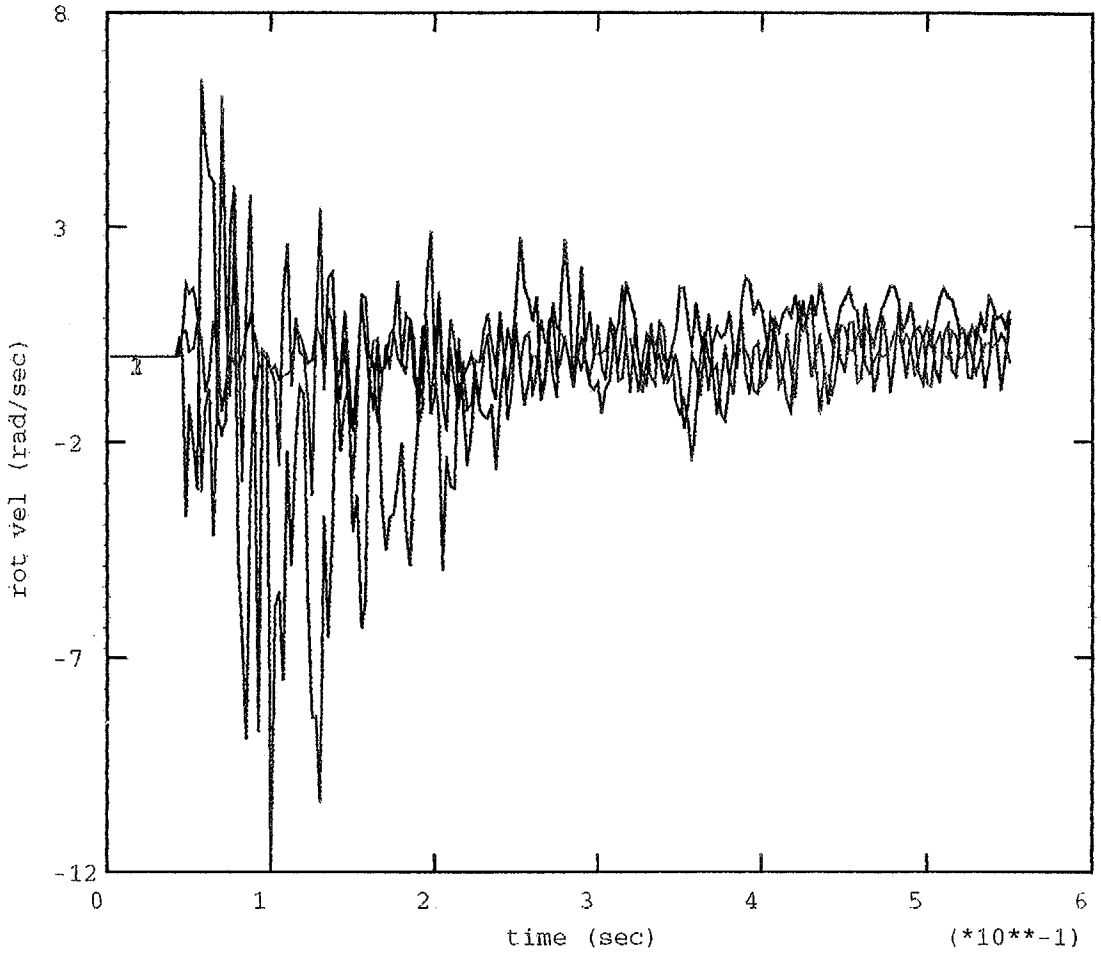

Figure C14. Lander C.G. Rotational Velocity Time-History for Impact 3

OBLIQUE IMPACT ON ROCKS, MARS3

LINE	VARIABLE	SCALE FACTOR
1	lander x disp	+1.00E+00
2	lander y disp	+1.00E+00
3	lander z disp	+1.00E+00

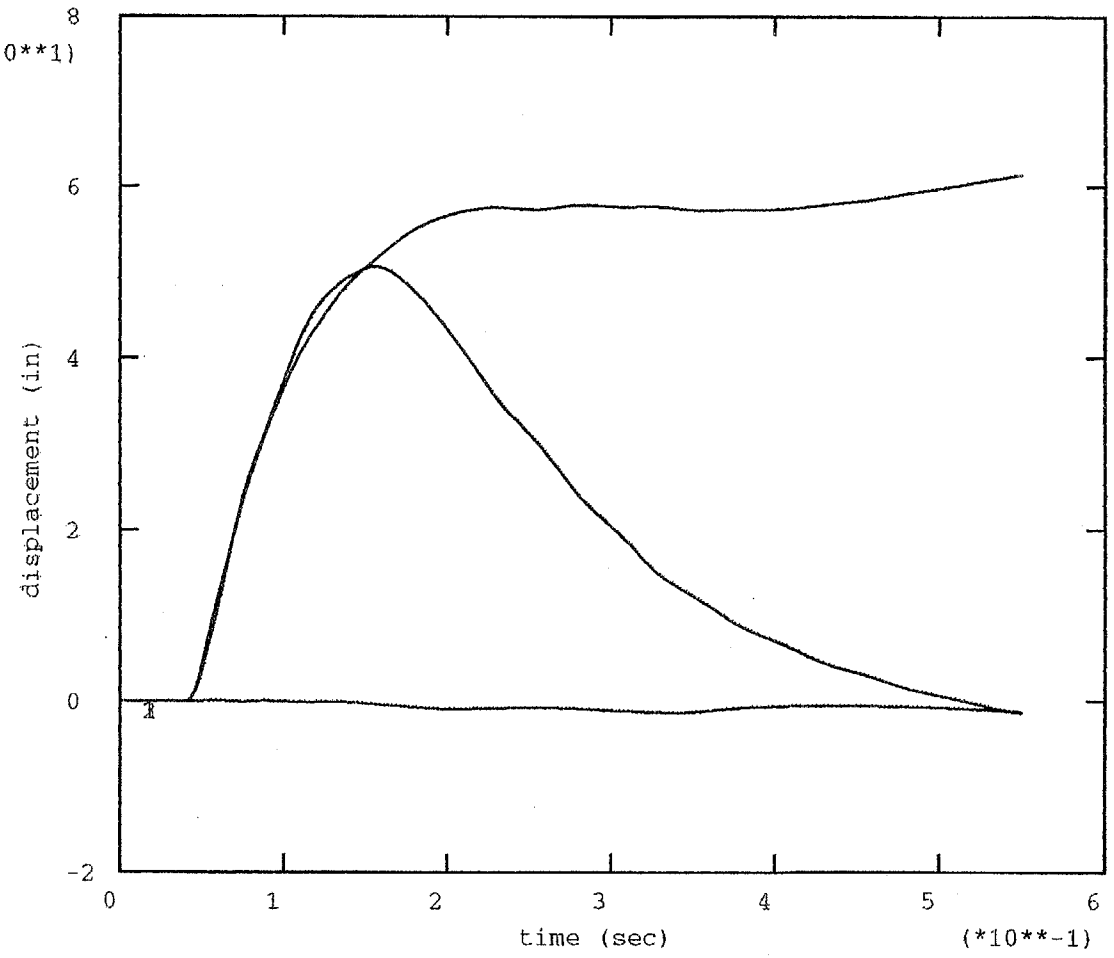

Figure C15. Lander C.G. Displacement Time-History for Impact 3

OBLIQUE IMPACT ON ROCKS, MARS3

LINE	VARIABLE	SCALE FACTOR
1	bag 1 tendon 1	+1.00E-01
2	bag 1 tendon 2	+1.00E-01
3	bag 1 tendon 4	+1.00E-01
4	bag 1 tendon 5	+1.00E-01
5	bag 1 tendon 6	+1.00E-01

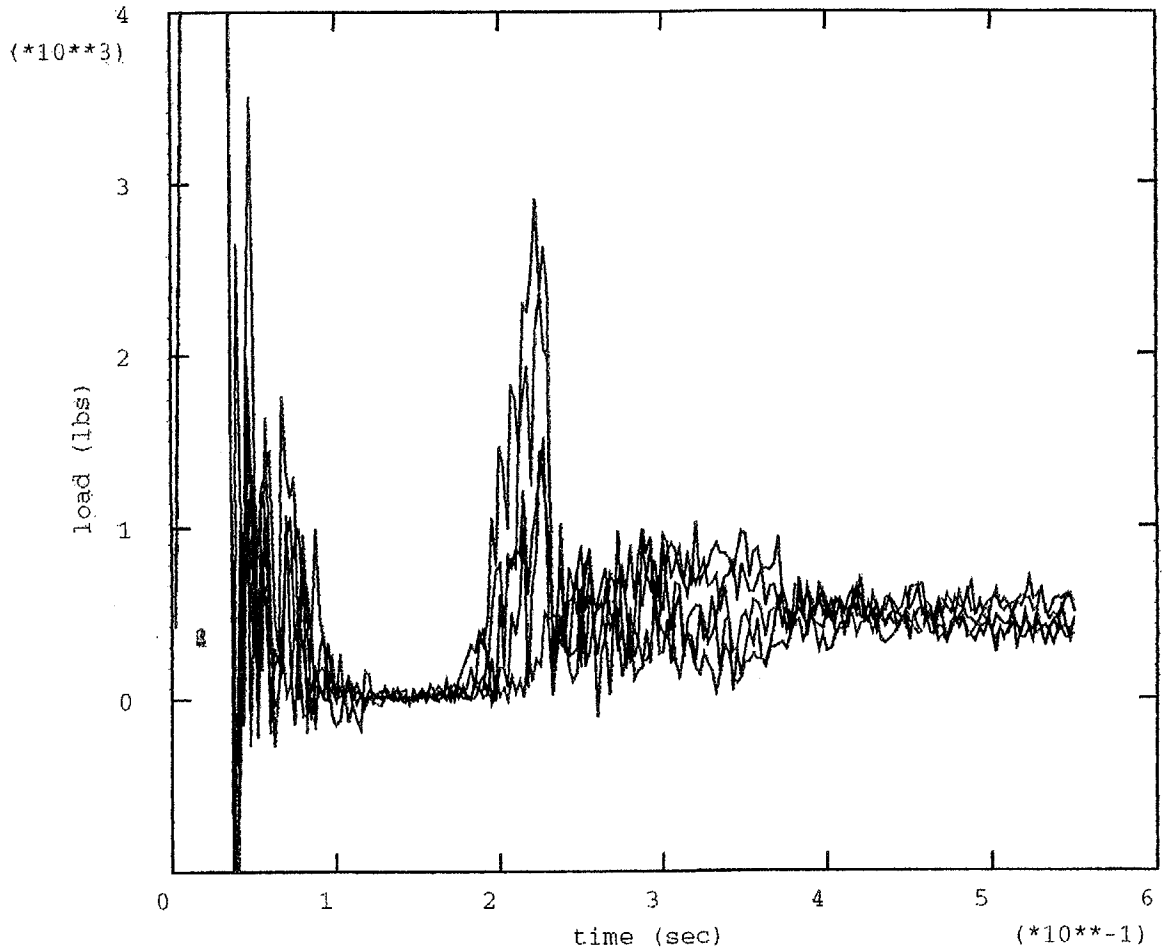

Figure C16. Bag 1 Tendon Force Time-History for Impact 3

OBLIQUE IMPACT ON ROCKS, MARS3

LINE	VARIABLE	SCALE FACTOR
1	bag 2 tendon 1	+1.00E-01
2	bag 2 tendon 2	+1.00E-01
3	bag 2 tendon 3	+1.00E-01
4	bag 2 tendon 4	+1.00E-01
5	bag 2 tendon 5	+1.00E-01
6	bag 2 tendon 6	+1.00E-01

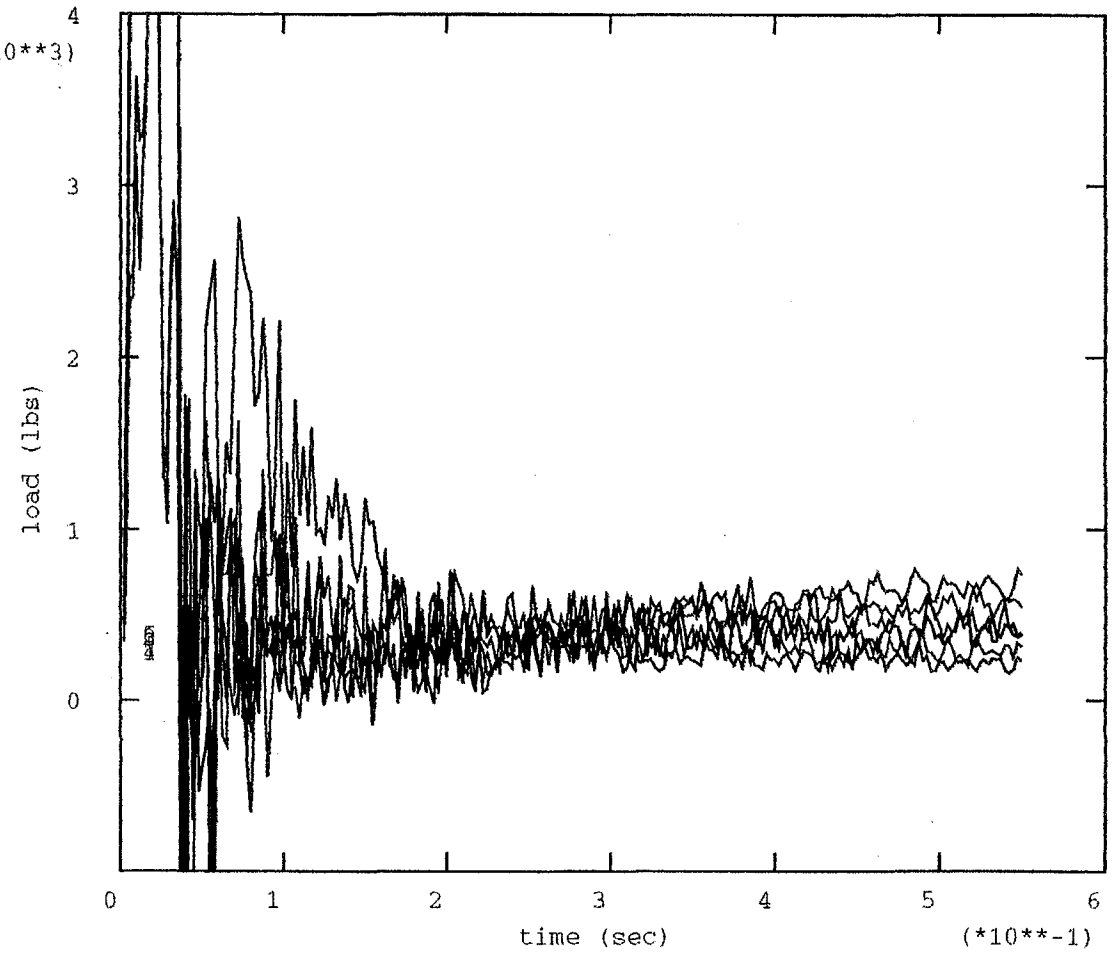

Figure C17. Bag 2 Tendon Force Time-History for Impact 3

OBLIQUE IMPACT ON ROCKS, MARS3

LINE	VARIABLE	SCALE FACTOR
1	bag 3 tendon 1	+1.00E-01
2	bag 3 tendon 2	+1.00E-01
3	bag 3 tendon 3	+1.00E-01
4	bag 3 tendon 4	+1.00E-01
5	bag 3 tendon 5	+1.00E-01
6	bag 3 tendon 6	+1.00E-01

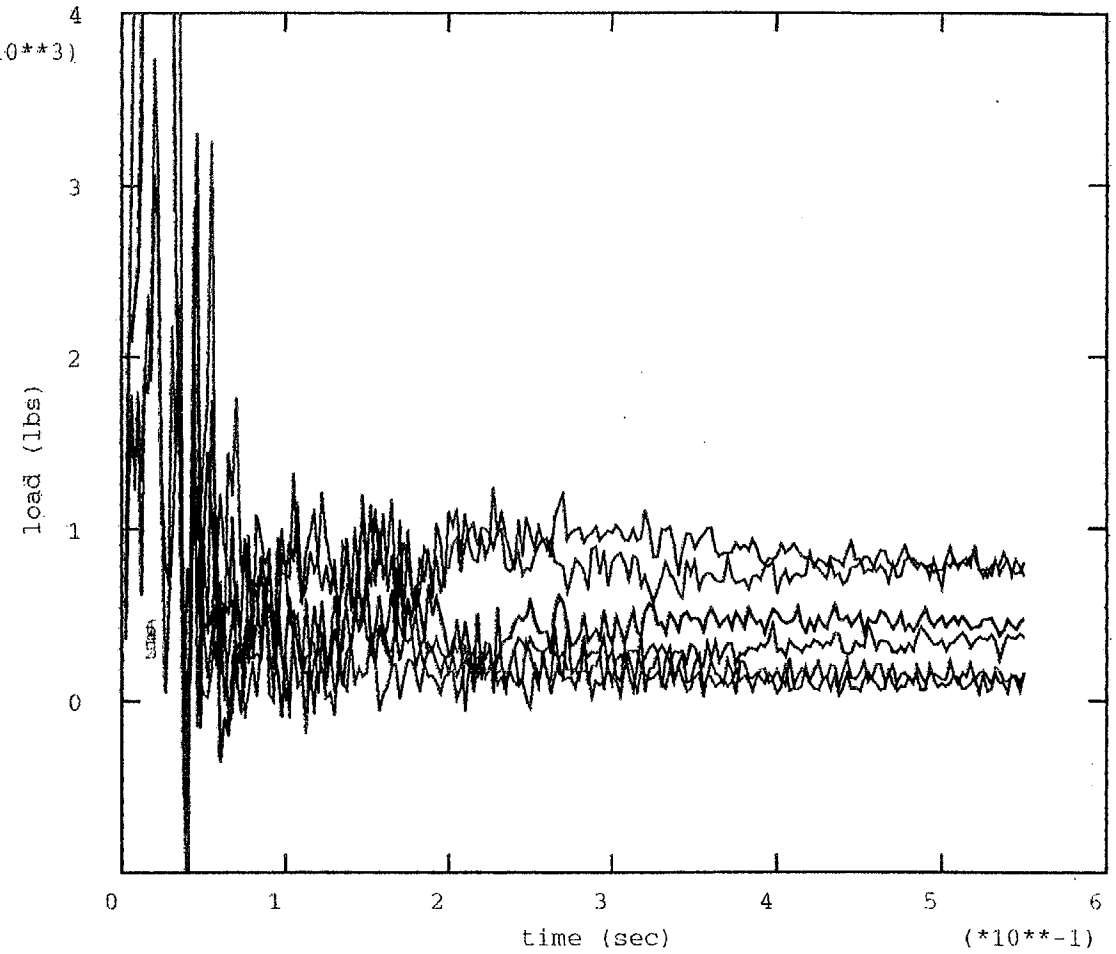

Figure C18. Bag 3 Tendon Force Time-History for Impact 3

OBLIQUE IMPACT ON ROCKS, MARS3

LINE	VARIABLE	SCALE FACTOR
1	bag 4 tendon 1	+1.00E-01
2	bag 4 tendon 2	+1.00E-01
3	bag 4 tendon 3	+1.00E-01
4	bag 4 tendon 4	+1.00E-01
5	bag 4 tendon 5	+1.00E-01
6	bag 4 tendon 6	+1.00E-01

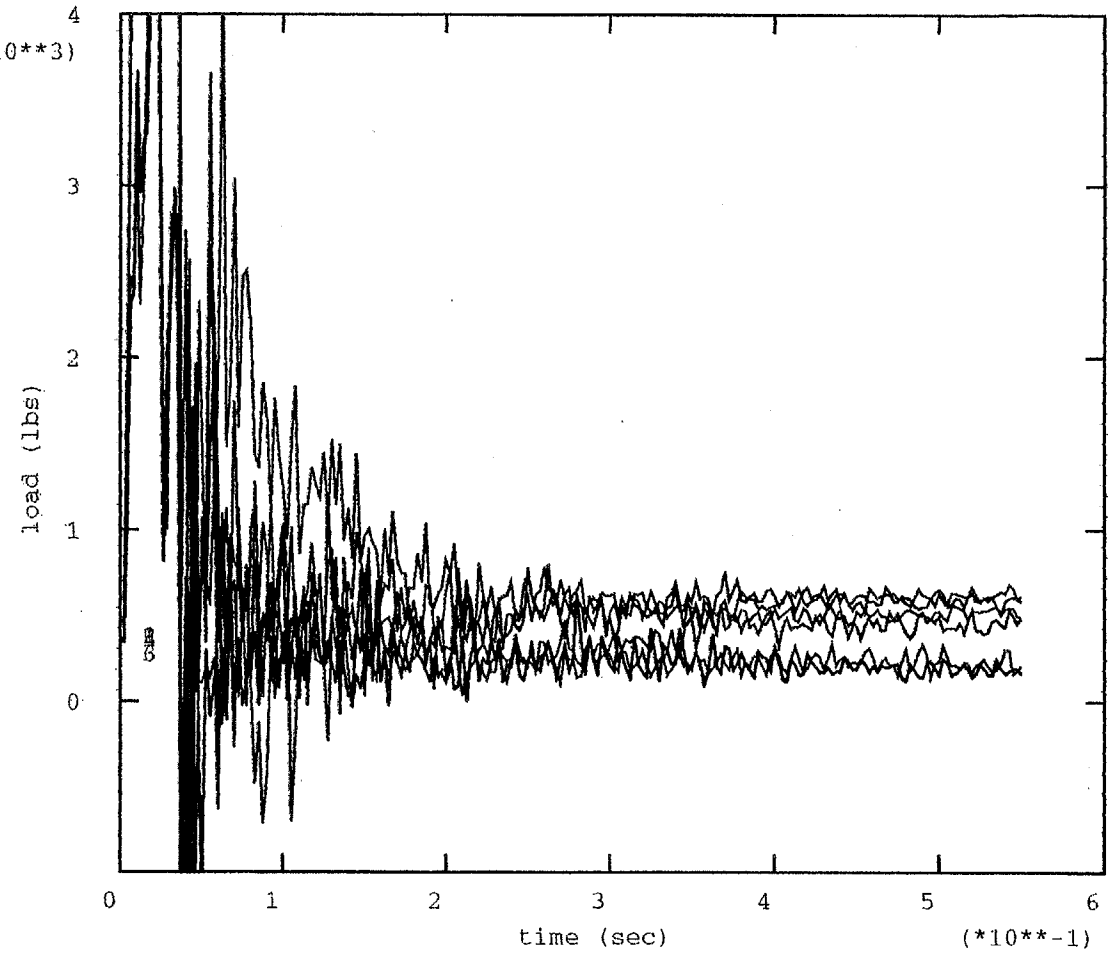

Figure C19. Bag 4 Tendon Force Time-History for Impact 3

OBLIQUE IMPACT ON ROCKS, MARS3

LINE	VARIABLE	SCALE FACTOR
1	2-4 in-line	+2.47E+00
2	2-4 norm	+1.58E+00
3	2-3 in-line	+2.47E+00
4	2-3 norm	+1.58E+00
5	3-4 in-line	+2.47E+00
6	3-4 norm	+1.58E+00

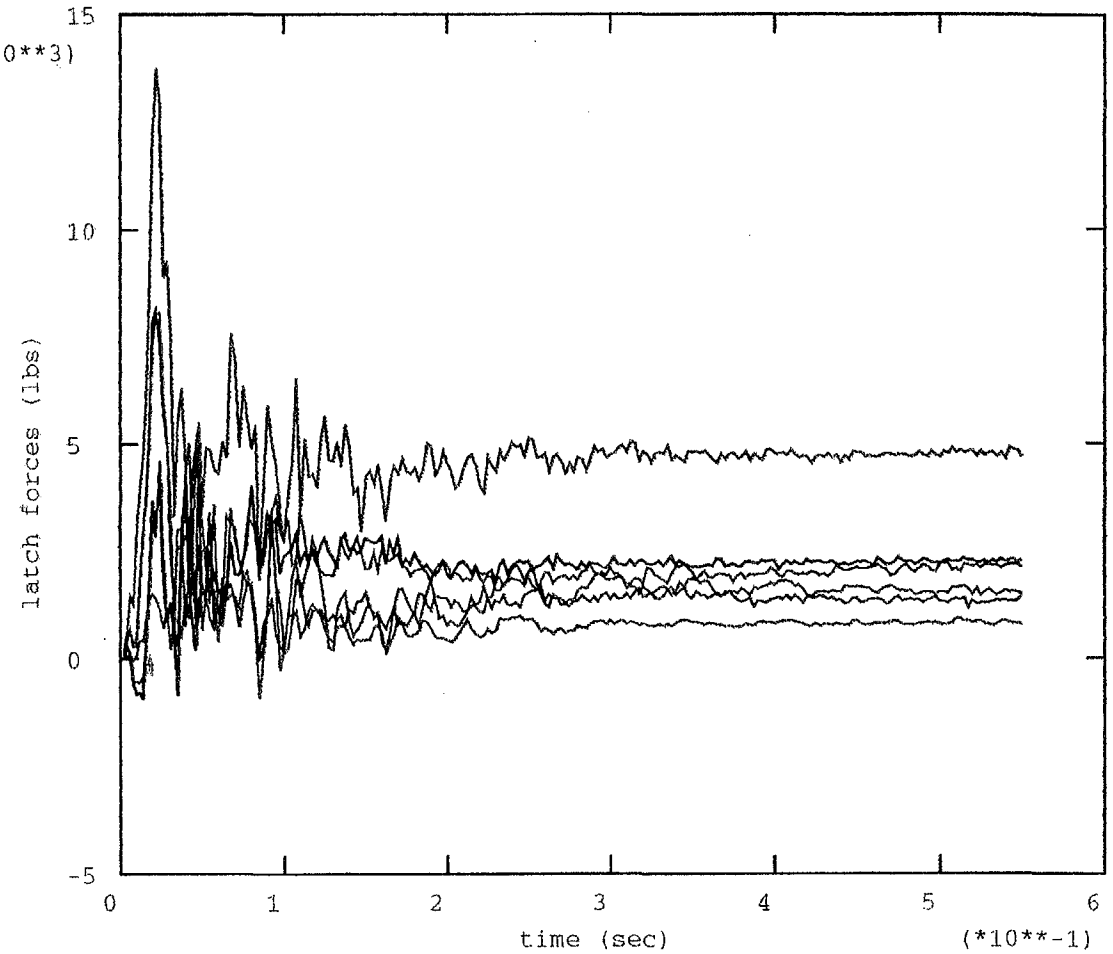

Figure C20. Latch Force Time-History for Impact 3

OBLIQUE IMPACT ON ROCKS, MARS3

LINE	VARIABLE	SCALE FACTOR
1	p4 in-line	+2.71E+00
2	p4 norm	+2.38E+00
3	p4 in-line	+2.71E+00
4	p4 norm	+2.23E+00
5	p2 in-line	+2.71E+00
6	p2 norm	+2.23E+00
7	p3 in-line	+2.71E+00
8	p3 norm	-2.67E-01
10	p3 norm	+3.05E+00
11	p3 in-line	+2.67E+00
12	p3 norm	+3.05E+00

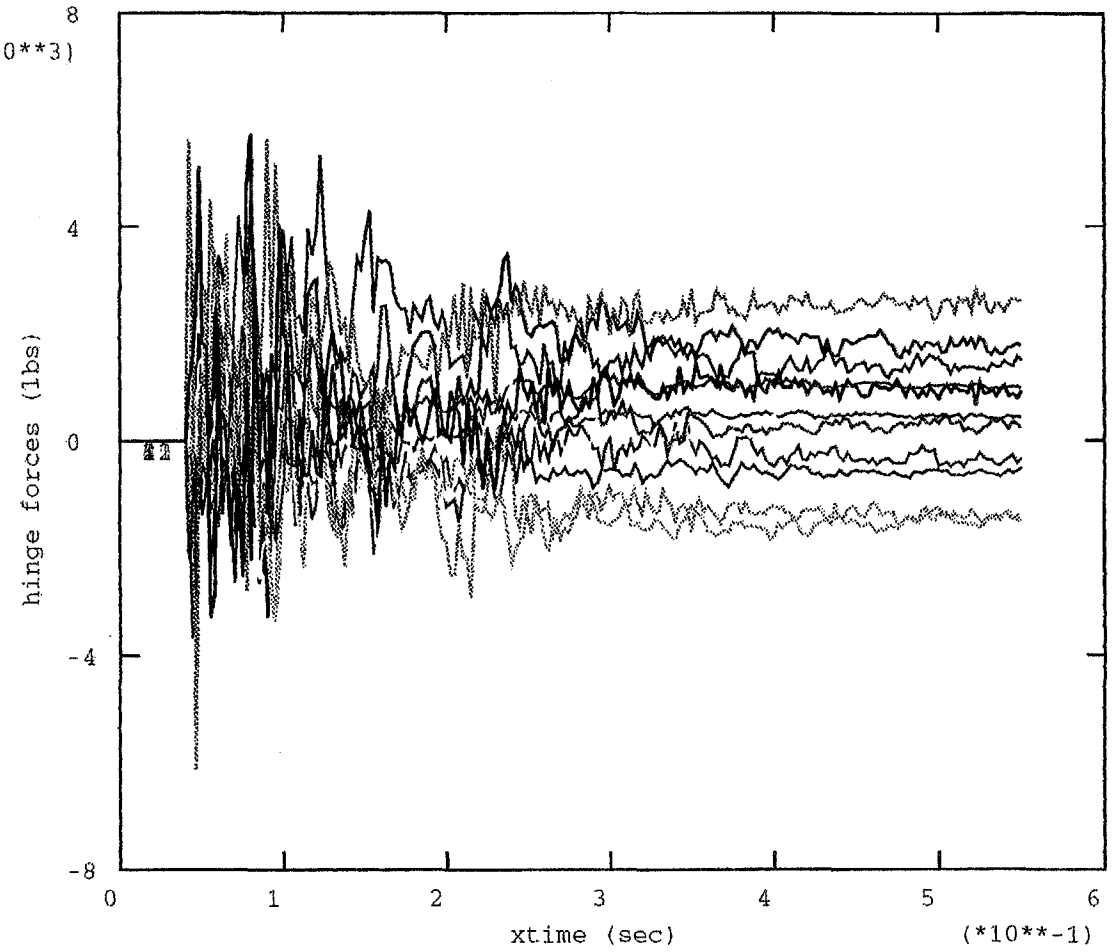

Figure C21. Hinge Force Time-History for Impact 3

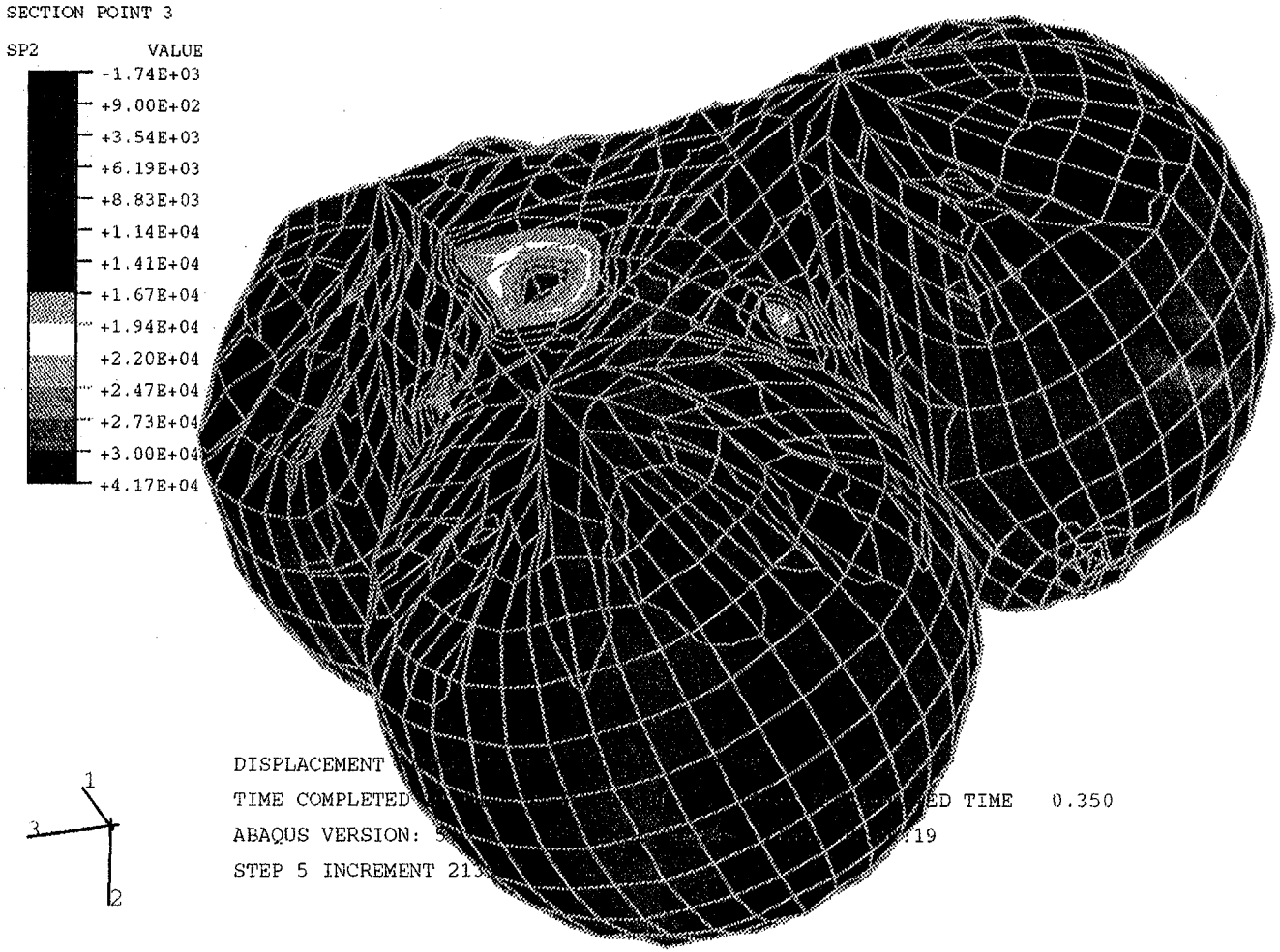

Figure C22. Maximum Principal Stress for Lander Side of Bottom Airbag for Impact 3

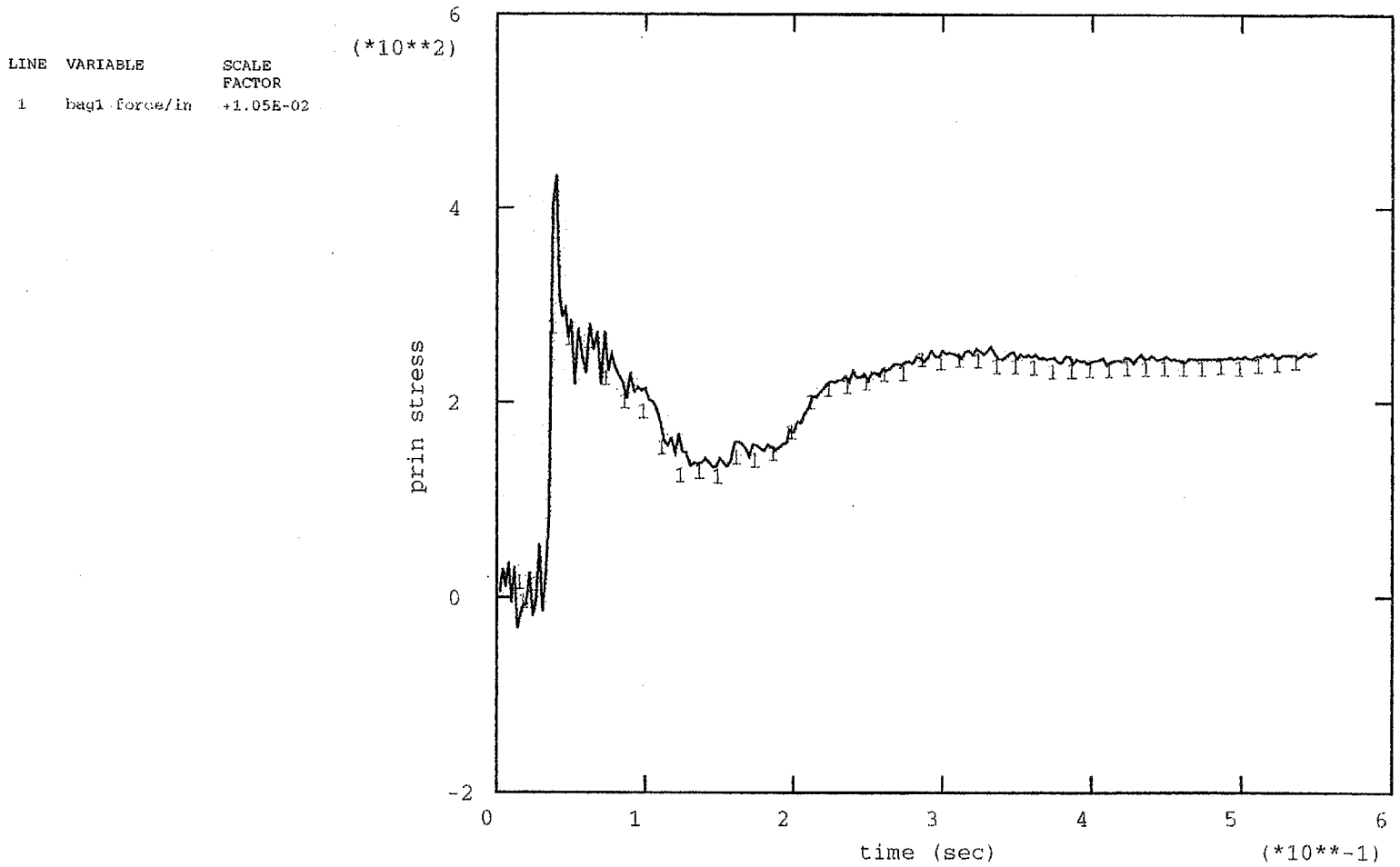

Figure C23. Fabric Force Time-History for Lander Side of Airbag 1 for Impact 3

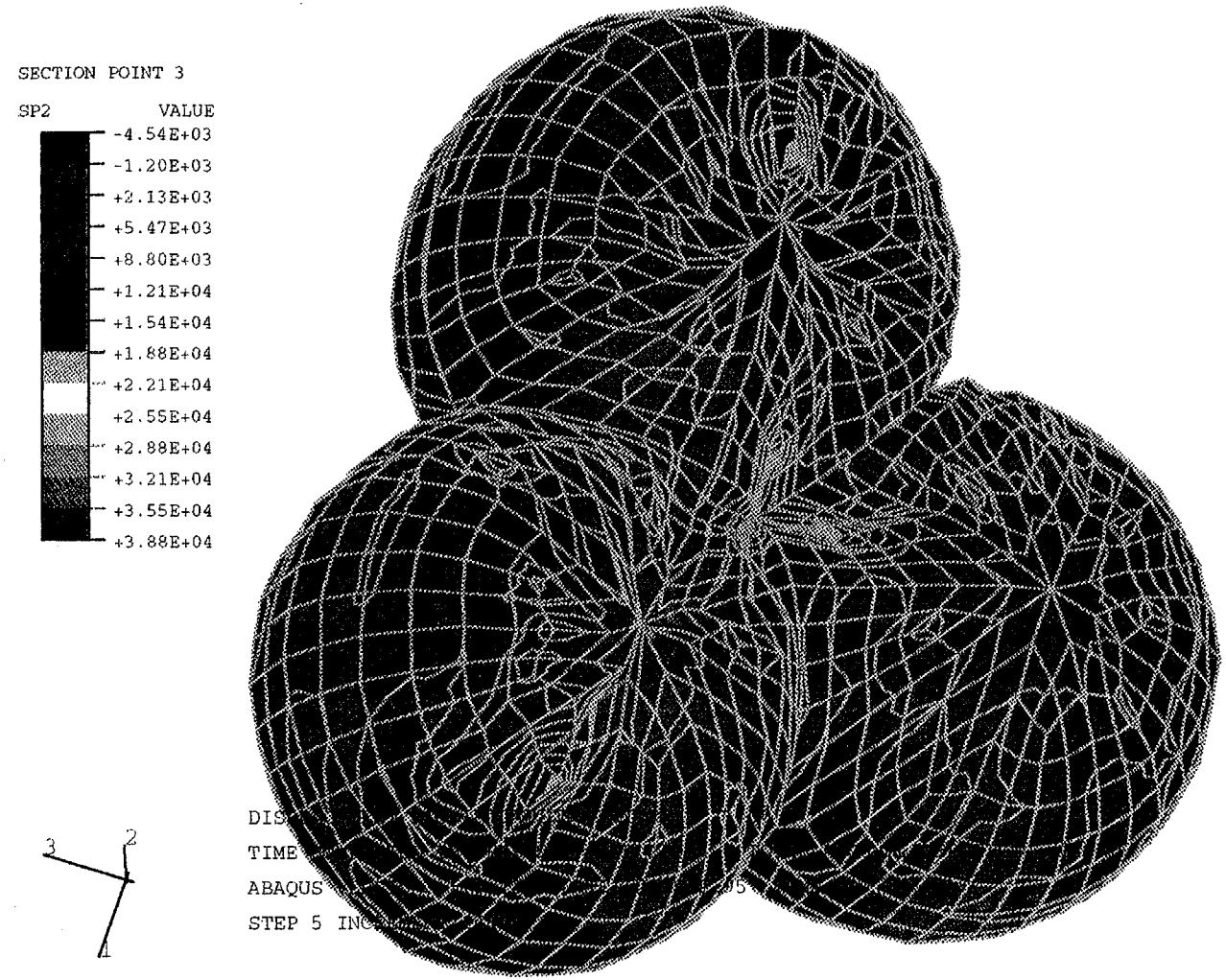

Figure C24. Maximum Principal Stress for Bottom of Bottom Airbag for Impact 3

LINE	VARIABLE	SCALE FACTOR
1	tear for/in	+1.05E-02

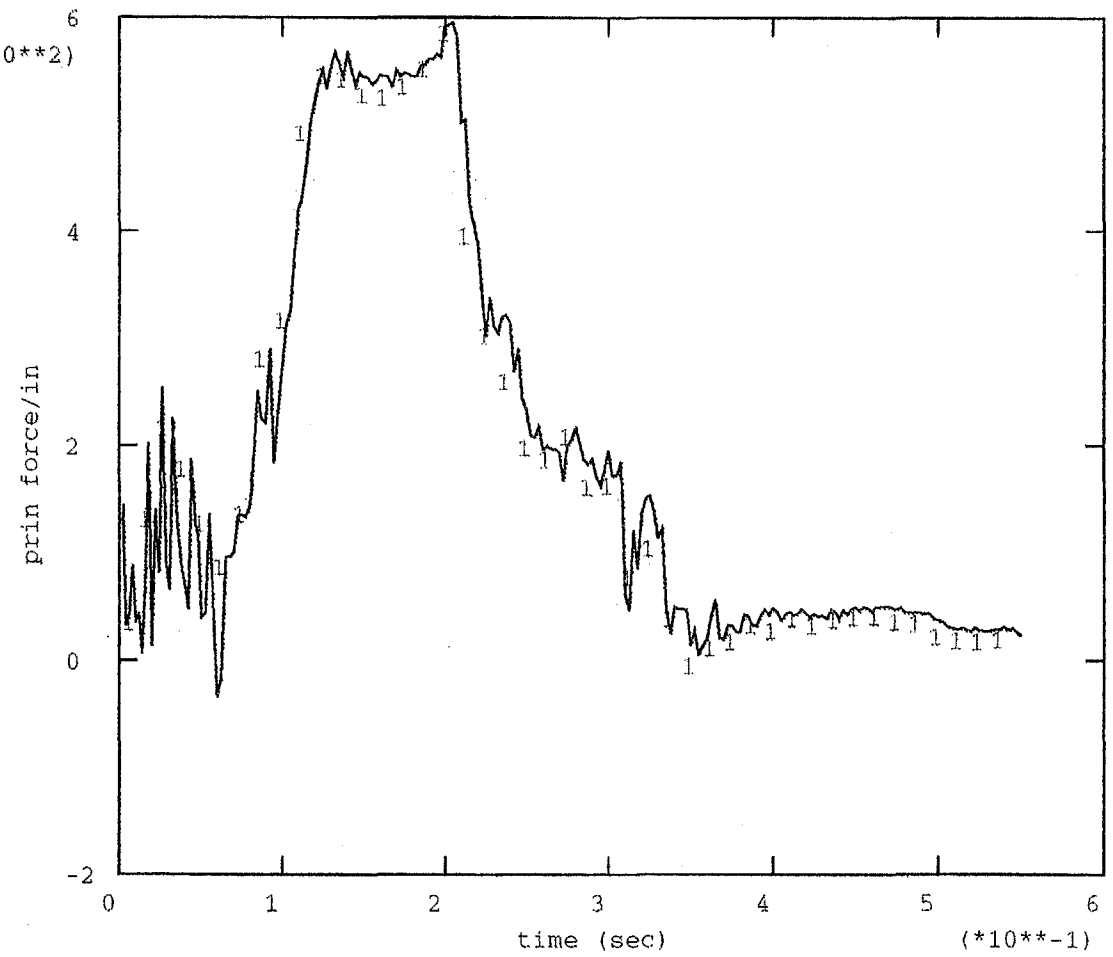

Figure C25. Bottom Portion of Airbag 1 Fabric Force Time-History For Impact 3

Appendix D

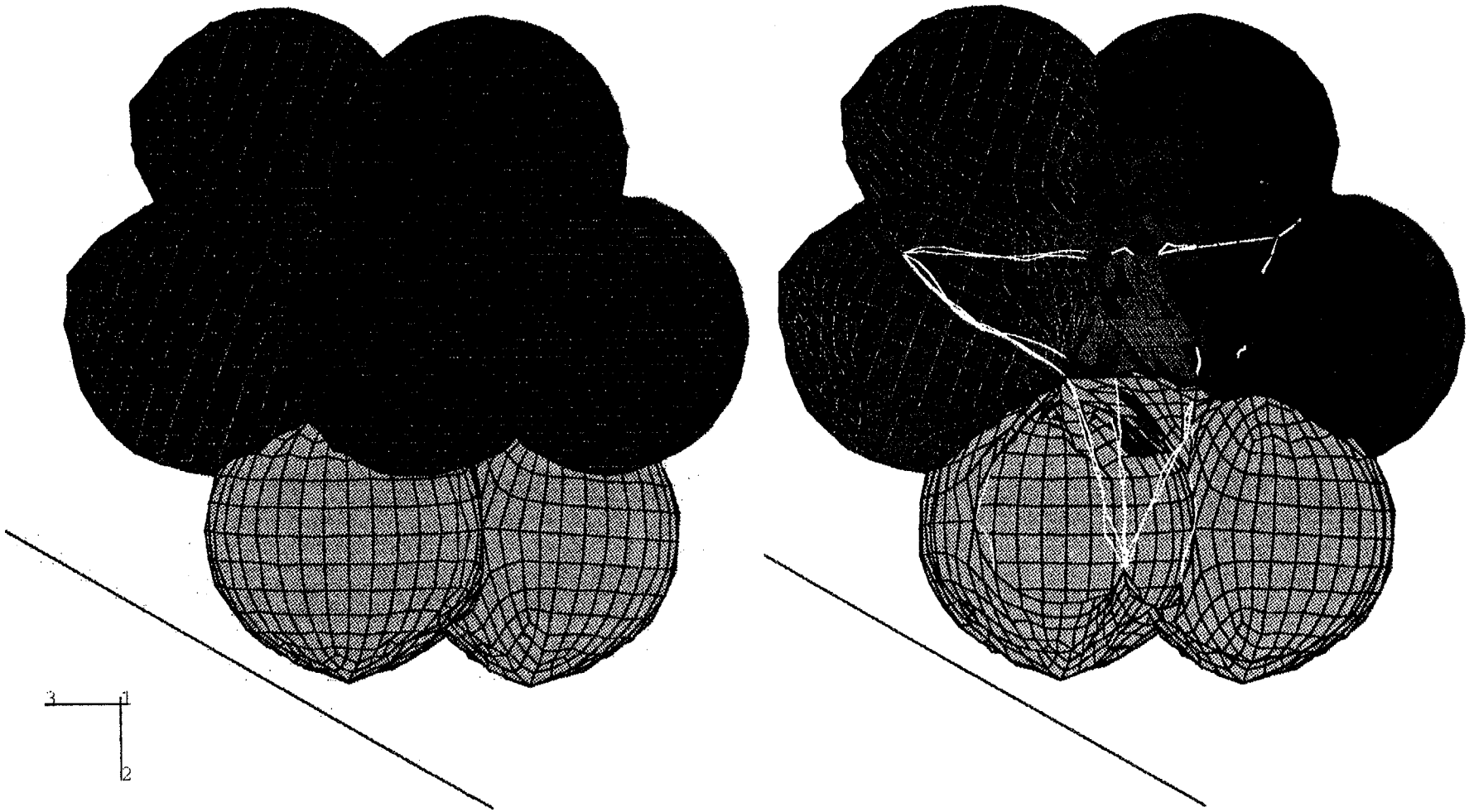

Figure D1. Deformed Mesh at 0 msec Into Impact 4

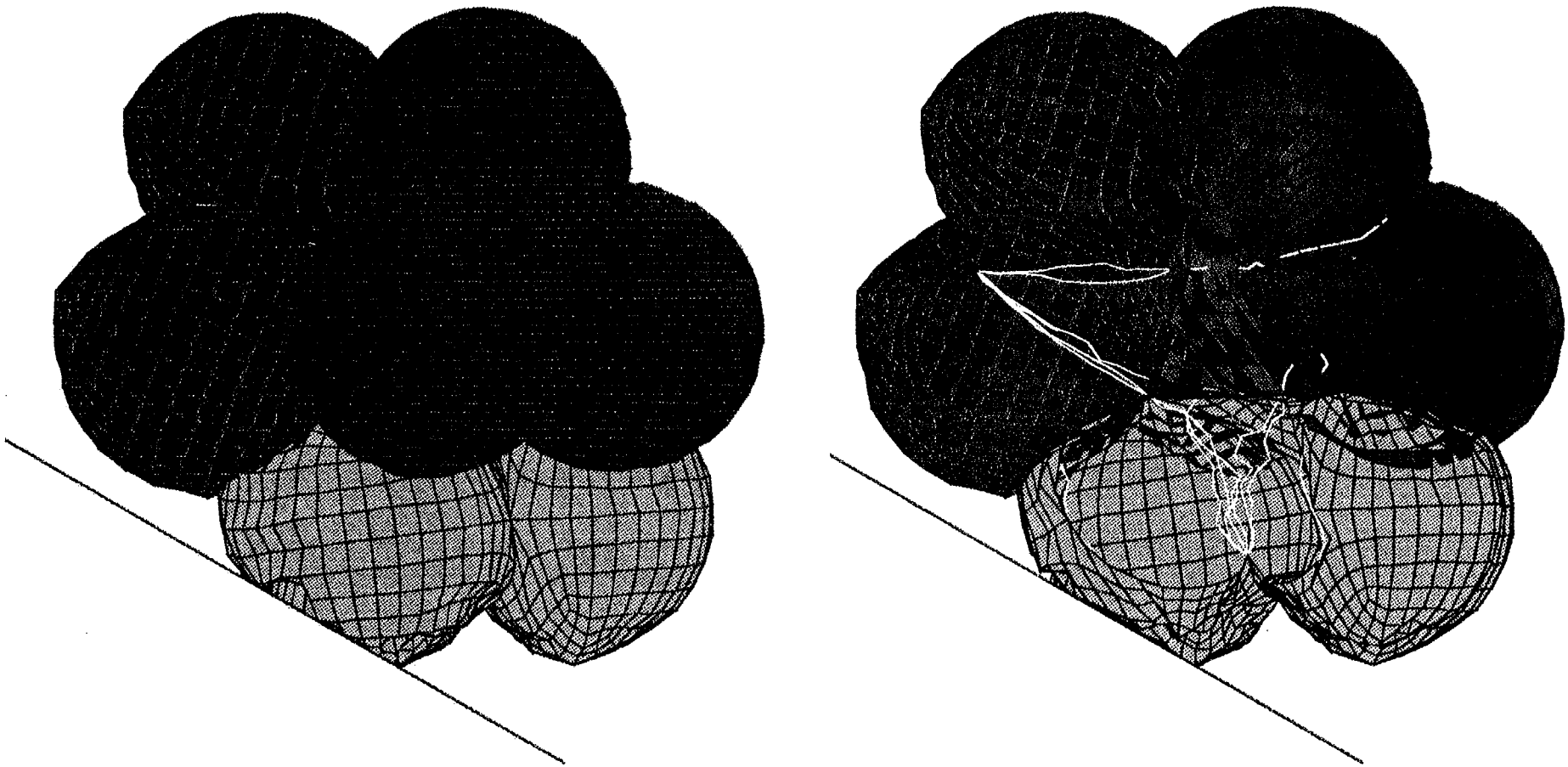

Figure D2. Deformed Mesh at 37.5 msec Into Impact 4

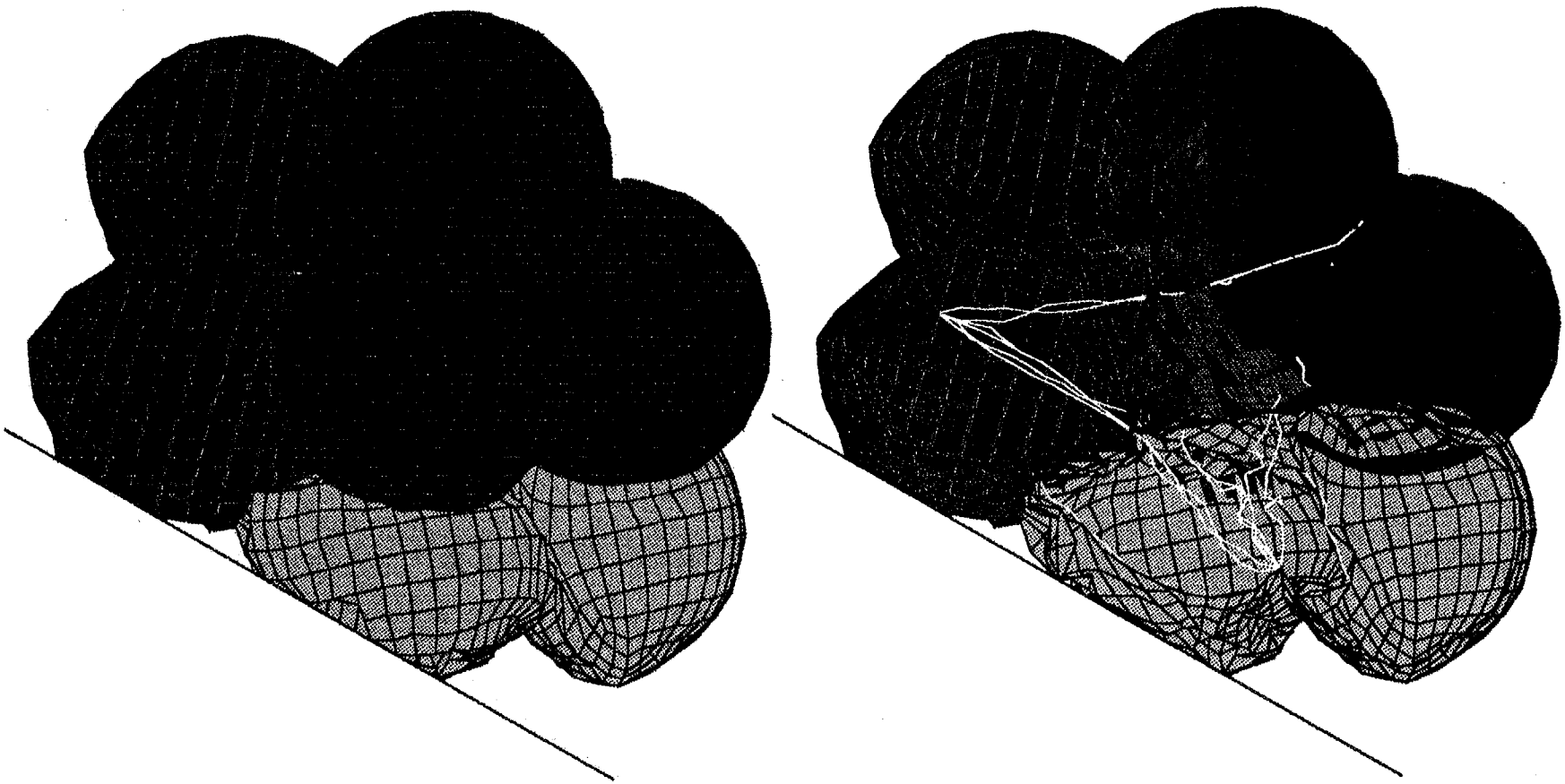

Figure D3. Deformed Mesh at 75 msec Into Impact 4

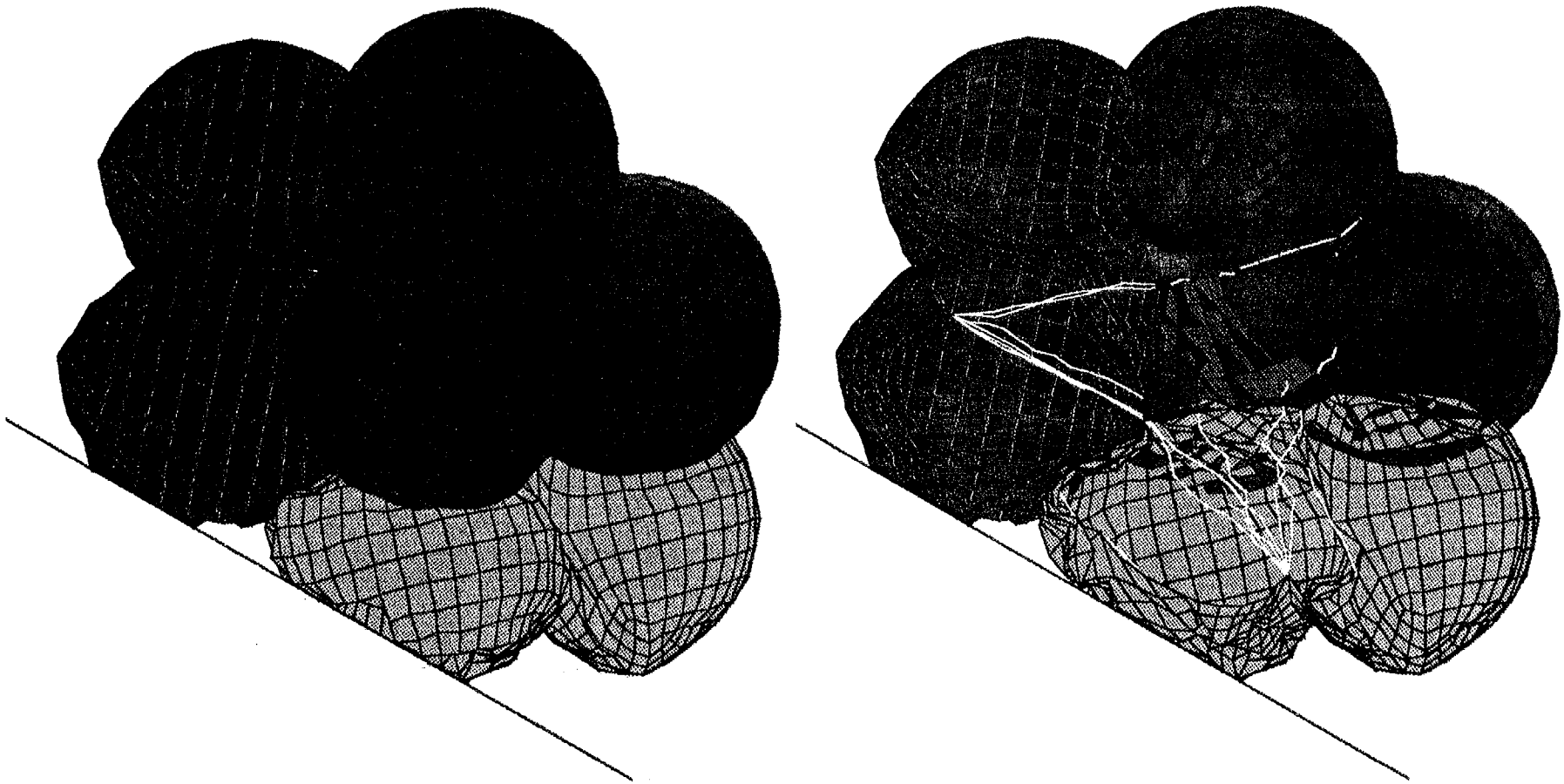

Figure D4. Deformed Mesh at 112.5 msec Into Impact 4

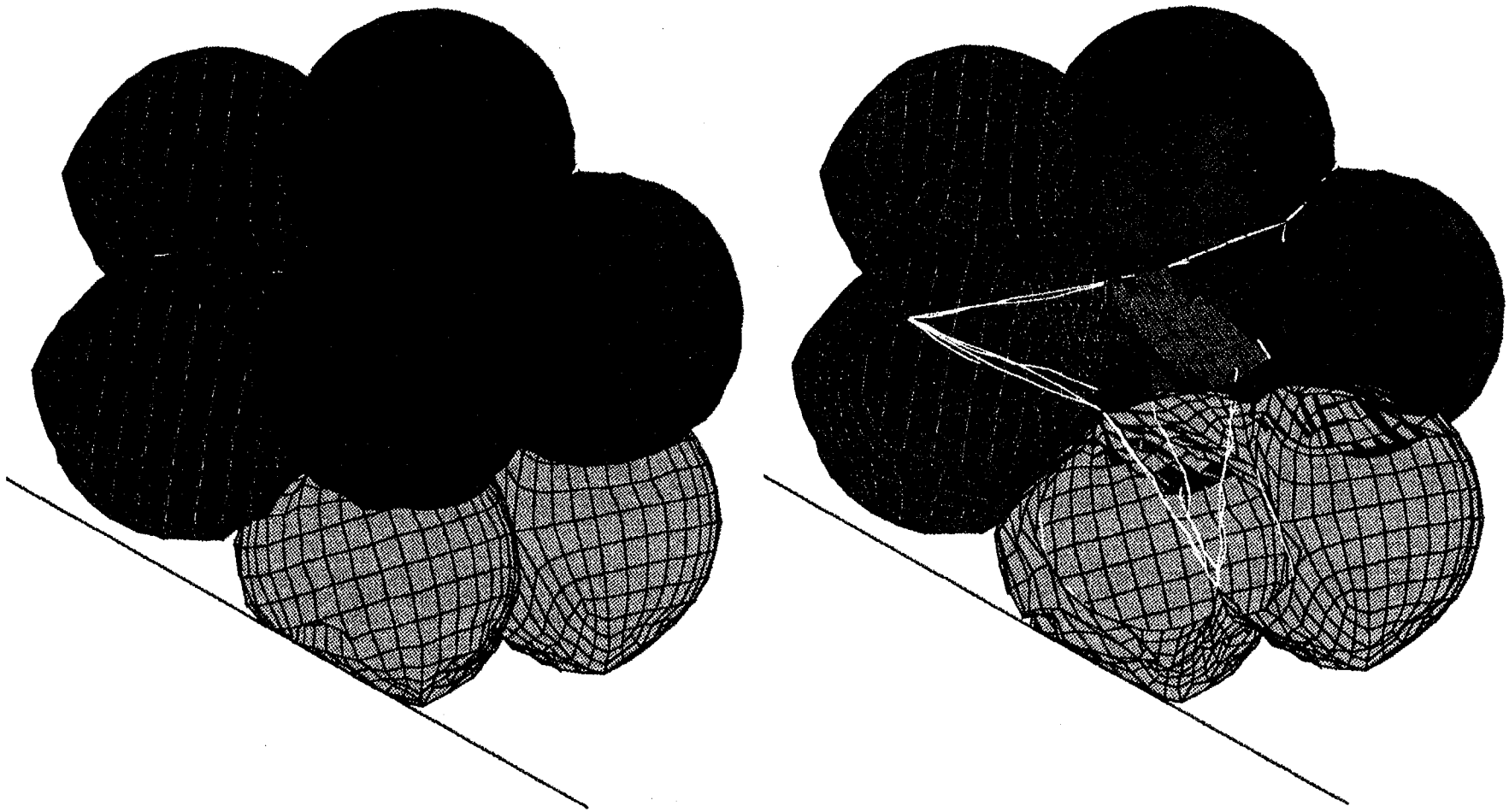

Figure D5. Deformed Mesh at 150 msec Into Impact 4

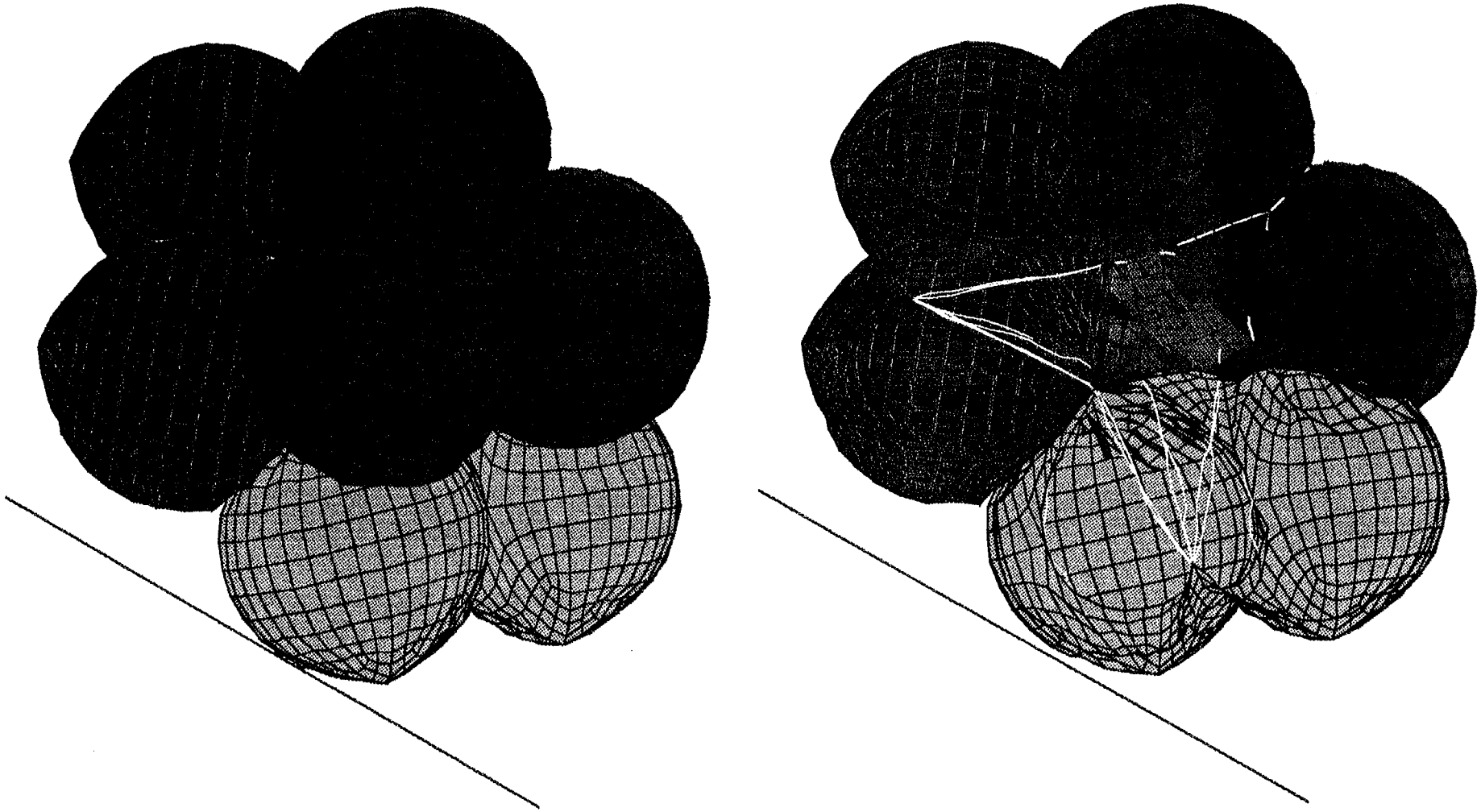

FiBure D6. Deformed Mesh at 187.5 msec Into Impact 4

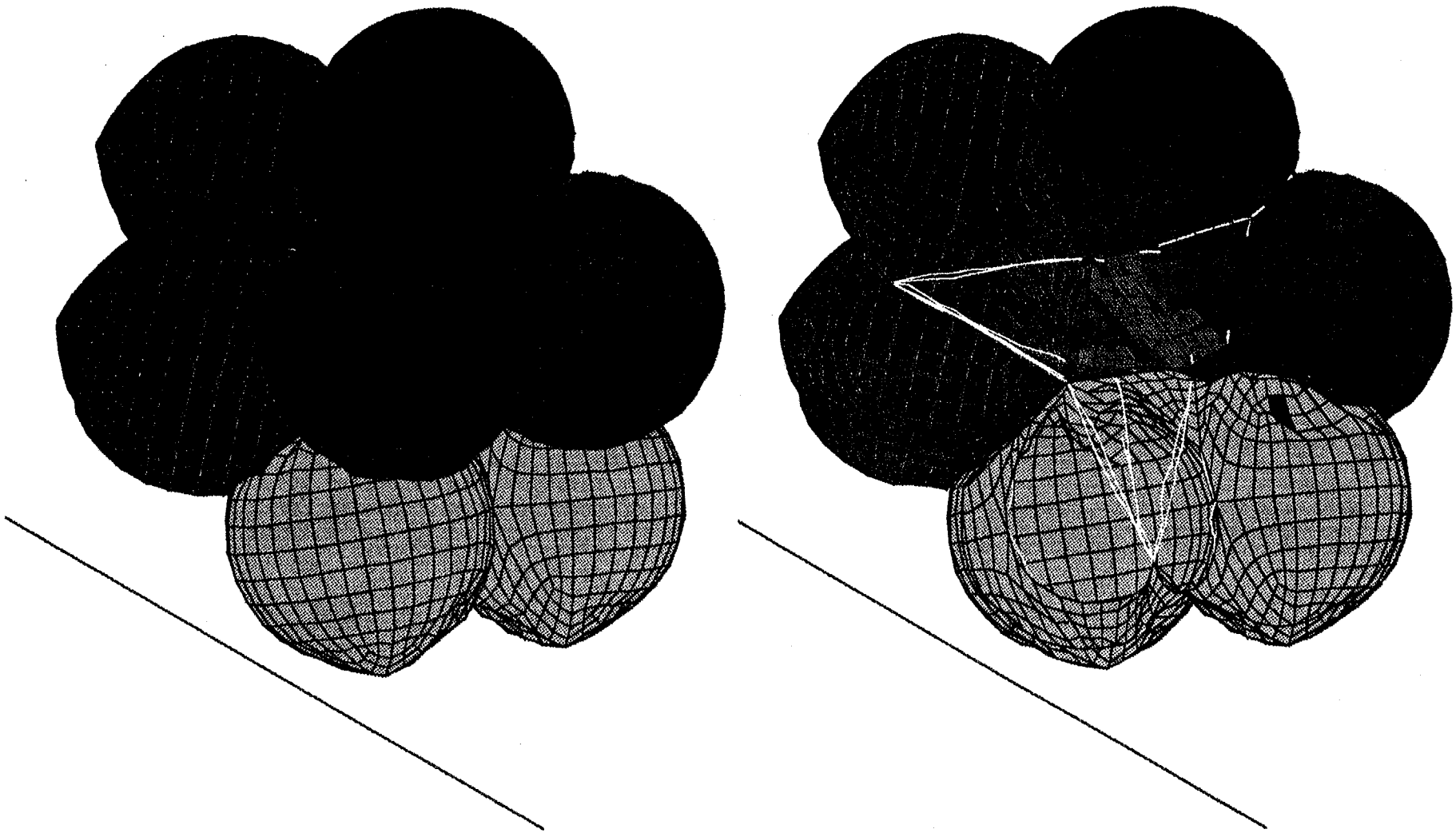

Figure D7. Deformed Mesh at 225 msec Into Impact 4

Mars 4 - Oblique impact at 20 m/sec, 30 degree inclined plane

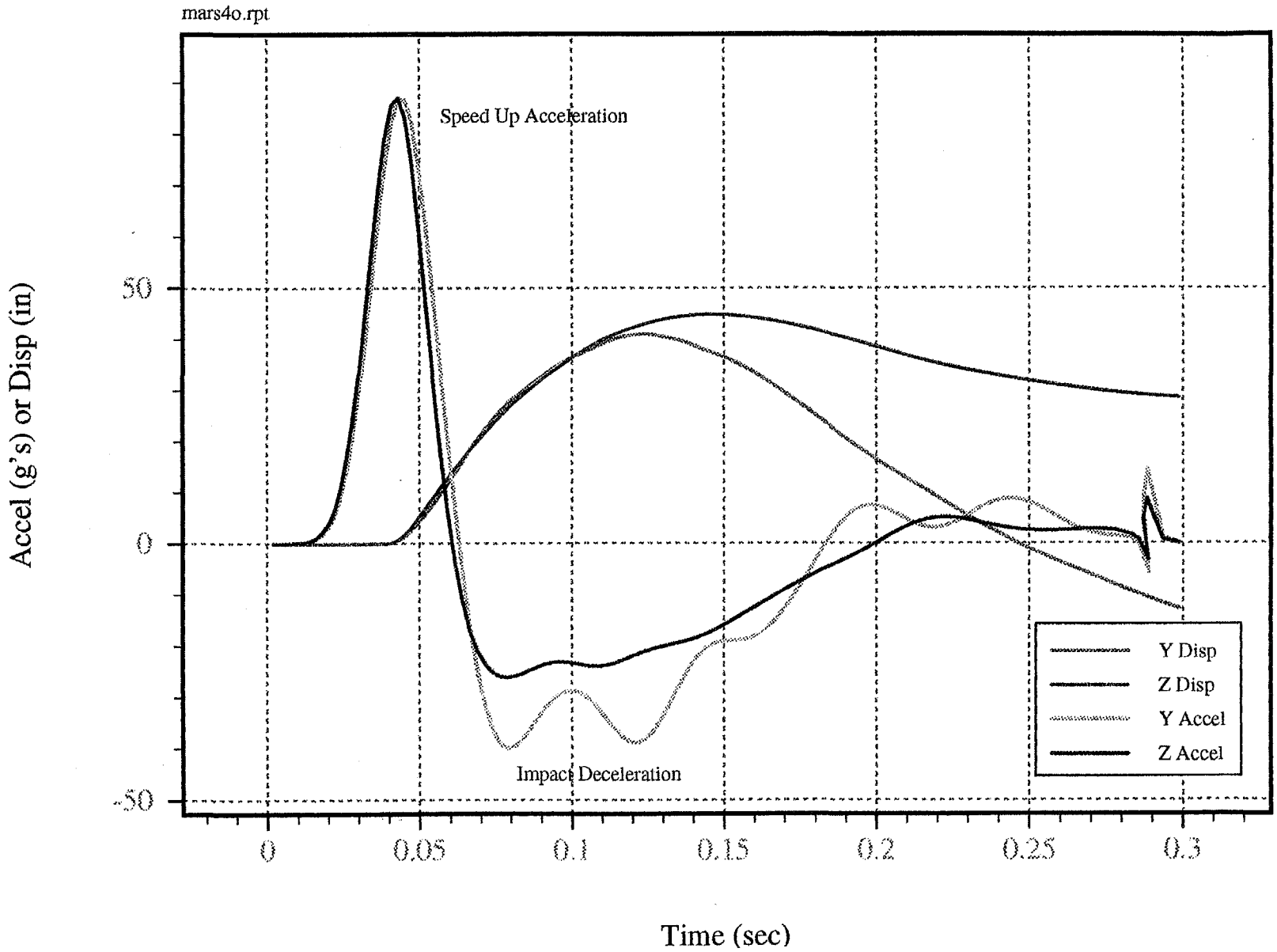

Figure D8. Lander C.G. Acceleration Time-History for Impact 4

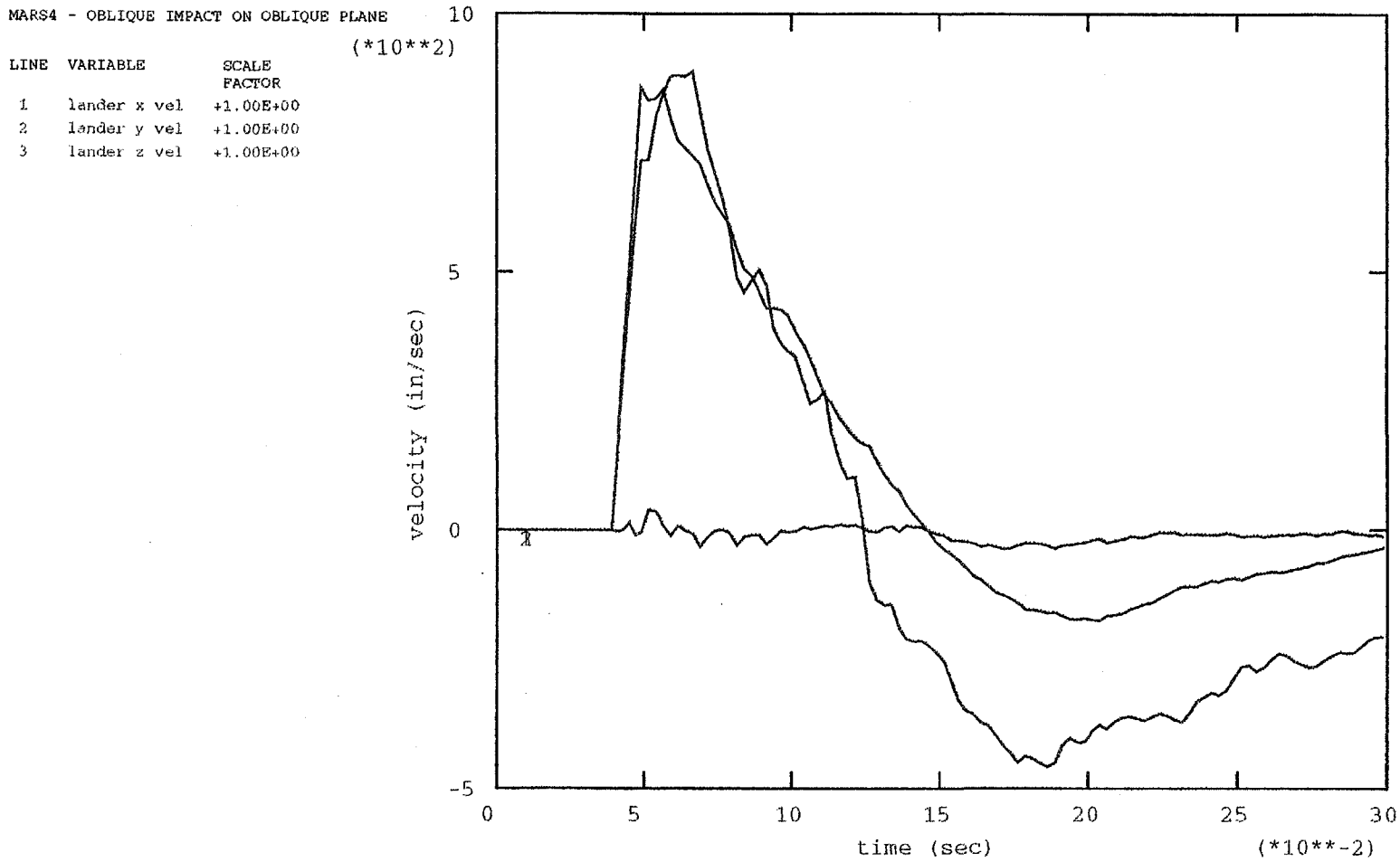

Figure D9. Lander C.G. Velocity Time-History for Impact 4

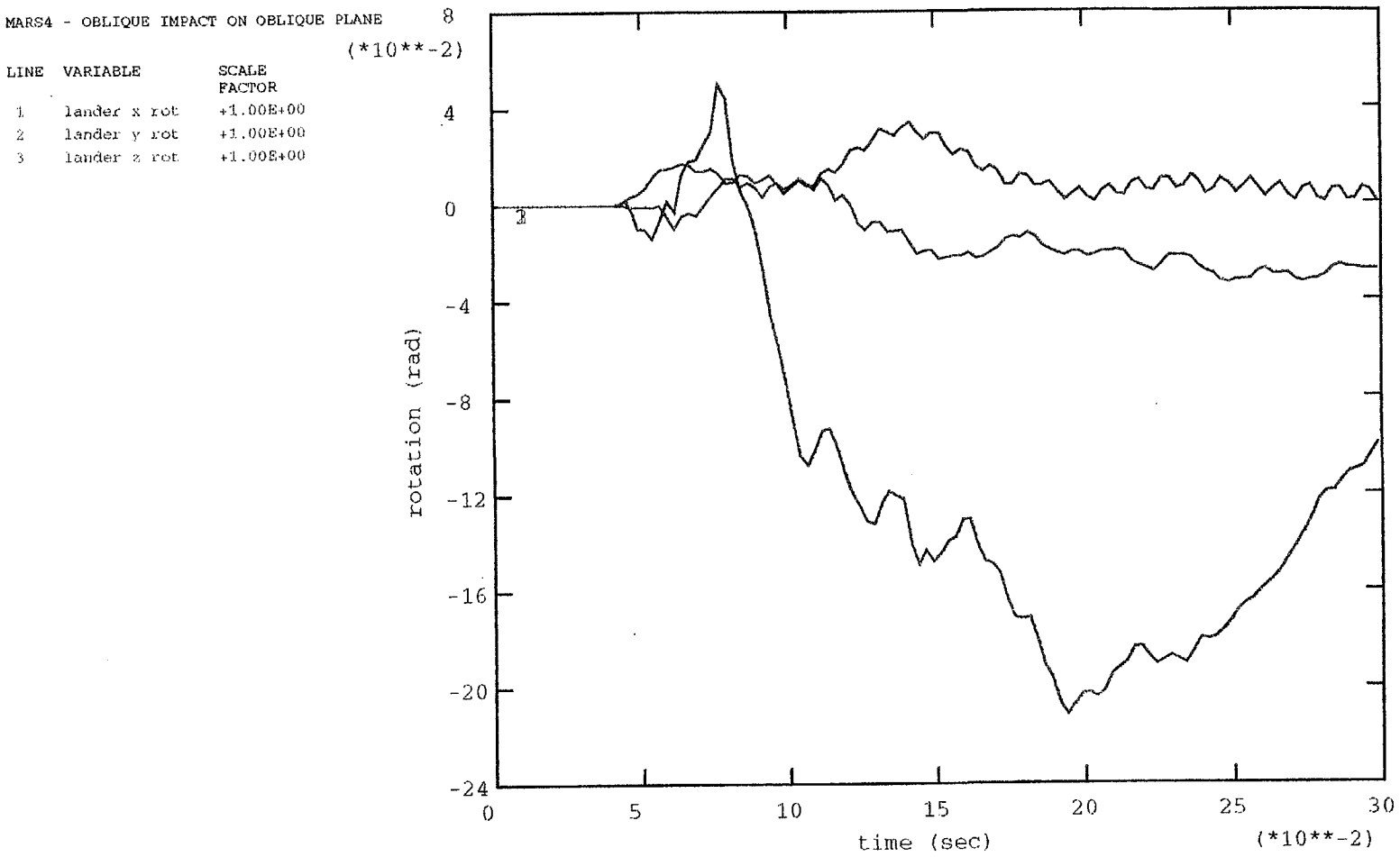

Figure D10. Lander C.G. RotationTime-History for Impact 4

MARS4 - OBLIQUE IMPACT ON OBLIQUE PLANE

LINE	VARIABLE	SCALE FACTOR
1	land x rot vel	+1.00E+00
2	land x rot vel	+1.00E+00
3	land x rot vel	+1.00E+00

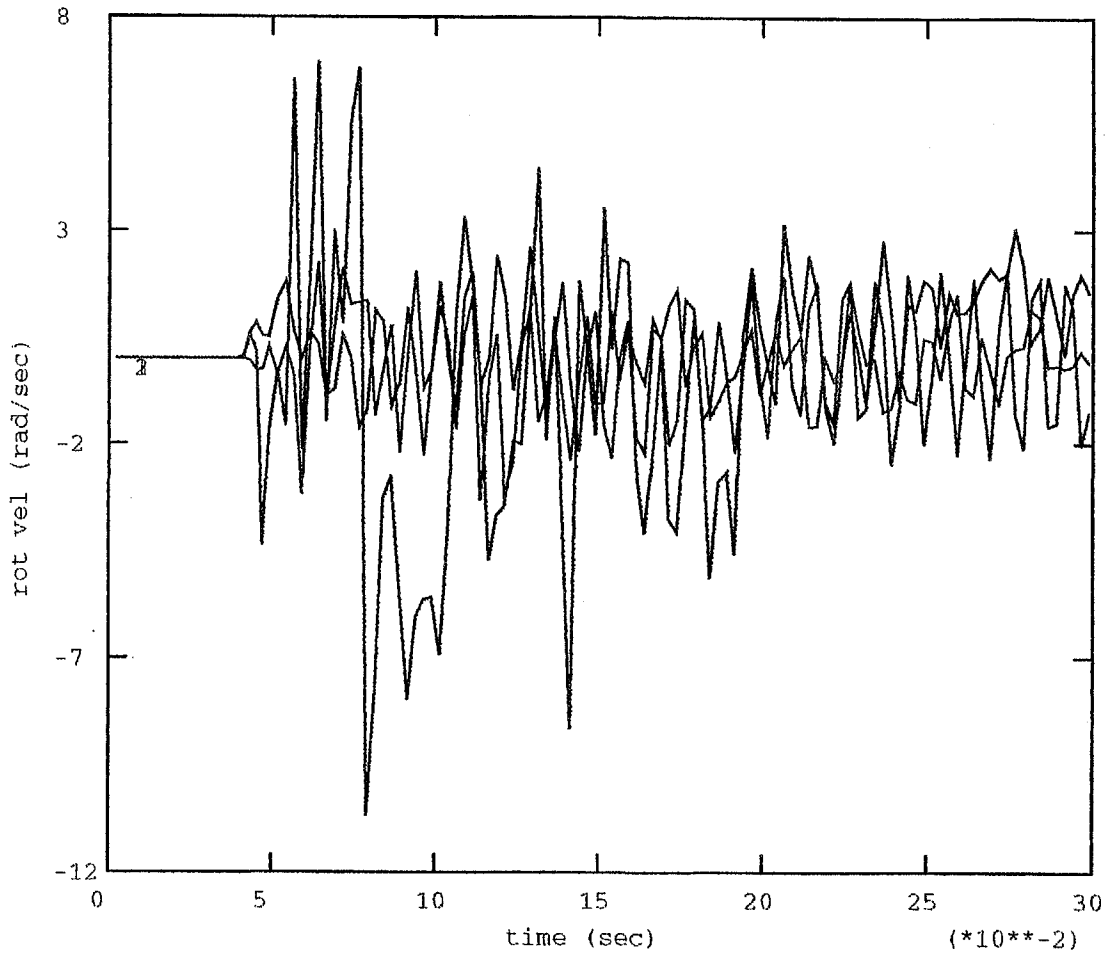

Figure D11. Dander C.G. Rotational Velocity Time-History for Impact 4

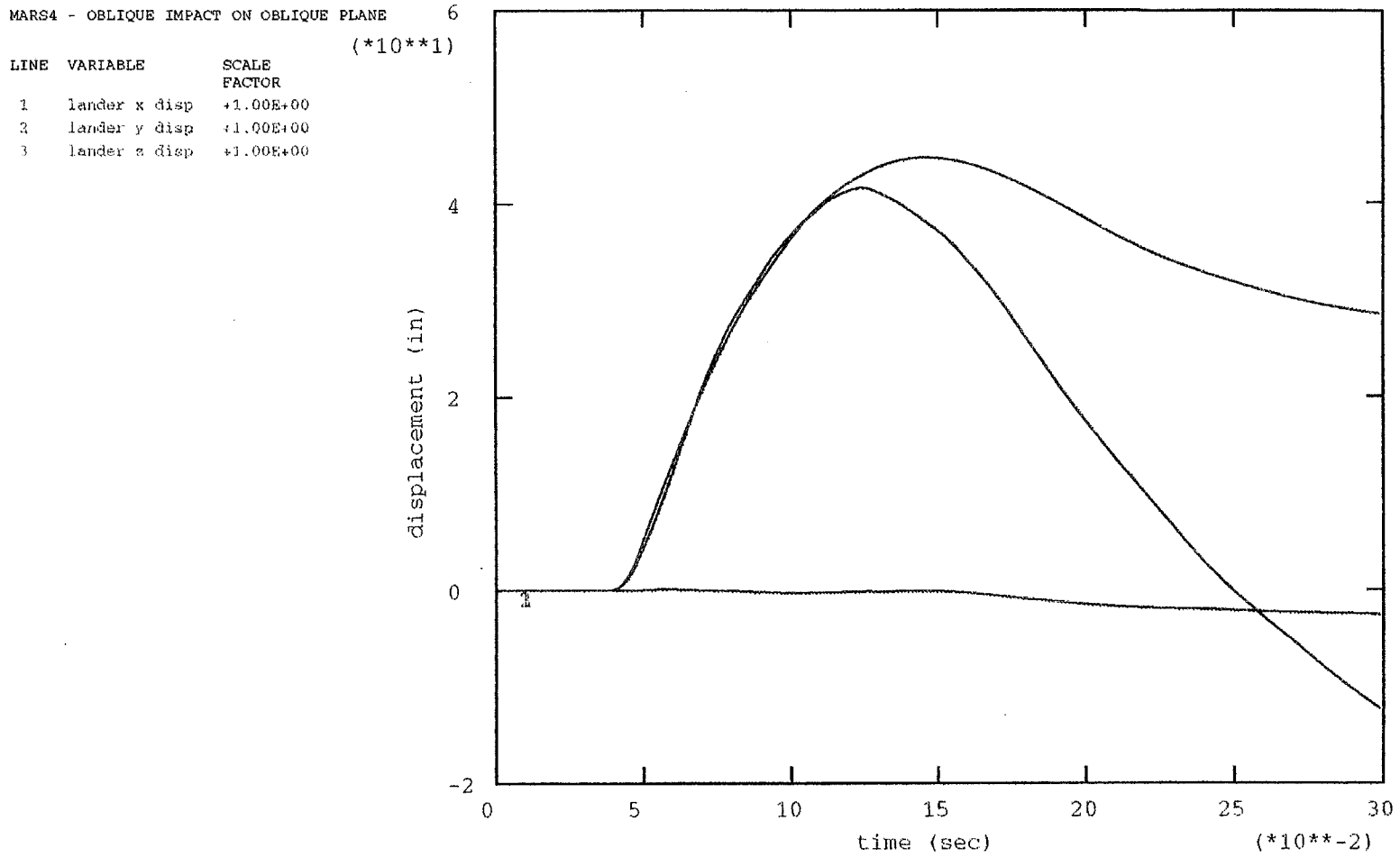

Figure D12. Lander C.G. Displacement Time-History for Impact 4

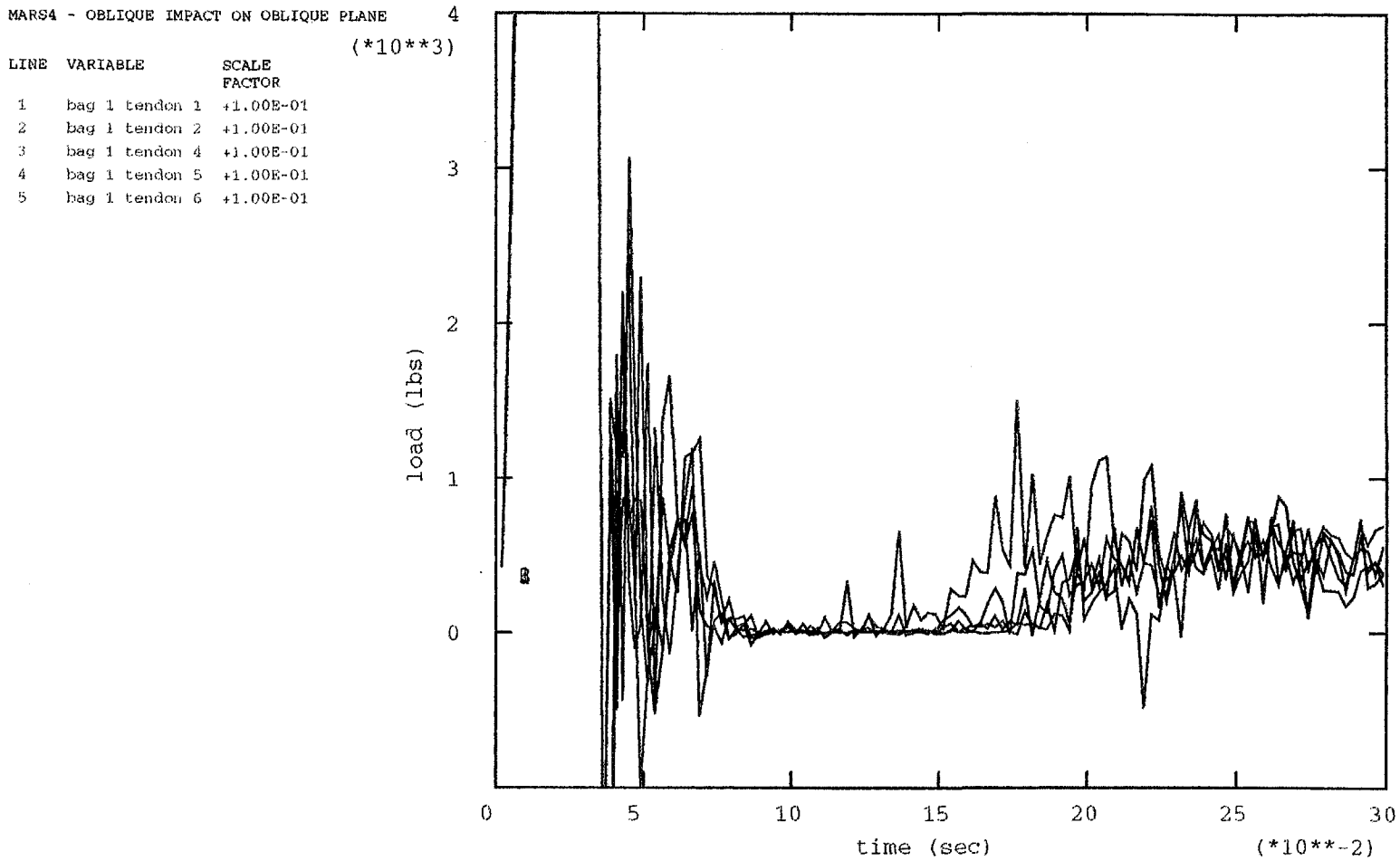

Figure D13. Bag 1 Tendon Force Time-History for Impact 4

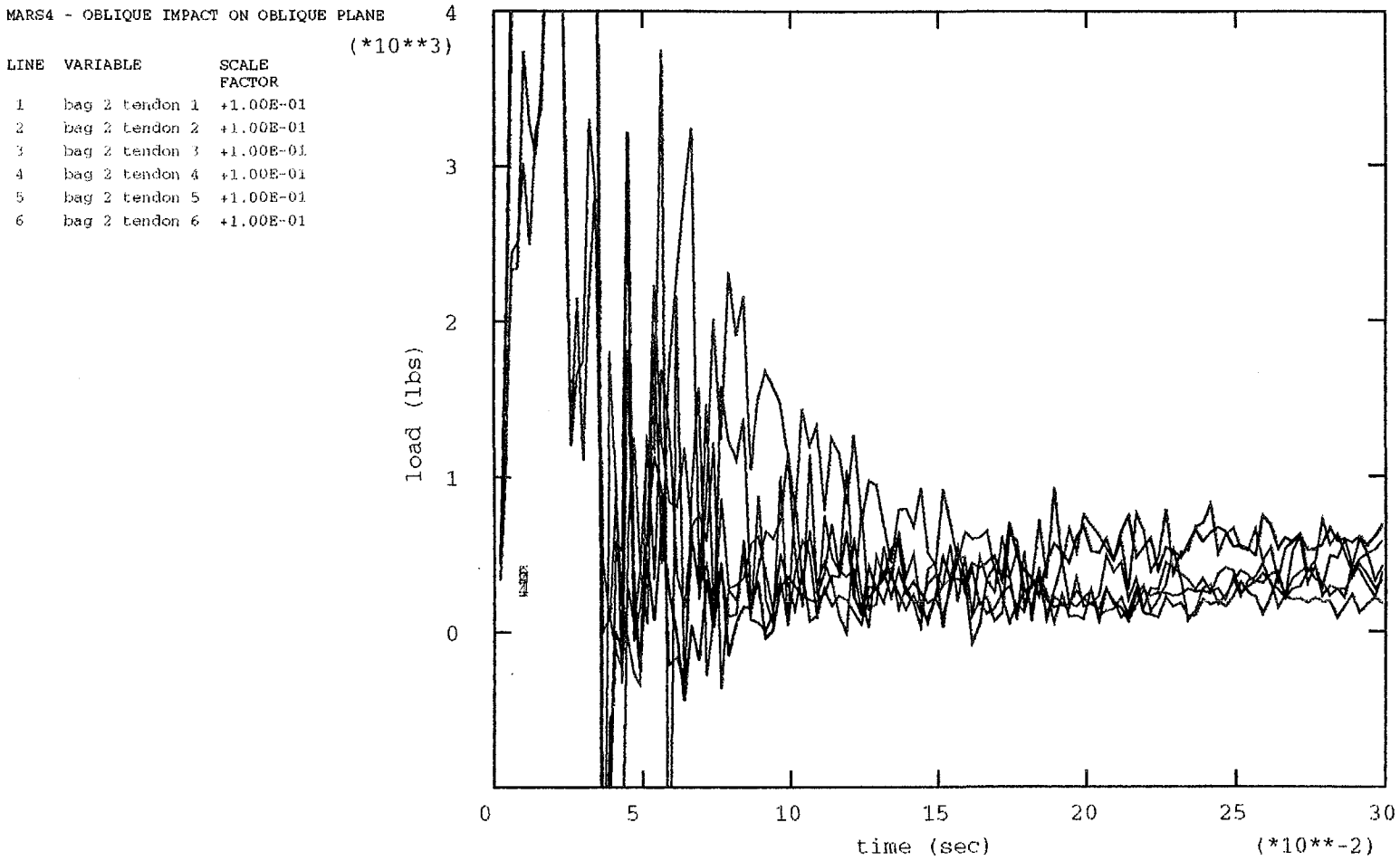

Figure D14. Bag 2 Tendon Force Time-History for Impact 4

MARS4 - OBLIQUE IMPACT ON OBLIQUE PLANE

LINE	VARIABLE	SCALE FACTOR
1	bag 3 tendon 1	+1.00E-01
2	bag 3 tendon 2	+1.00E-01
3	bag 3 tendon 3	+1.00E-01
4	bag 3 tendon 4	+1.00E-01
5	bag 3 tendon 5	+1.00E-01
6	bag 3 tendon 6	+1.00E-01

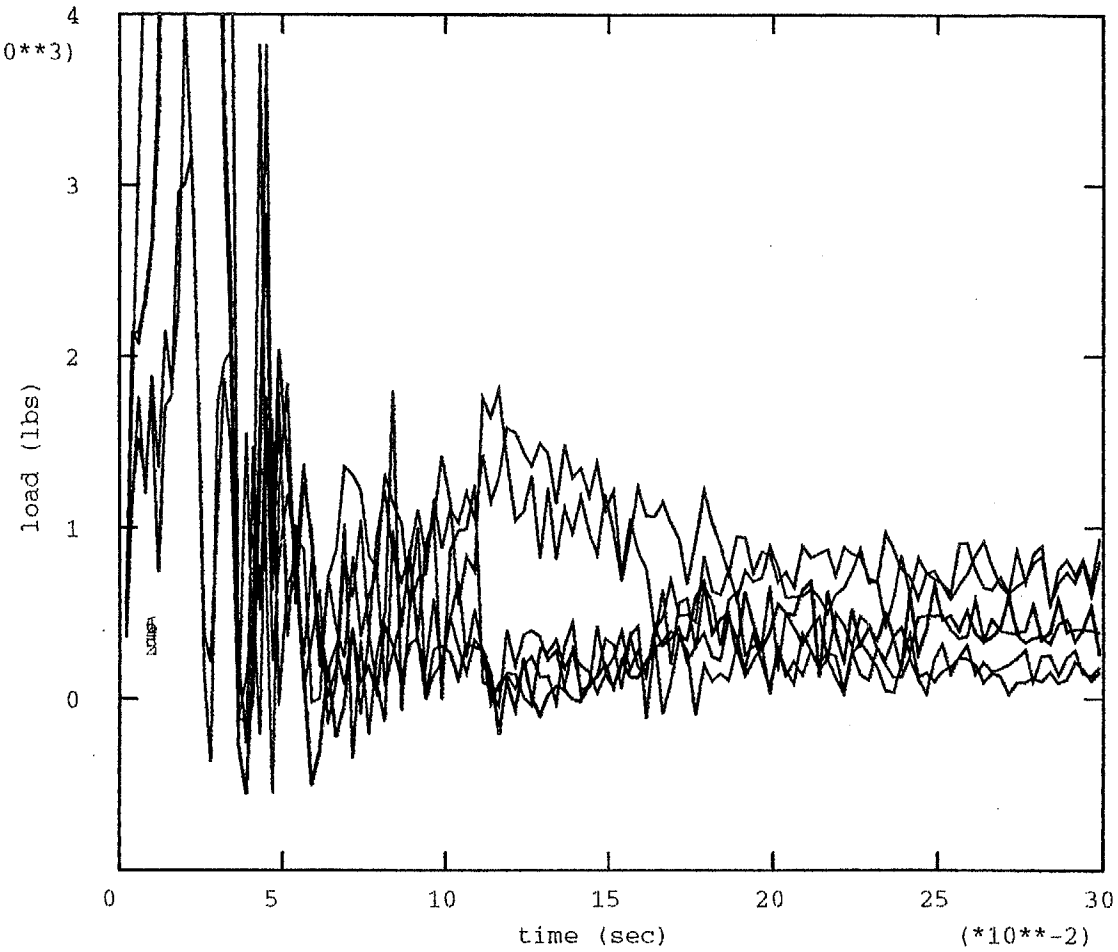

Figure D15. Bag 3 Tendon Force Time-History for Impact 4

MARS4 - OBLIQUE IMPACT ON OBLIQUE PLANE

LINE	VARIABLE	SCALE FACTOR
1	bag 4 tendon 1	+1.00E-01
2	bag 4 tendon 2	+1.00E-01
3	bag 4 tendon 3	+1.00E-01
4	bag 4 tendon 4	+1.00E-01
5	bag 4 tendon 5	+1.00E-01
6	bag 4 tendon 6	+1.00E-01

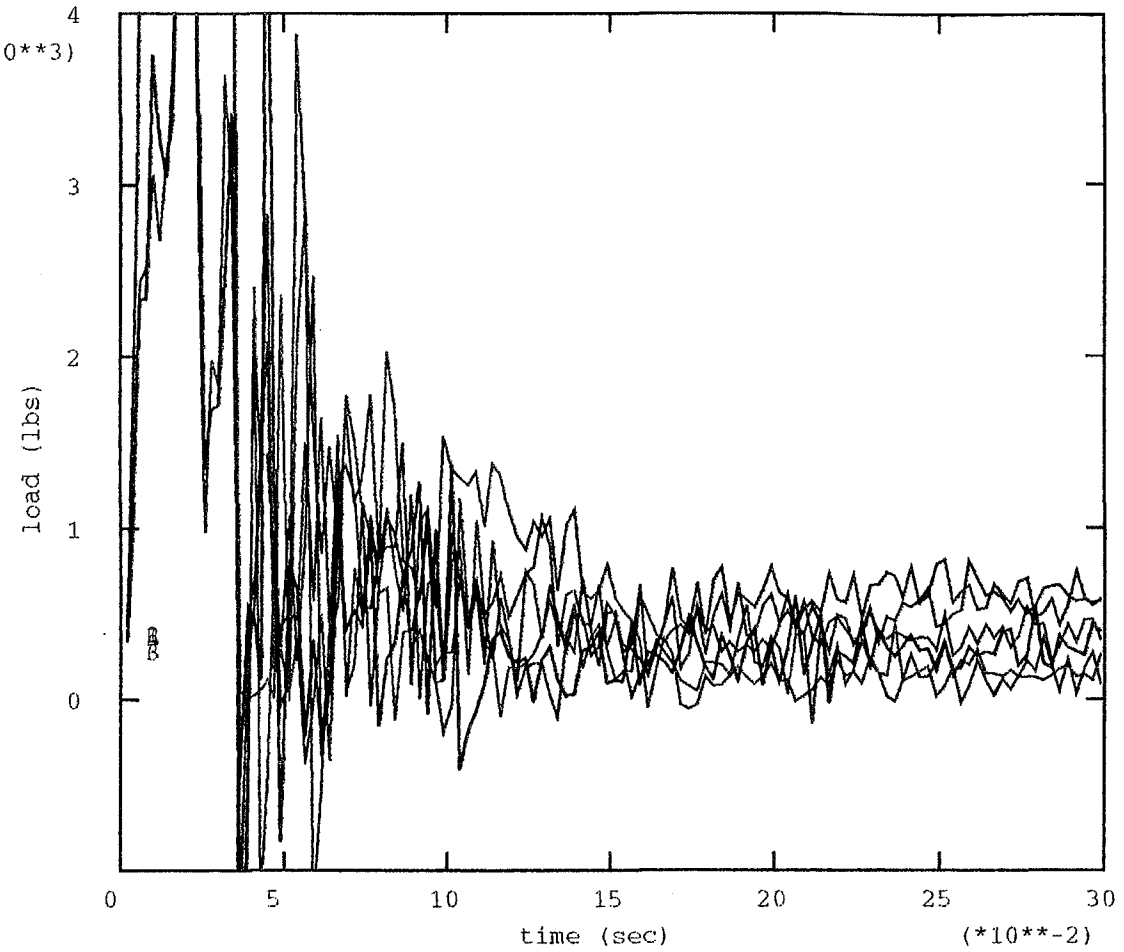

Figure D16. Bag 4 Tendon Force Time-History for Impact 4

MARS4 - OBLIQUE IMPACT ON OBLIQUE PLANE

LINE	VARIABLE	SCALE FACTOR
1	2-4 in-line	+2.47E+00
2	2-4 norm	+1.58E+00
3	2-3 in-line	+2.47E+00
4	2-3 norm	+1.58E+00
5	3-4 in-line	+2.47E+00
6	3-4 norm	+1.58E+00

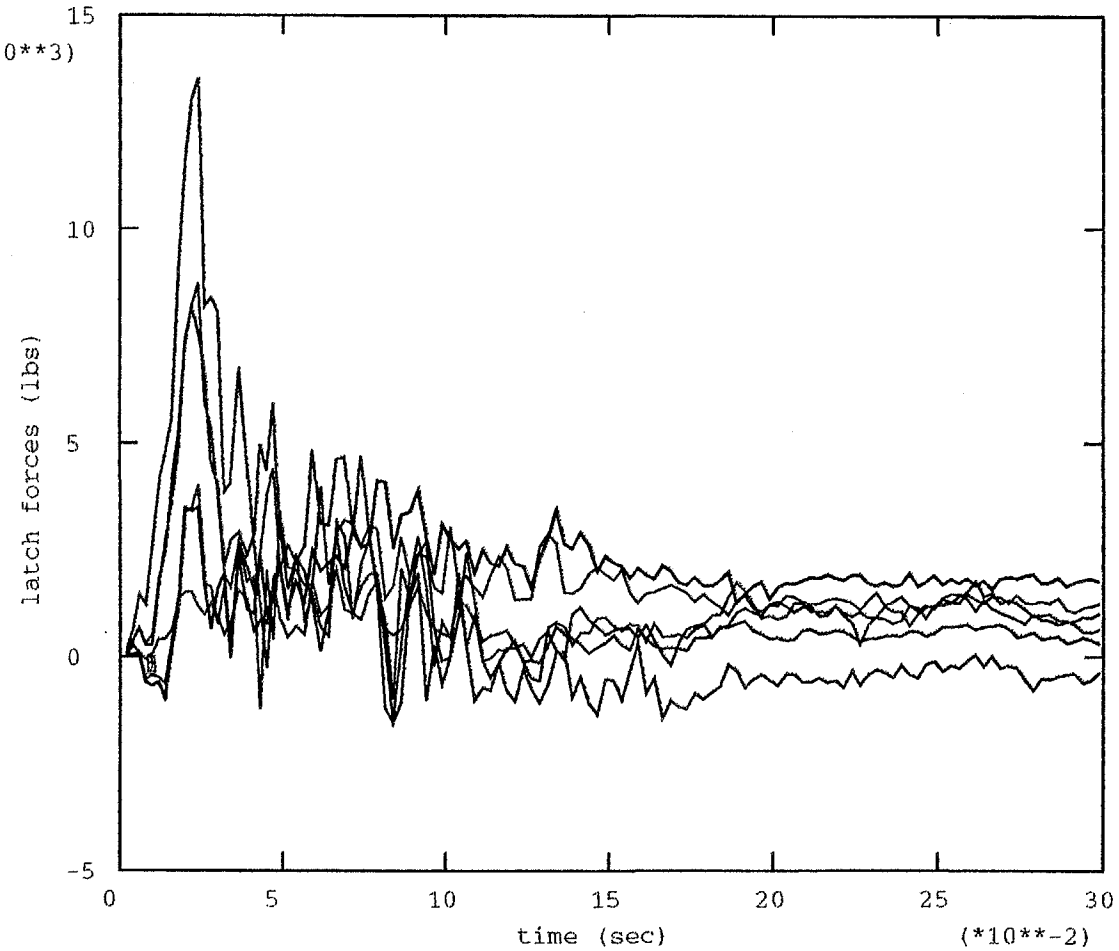

Figure D17. Latch Force Time-History for Impact 4

MARS4 - OBLIQUE IMPACT ON OBLIQUE PLANE

LINE	VARIABLE	SCALE FACTOR
1	p4 in-line	+2.71E+00
2	p4 norm	+2.38E+00
3	p4 in-line	+2.71E+00
4	p4 norm	+2.23E+00
5	p2 in-line	+2.71E+00
6	p2 norm	+2.23E+00
7	p2 in-line	+2.71E+00
8	p2 norm	+2.23E+00
9	p3 in-line	+2.07E+00
10	p3 norm	+3.05E+00
11	p3 in-line	+2.07E+00
12	p3 norm	+3.05E+00

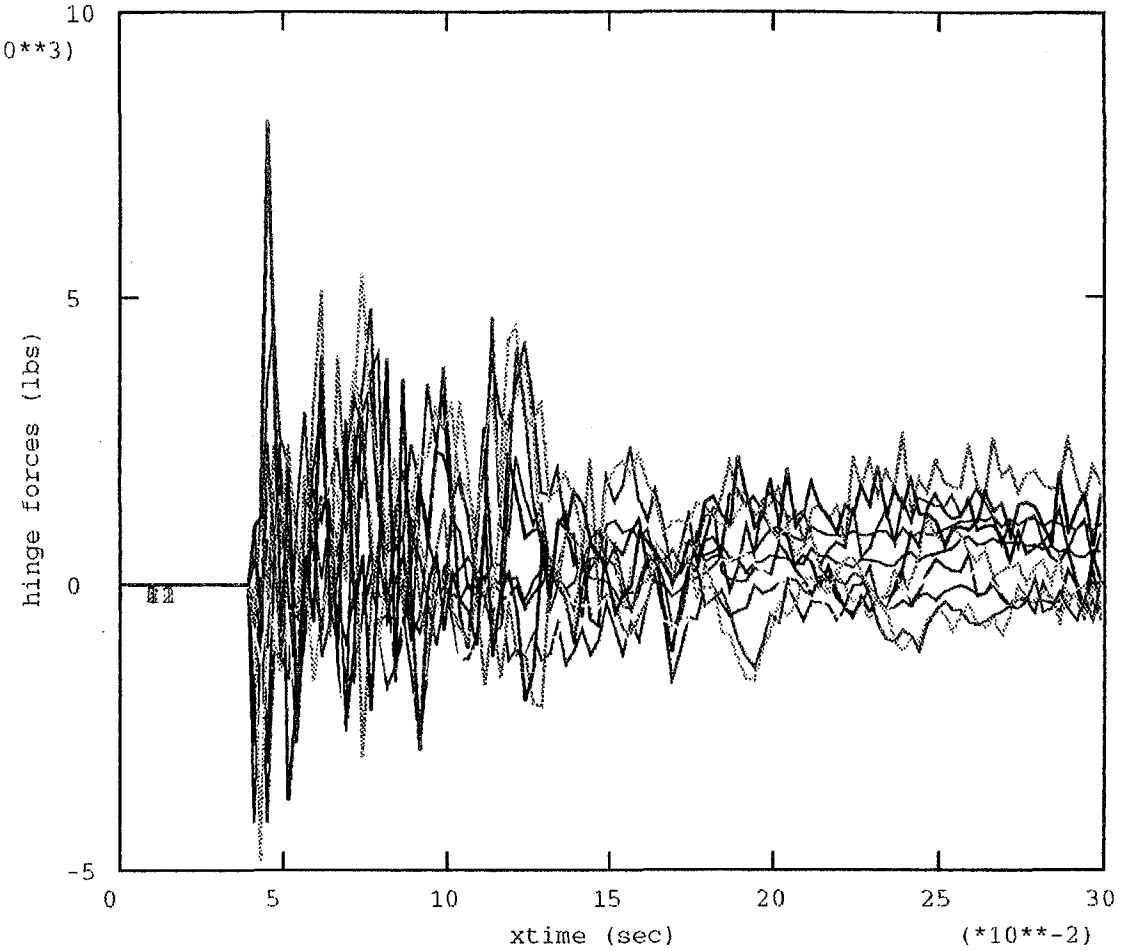

Figure D18. Hinge Force Time-History for Impact 4

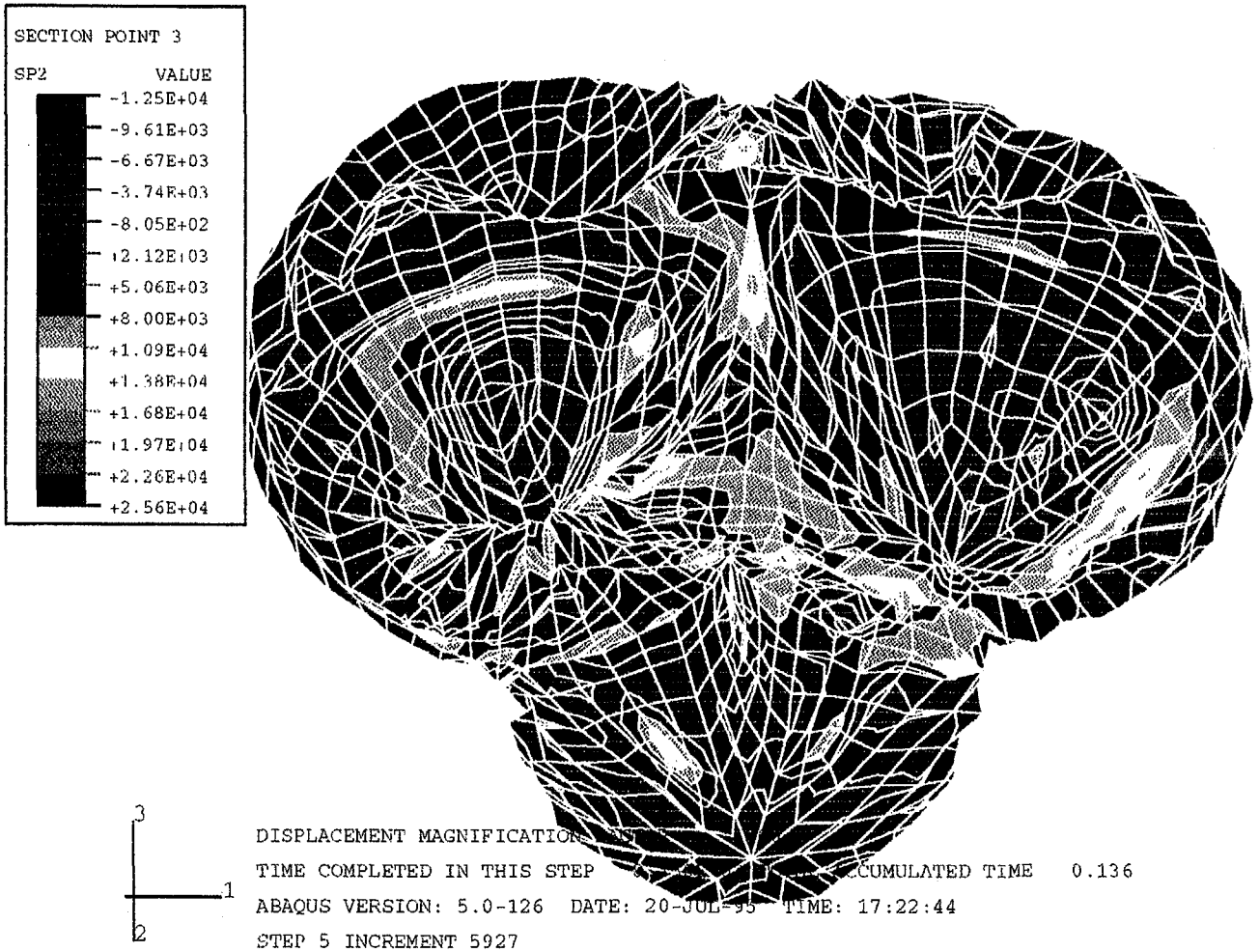

Figure D19. Maximum Principal Stress Distribution, Bottom Airbag, for Impact 4

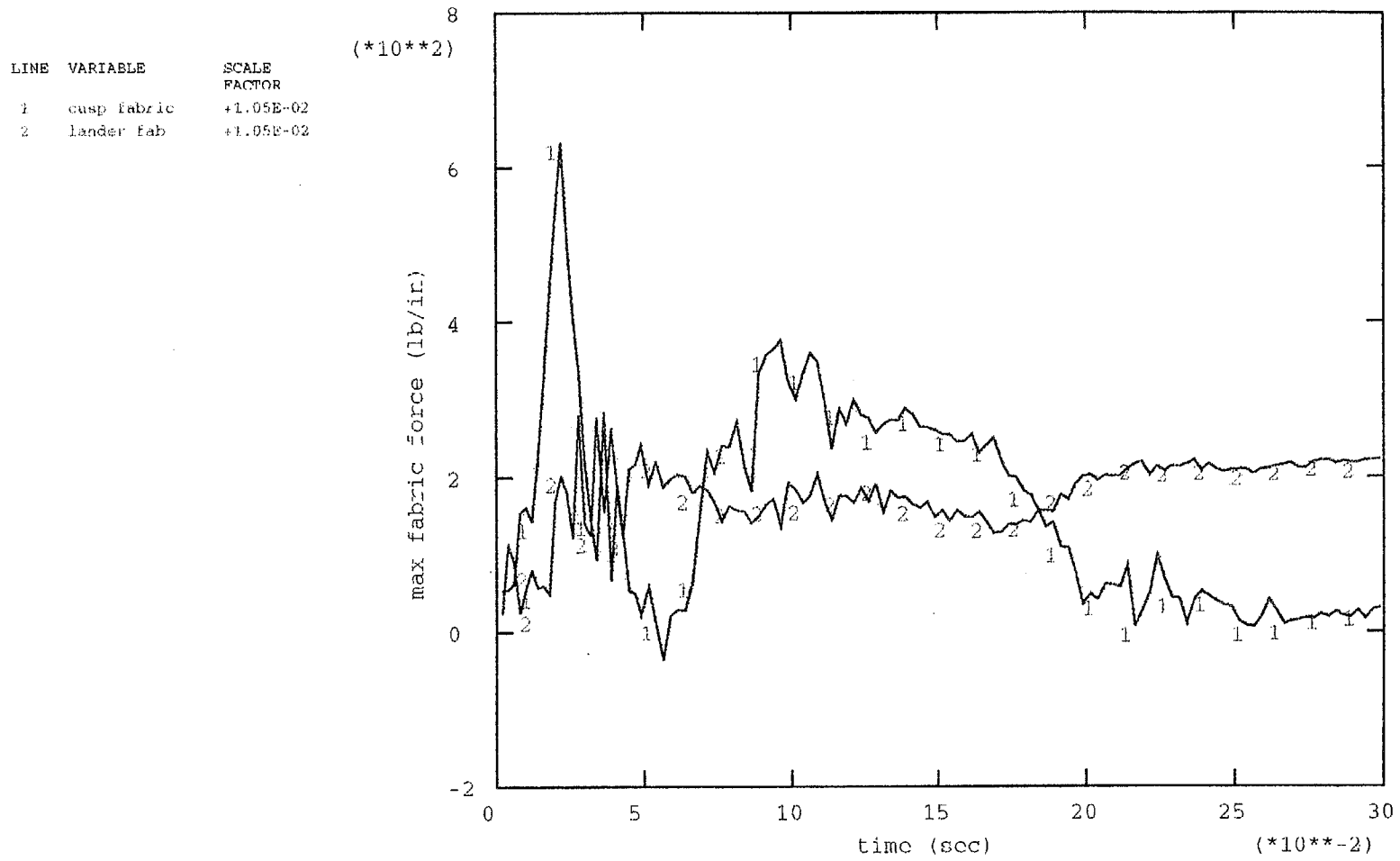

Figure D20. Maximum Fabric Force Time-History for Impact 4

Distribution

Brian Muirhead, JPL
Jet Propulsion Laboratory
4800 Oak Grove Drive
Pasadena, California 91109

Tom Rivellini, JPL
Jet Propulsion Laboratory
4800 Oak Grove Drive
Pasadena, California 91109

MS 0841	9100	P. Hommert
MS 0828	9104	R. K. Thomas
MS 0836	9116	C. W. Peterson
MS 0437	9117	K. W. Gwinn (10)
MS 0437	9117	H. S. Morgan
MS 0437	9117	K. E. Metzinger
MS 0872	14311	D. E. Waye
MS 9018	8940-2	Central Tech Files
MS 0899	4916	Technical Library (2)
MS 0619	00111	Review &Approval Desk for DOE/OSTI (1)